FINAL PERFORMANCE REPORT

Project Title: Exposure and Risk Assessment for Infectious Aerosols

Grant Number: 5 K01 OH00155

Funding Agency: National Institute for Occupational Safety and Health
U.S. Centers for Disease Control and Prevention

Principal Investigator: Mark Nicas, PhD, CIH, Adjunct Associate Professor

Academic Sponsor: Robert C. Spear, PhD, Professor

Academic Institution: School of Public Health
University of California
Berkeley, CA 94720

Table of Contents

List of Figures

Figure 9 - Costs and residual disease risks at 12 years for alternative *M. tb* infection screening intervals given an annual rate of infection of 0.5%, costs of $10 per PPD skin test and $10,000 per TB disease case, and an imperfect screening program with $p = 0.88$.

Figure 10 - Predicted cumulative infection risk parameter D since the time (days) of TB patient admission for a single infectious patient in a hospital ward.

Figure 11 - Predicted infection risk parameter D for a scenario involving exposure of 13 health care workers for 150 minutes to a highly infectious TB patient during a broncho-scopy procedure. The efficacy of wearing four alternative respirator devices and increasing the air cleaning rate (the effective ventilation rate) in ACH is shown.

Figure 12 - A schematic representation of the zones and air flows in a room divided into an upper zone, lower zone and near-field zone.

Figure 13 - The decay in the viable *M. bovis* concentration according to the three-zone model, where the initial concentration is 100 per m^3 in all three zones. Model parameter values are as follows: $V_U = 11.2\ m^3$, $V_L = 50.7\ m^3$, $V_{NF} = 2.1\ m^3$, $Q = 2\ m^3/min$, $\beta_1 = 28\ m^3/min$, $\beta_2 = 9.6\ m^3/min$, $k_1 = .00235\ min^{-1}$, $k_2 = 1.28\ min^{-1}$.

Figure 14 - A hypothetical two-zone room containing a near-field zone around a contaminant emission source; the remainder of the room constitutes the far-field zone.

Figure 15 - The *M. tb* particle concentrations in the near-field and far-field zones in the first 60 seconds following a pulse release of 10 particles into the near field at time zero. The solid-line curves are the expected near-field and far-field particle concentrations. The dotted line immediately above each expected concentration curve is the approximate 95th percentile value for the corresponding particle concentration.

Figure 16 - The distribution of approximate *M. tb* infection risk values across 10^5 simulations of a near-field/far-field scenario in which a health care worker is in the near field of a tuberculosis patient for five minutes immediately after the patient emits 10 *M. tb* particles. For this distribution, $E[R] \cong .0069$ and $SD[R] \cong .0017$.

Figure 17– The 100 x 100 single-step transition probability matrix **P** for the particle position along a 10-m room axis divided into one hundred 0.1-m segments.

Figure 18 – The expected particle concentrations at three room positions predicted by Markov models I and II following the pulse release of 2700 particles at source midpoint position ($x = 1.1$ m, $y = 1.5$ m, $z = 1.5$ m). The receptor midpoint positions are: (1) $x = 0.1$ m, $y = 1.5$ m, $z = 1.5$ m; (2) $x = 2.1$ m, $y = 1.5$ m, $z = 1.5$ m; and (3) $x = 2.9$ m, $y = 1.5$ m, $z = 1.5$ m. The room is 3 m x 3 m x 3 m, and receives no air supply.

Figure 19 – The expected particle concentrations at receptor midpoint position (x = 0.1 m, y = 1.5 m, z = 1.5 m) predicted by Markov models I and II following the pulse release of 2700 particles at source midpoint position (x = 1.1 m, y = 1.5 m, z = 1.5 m). The room is 3 m x 3 m x 3 m, and receives 6 nominal air changes per hour. The receptor position adjoins an air inlet and is 1 m upstream from the release position.

Figure 20 – The expected particle concentrations at receptor midpoint position (x = 2.1 m, y = 1.5 m, z = 1.5 m) predicted by Markov models I and II following the pulse release of 2700 particles at source midpoint position (x = 1.1 m, y = 1.5 m, z = 1.5 m). The room is 3 m x 3 m x 3 m, and receives 6 nominal air changes per hour. The receptor position is in the room interior and 1 m downstream from the release position.

Figure 21 – The expected particle concentrations at receptor midpoint position (x = 2.9 m, y = 1.5 m, z = 1.5 m) predicted by Markov models I and II following the pulse release of 2700 particles at source midpoint position (x = 1.1 m, y = 1.5 m, z = 1.5 m). The room is 3 m x 3 m x 3 m, and receives 6 nominal air changes per hour. The receptor position adjoins an air outlet and is 1.8 m downstream from the release position.

Figure 22 – The expected particle concentrations at source midpoint position (x = 1.1 m, y = 1.5 m, z = 1.5 m) following the pulse release of 2700 particles predicted by Markov model II with a barrrier immediately upstream of the source position (the solid-line curve) or with no barrier (the dashed-line curve). The room is 3 m x 3 m x 3 m, and receives 6 nominal air changes per hour.

List of Tables

Table 1 - The mean number of total infections plus or minus one standard deviation at five years without accounting for subsequent TB disease among health care workers.

Table 2 - The mean number of total and secondary infections plus or minus one standard deviation, and the mean number of disease cases plus or minus one standard deviation, at five years when accounting for subsequent TB disease among health care workers but no close contacts.

Table 3 - The mean number of total and secondary infections plus or minus one standard deviation, and mean number of disease cases plus or minus one standard deviation, at five years when accounting for subsequent TB disease among health care workers plus close contacts.

Table 4 - The mean plus or minus one standard deviation of the total number of infections, the number of secondary infections, and the total number of disease cases at the end of five years, given 5 vs. 50 TB patients admitted annually on average, constant patient infectivity, PPD skin testing programs of varying test frequency, and 0% vs. 90% successful participation.

Table 5 - The mean plus or minus one standard deviation of the total number of infections, the number of secondary infections, and the total number of disease cases at the end of five years, given 5 vs. 50 TB patients admitted annually on average, a PPD skin testing program with a 6-month testing frequency and 90% successful participation, for three distributions of patient infectivity values: (*i*) constant infectivity; (*ii*) uniformly distributed infectivity; and (*iii*) binary infectivity.

Table 6 - The mean plus or minus one standard deviation of the total number of infections, the number of secondary infections, and the total number of disease cases at the end of five years, given 1, 3 or 5 immmunocompromised workers in the cohort and given no PPD skin testing program in place.

Table 7 - The mean plus or minus one standard deviation of the total number of infections, the number of secondary infections, and the total number of disease cases at the end of five years, given zero (0) versus five (5) immmunocompromised health care workers in the cohort and given PPD skin testing programs of varying test frequency

Table 8 - The total cost (TC) and the cost per disease case prevented (C/DCP) in thousands of dollars at 12 years given different annual rates of infection, alternative screening intervals, 1000 initially susceptible employees, and a perfect screening program, $p = 1.0$ (0% false negative error in skin testing, 0% noncompliance with testing, 0% failure of prophylaxis).

Table 9 - The total cost (TC) and the cost per disease case prevented (C/DCP) in thousands of dollars at 12 years given different annual rates of infection, alternative screening intervals, 1000 initially susceptible employees, and an imperfect screening program, $p = 0.88$ (5% false negative error in skin testing, 0% noncompliance with testing, 7% failure of prophylaxis).

Table 10 - Three-zone model parameters for the *M. bovis* UVGI room study

Section 1 – Significant Findings

I. A stochastic simulation model was developed to describe *M. tuberculosis* (*M. tb*) infection and disease incidence among a hospital health care worker (HCW) cohort. The model provides results that reasonably adhere to several published observations: (*i*) the simulated annual HCW infection rates fall within the range of annual HCW infection rates reported for a sample of U.S. hospitals; (*ii*) the simulated HCW infection rates increase with more TB patient admissions, as do reported infection rates among hospital HCW's; and (*iii*) the ratio of simulated primary to secondary TB disease cases is similar to reported primary-to-secondary TB disease ratios among hospital HCW's; a primary case is due to infection by a TB patient, while a secondary case is due to infection by a coworker with TB disease.

II. The stochastic simulation model was used to investigate the effect of variability in TB patient infectivity on *M. tb* infection and disease outcomes in HCW cohorts. There were two important findings. First, as variability in patient infectivity increases, so does variability in infection incidence among HCW cohorts. Second, a binary type of patient infectivity (i.e., most patients have low infectivity but a few are highly infectious) generates the largest variability in infection incidence. A binary patient infectivity adheres to the common view that most TB patients are not infectious, but that a few are "dangerous disseminators."

III. The stochastic simulation model was used to investigate the cohort-level impact of the presence of immunocompromised HCW's who are more susceptible to TB disease subsequent to *M. tb* infection. HCW's who develop TB disease become secondary sources of infection for their coworkers. The primary finding was that the presence of immmunocompromised workers causes only a slight increase in incidence of secondary *M. tb* infection and TB disease at the cohort level.

IV. A component reliability analysis of a hospital TB control program was performed to inform cost efficacy decision-making. Alternative pathways for a HCW developing TB disease in the presence of a TB control program were delineated, and HCW disease risk was specified as a function of the reliability of the four major components of the program (rapid identification of TB disease in presenting patients, environmental controls including respiratory protection, infection screening, antibiotic prophylaxis). There were two important findings. First, for hospital staff as a whole, the rapid identification of suspected TB disease in a presenting patient is the most important component. Second, once TB disease in a presenting patient is identified, environmental controls constitute the most important component.

V. An analytical risk model was developed to examine the cost-efficacy of alternative screening intervals for *M. tb* infection among HCW's, where efficacy is the reduction in TB disease incidence among infected HCW's. Screening constituted PPD skin testing of individuals known to be PPD-negative on their last skin test. The 12-year cumulative TB disease risk of 1 per 1000 for the general U.S. population was used as a benchmark goal. The major finding was that among HCW's subject to a relatively "low" annual infection risk of 0.5%, an infection screening interval of 6 months rather than 12 months is necessary to limit the 12-year TB disease risk to 1 per 1000.

VI. A source-pathway-receptor engineering construct was developed to assess the effectiveness of alternative control measures (primarily environmental controls) for preventing *M. tb* infection among hospital HCW's, and thereby inform cost efficacy decision-making. Because the construct permits quantifying infection risk, it permits examining the cost-efficiacy of various control measures. There were two important findings. First, for those HCW's who do not enter TB patient isolation rooms, the rapid identification of suspected TB disease in a presenting patient is substantially more effective than increasing the airborne *M. tb* removal rate via increased mechanical ventilation, air filtration of recirculating air, and ultraviolet disinfection of air. Second, for those HCW's who enter TB patient isolation rooms, personal respiratory protection is substantially more effective than increasing the *M. tb* removal rate from room air via increasing effective room ventilation.

VII. A three-zone model of air flow in a TB patient isolation room was developed to evaluate previously published data on the efficacy of upper-room air ultraviolet germicidal irradition (UVGI). The upper portion of the room irradiated with UV light is one zone, a near-field zone surrounding the TB patient in the lower portion of the room is the second zone, and the remainder of the lower portion of the room is the third zone. Air within each zone is perfectly mixed, but there is limited air exchange between contiguous zones. There were two import-ant findings. First, if one examines the decay in viable bacilli concentrations in each zone starting from some initial level, the slopes of the logarithm of concentration versus time for the three zones will quickly attain a similar value, even though the effective ventilation rate in each zone is different. Second, by examining the slope of viable *M. bovis* concentration decay in a test room with and without upper-room air UVGI in operation, previous investigators likely overestimated the efficacy of UVGI in reducing viable bacilli concentrations near the emission source (the TB patient).

VIII. A Markov model was developed to describe a two-zone model of air flow in a TB patient isolation room not subject to upper-room air UVGI. The near-field zone surrounding the TB patient is one zone, and the remainder of the room is the second zone. Air within each zone is perfectly mixed, but there is limited interzonal air exchange. Markov modeling is well suited to describe airborne particle concentrations where small numbers of particles are present, as is generally the case for *M. tb* aerosol emissions. The most important finding was that the probabilistic nature of the *M. tb* particle concentration needs to be considered when designing exposure controls; it is not sufficient to base decisions on the expected particle concentration.

IX. Markov chain techniques were used to formulate a more general multi-state model of contaminant dispersion in room air due to turbulent diffusion and advection, and contaminant removal via exhaust air flows and other mechanisms such as particle settling. There were two important findings. First, the multi-zone Markov model provides a more realistic description of contaminant concentrations at different room positions than do previosuly published turbulent diffusion models or multi-zone models. Second, the effect of an in-room barrier to contaminant dispersion is to increase the average contaminant concentration near the barrier.

Section 2 – Usefulness of Findings

The overall outcome of this project has been the development of a quantitative framework for the risk assessment and risk management of occupational TB transmission in a hospital setting. Further, the engineering elements of the source-pathway-receptor construct for airborne infection can be generalized to other infectious aerosols of occupational concern. The simulation model describes the dynamic nature of TB infection and disease incidence among HCW's. Unlike previous models, it accounts for the secondary spread (worker-to-worker) of TB among hospital staff, which is a phenomenon that is difficult to describe by analytical means for a relatively small group. The simulation model clearly shows that an employee infection surveillance program serves two important roles – reducing the incidence of primary TB disease (via early detection of new nosocomial infections among HCW's, with followup antibiotic prophylaxis), and thereby minimizing the secondary transmission of TB disease.

The simulation model also demonstrates that a binary type of TB patient infectivity variability (i.e., most patients impart a low risk of infection, but some are highly infectious) can lead to great deal of variability or uncertainty in the incidence of infection and disease among HCW's. For example, based on the previous several years' experience, an entire facility might be deemed "low risk", yet the next year's incidence values might be substantially greater. A binary type of patient infectivity adheres to the common view held by infection control professionals that most TB patients are not infectious, but that a few are "dangerous disseminators". The implication is that every facility should maintain a high level of suspicion of TB disease in presenting patients, and have the respiratory isolation facilities needed to house such patients at least on a temporary basis.

The simulation model also indicates that TB infection among immunocompromised HCW's is not expected to cause a significant impact on secondary TB transmission at the HCW cohort level. Because TB infection can have severe personal consequences for an immunocompromised HCW, it is necessary to provide specific counseling to such HCW's as recommended by the 1994 CDC guidelines. Further, it is appropriate to offer such HCW's alternative assignments (to be accepted voluntarily) that decrease their degree of exposure to TB patients. However, there is no justification for making mandatory reassignments based on the idea of protecting coworkers.

The Markov models of contaminant dispersion in indoor air provide a relatively simple and explicitly probabilistic description of the transport and fate of airborne particles such as *M. tb* aerosol. These models indicate that increasing mechanical dilution ventilation has a limited ability to decrease a HCW's infection risk if most of that risk occurs while the HCW is in close proximity to the TB patient. That is, one can picture a near field zone surrounding a TB patient in which exposure of the HCW occurs. Mechanical dilution ventilation (and other particle removal or inactivation mechanisms such as upper-room air ultraviolet germicidal irradiation) that operate outside this near field zone will have a limited effect on reducing exposure intensity at the HCW's position near the TB patient.

The Markov modeling approach has broad applications to describing concentrations of indoor air contaminants other than infectious aerosols. Such models are useful in making retrospective and prospective exposure estimates in a wide variety of settings, and are tools for prioritizing air sampling efforts. The multi-state construct termed Markov model II also shows that the presence of in-room barriers to contaminant diffusion and advection are important to consider in some circumstances, because such barrers can substantially increase a worker's exposure intensity by keeping contaminant close to the individual for a longer period.

The three-zone model analysis of published data regarding upper-room air ultraviolet germicidal irradiation shows that previous investigators likely overstimated the efficacy of this means of infection control. The analysis has the following broader application. Determinations of an enginering control's efficacy in reducing the steady-state or long-term average airborne contaminant concentration should not be based on analyzing slopes of concentration decay curves, but on steady-state measurements, because decay slope values can be misleading. The effective contaminant removal rate at different room positions may differ markedly (leading to different average contaminant levels at these room positions), yet the slopes of concentration decay curves at these same room positions can be similar in value.

The analytical model developed for the effect of an *M. tb* infection screening program in reducing nosocomial TB disease among HCW's is apparently the first effort at quantifying the cost-efficacy of alternative screening intervals. The analytical formulae permit risk managers to design a screening program based on the estimated annual rate of infection in a facility and a defined target risk of disease (suggested to be 1 per 1000 in a 12-year interval).

The component reliability analysis and the source-pathway-receptor engineering construct provide a general framework for cost-efficacy analysis of TB control measures. Cataloguing of current dollar costs for different control measures, and comparisons of specific controls (e.g., in-room air filter #7 versus Type N95 respirator #20), were not pursued in this project. The reason is that costs continually chang as new technology is developed and market demand fluctuates, and a final cost analysis depends not only on the current dollar values of implementing different measures, but on the degree of risk currently experienced by a facility. In this context, it is the ability to estimate reductions in infection and disease risk afforded by different measures that is important to develop.

The component reliability analysis shows that if a facility has a poor record in identifying TB disease in presenting patients, expenditures to increase the general level of suspicion and efficiency of identifying and isolating TB patients will be most cost-effective. On the other hand, if the facility is already highly efficient in identifying and isolating TB patients, expenditures to increase the efficency of environmental controls will be most cost-effective, particularly among HCW's who attend TB patients. The source-pathway-receptor construct shows that for HCW's who enter TB patient isolation rooms, personal respiratory protection is substantially more effective than increasing the *M. tb* removal rate from room air via increasing effective room ventilation. The latter conclusion is also supported by the two-zone Markov model, as previously described.

Section 3 – Abstract

The general aim was to develop a quantitative framework for estimating *M. tb* infection and TB disease incidence among HCW's in a hospital setting, such that the framework could inform risk management decisions. A stochastic simulation model was developed to describe *M. tb* infection and disease incidence among a hospital HCW cohort. The model provided results that reasonably adhered to published observations. Application of the model showed that a binary type of patient infectivity (i.e., most patients have low infectivity but a few are highly infectious) generates substantial variability in infection incidence. A binary patient infectivity adheres to the common view that most TB patients are not infectious, but that a few are "dangerous disseminators." Application of the simulation model also showed that infection among immunocompromised HCW's causes only a slight increase in incidence of secondary *M. tb* infection and TB disease at the HCW cohort level, although TB disease in immunocompromised individuals has severe personal consequences.

To provide an analytical framework for investigating cost-efficacy, a component reliability analysis of a hospital TB control program was performed to identify the most important control measures. For hospital staff as a whole, the rapid identification of suspected TB disease in presenting patients is the most important measure, but once TB disease in a presenting patient is identified, applying highly efficient environmental controls is the most important measure. With regard to the infection surveillance component of the TB control program, an analytical risk model was developed to examine the cost-efficacy of alternative screening intervals for new infection among HCW's. Efficacy was the reduction in TB disease incidence among HCW's, with the U.S. population TB disease risk taken as the target goal. It was shown that among HCW's subject to a relatively "low" annual infection risk of 0.5%, an infection screening interval of 6 months rather than 12 months is necessary to meet the target risk level, yet this interval is only slightly less cost effective than using a 12-month interval. A source-pathway-receptor engineering construct was developed to assess the efficacy of alternative control measures (primarily environmental controls) for preventing *M. tb* infection. Similar to the finding of the component reliabiity analysis, it was shown that for HCW's who do not attend TB patients, the rapid identification of suspected TB disease in a presenting patient is substantially more effective than increasing the effective ventilation rate via increased mechanical ventilation, air filtration of recirculating air, and ultraviolet disinfection of air. However, for those HCW's who directly attend TB patients, personal respiratory protection is substantially more effective than increasing effective ventilation. A related engineering model showed that a previous analysis of upper-room air ultraviolet germicidal irradiation likely overestimated the efficiacy of this control technique.

Markov models of contaminant dispersion in indoor air were developed. It was shown that Markov models provide a relatively simple and explicitly probabilistic description of the transport and fate of airborne particles such as *M. tb* aerosol. These models indicate that increasing mechanical dilution ventilation has a limited ability to decrease a HCW's infection risk if most of that risk occurs while the HCW is in close proximity to the TB patient. The Markov modeling approach has broad applications to describing concentrations of indoor air contaminants other than infectious aerosols.

Section 4 – Background

An increased incidence of active pulmonary tuberculosis (TB) in the U.S. population in the early 1990's, combined with nosocomial outbreaks of multidrug resistant TB, has led to renewed concern for TB transmission among health care workers (HCWs).[1,2,3] Infection usually occurs via inhalation of respirable particles carrying viable *M. tb* bacilli which are emitted in respiratory aerosols by persons with pulmonary TB. It is estimated that 10% of infected persons eventually develop clinical disease absent receiving prophylactic antibiotic therapy, and that half of these cases occur in the first year following infection.[4]

Prior to the advent of antibiotic therapy in the 1950's, HCWs experienced high rates of *M. tb* infection, and substantial numbers developed active TB.[3] Rates of *M. tb* infection currently reported for HCWs are much lower. In a mail questionnaire survey of hospital epidemiologists, employee infection rates in 1992 as reported for 109 hospitals had a median value of 0.5% (range: 0 - 7.7%).[5] In an ongoing prospective cohort study involving 29,000 HCWs, the cohort annual infection rate is reported to be approximately 1%.[6] Infection rates for particular groups of HCWs can be considerably higher.[7]

In 1992, NIOSH issued recommendations on respiratory protection against *M. tb* aerosol.[8] In 1994, the CDC issued final guidelines for preventing TB transmission in health care facilities.[9] Although these recommendations and guidelines promoted integrated TB control programs, they treated risk reduction in a qualitative rather than quantitative fashion. Three examples are as follows. The 1994 CDC guidelines recommended that: (1) HCW's wear Type N95 filtering-facepiece respirators when attending TB patients; (2) TB patient isolation rooms receive at least six air changes per hour of ventilation air; and (3) susceptible HCW's subject to a "low" risk of infection receive PPD skin testing at 12 month intervals. For all three examples, there was no quantitative discussion of the baseline degree of infection and disease risk assumed, and no quantification of the estimated reduction in risk to be achieved by the recommended control. The general purpose of the project was to develop a quantitative framework for estimating *M. tb* infection and TB disease incidence among HCW's in a hospital setting, such that the framework would inform risk management decisions. It was expected that elements of the approach for TB could be generalized to other infectious aerosols of occupational concern.

Section 5 – Specific Aims

At the outset, this three-year project had four specific aims:

(*i*) develop a stochastic simulation model of TB transmission among a cohort of hospital HCW's that accounts for variability in the number of TB patients admitted, variability among HCW's in infection risk, secondary transmission of TB from worker to worker, and variability in TB patient infectivity;

(*ii*) use the stochastic simulation model to investigate the impact of TB infection among immunocompromised HCW's, for example, those with active HIV infection;

(*iii*) develop a field method for determining the local purging flowrate in TB patient and treatment rooms; and

(*iv*) use the stochastic model and analytical methods to investigate the cost efficacy of alternative infection/disease control measures.

In the third year of the project, it became evident that aim (*iii*) could not be completed due to technical difficulties encountered in the laboratory validation of the intended field method. NIOSH/CDC grant management officers were informed of the problem, and it was mutually agreed that aim (*iii*) would be modified as follows: develop a multi-state Markov chain model to describe contaminant dispersion in indoor air. Because the intended Markov chain modeling work has application to assessing dilution ventilation efficacy, it was deemed consistent with the original aim.

As detailed in Section 6, original aims (*i*), (*ii*) and (*iv*), and modified aim (*iii*) were successfully completed.

Section 6 – Results

I. The Stochastic Simulation Model

The approach was to start with a simple construct and add complexity in a step-wise fashion. HCW's were classified into three groups (low, medium, high) with respect to their daily risk of infection due to the admission of a TB patient into the hospital. The number of susceptible workers initially in the three groups is denoted X, Y, and Z, respectively, where N = X + Y + Z. Simulations were based on N = 1000 individuals. The rationale for the classification was that workers in the first group would have very little occupational risk due to their lack of patient contact and physical separation from patient care areas (e.g., records clerks, pharmacists), that workers in the second group would have a higher risk due to their presence in TB patient care areas although without direct patient contact (e.g., ward clerks), and that workers in the third group would have the highest risk due to their providing services directly to TB patients (e.g., attending nurses and physicians). Two scenarios were examined with regard to the numbers of HCW's in the three groups. In the first scenario, X = 600, Y = 300, and Z = 100. In the second scenario, X = 850, Y = 100, and Z = 50.

The daily infection risk attributed to a given TB patient is treated as identical for all members of a given risk group, and initially all TB patients are treated as being equally infectious. Given the conditions of identical risk within a group and no difference in infectiousness between TB patients, the presence of one TB patient in the hospital imparts the following daily infection risks to members of the low-, medium- and high-risk HCW groups, respectively: $r_L = 10^{-5}$, $r_M = 10^{-4}$, and $r_H = 5 \times 10^{-4}$. These daily risks apply only while the TB patient is in the facility; the length of stay while infectious is set at 10 days for every TB patient. Note that if one TB patient were in the facility on every work day, and if there were 220 workdays in a year, the annual risk of infection in the low-, medium- and high-risk groups would be, respectively, .0022, .022, and 0.11. When two TB patients are in the hospital, the daily risks are doubled to $2r_L$, $2r_M$, and $2r_H$, respectively, and so forth. When no TB patients are in the hospital, the daily risk is set to zero for all susceptible workers. In reality, there is a background daily risk of nonoccupational *M. tb* infection on the order of 4×10^{-6}; the latter daily risk corresponds to an annual *M. tb* infection risk of .0015 as estimated for the general U.S. population.[10] For simplicity, this nonoccupational risk was ignored due to its negligible impact on the overall cohort risk given the posited values for r_L, r_M and r_H.

Two scenarios were examined with regard to the expected number of TB patients admitted annually, denoted T; these scenarios were T = 5 and T = 50. The corresponding expected number of TB patient admissions per day are T/365. The number of TB patients admitted on a given day, denoted S, is modeled as a Poisson random variable such that: $\Pr(S = s) = (T/365)^s \exp(-T/365)/s!$.

The simulation involved tracking the random events of TB patient admissions and occupational *M. tb* infections among the N = 1000 cohort members over a five-year period during

which members work on average 220 days per year. While the initial scenarios did not account for the development of TB among infected healthcare workers, later scenarios did incorporate this possibility, as will be described. To illustrate the basic simulation, consider the values previously posited for r_L, r_M and r_H, let T = 50 TB patients admitted annually on average, and let X = 600, Y = 300 and Z = 100. On day 1, a Poisson random variate S with an expected value of 50/365 is generated. If S = 0, no TB patients are admitted, the risk of infection is zero for all workers, and the simulation proceeds to day 2. However, if S = 1, one TB patient is admitted on day 1, and $r_L = 10^{-5}$, $r_M = 10^{-4}$, and $r_H = 5 \times 10^{-4}$. Next, a uniform random variate U_W is generated for each susceptible HCW to determine if the individual is assigned to work that day. If $U_W \leq 220/365$, the individual is on the job, whereas $U_W > 220/365$ signifies that the individual is not at work. For day 1 this results in approximately 362, 181, and 60 members of the low-, medium- and high-risk groups at work.

For each low-risk group member at work, another uniform random variate U_L is generated. If $U_L \leq .00001$, the individual becomes infected, whereas if $U_L > .00001$, the individual remains uninfected. Infected workers are removed from the remaining susceptibles in the group such that no double counting of infections occurs; from a biological standpoint this means that multiple infections are not permitted. A similar comparison pertains to each medium-risk and high-risk group member at work where, respectively, $U_M \leq .0001$ and $U_H \leq .0005$ signifies that infection occurs.

Consider the admission of one TB patient on day 1. On day 2, another Poisson random variate S is generated. If S = 0, no new TB patients are admitted on day 2. However, because the TB patient admitted on day 1 remains in the facility (and will remain through day 10), the infection risks on day 2 are still: $r_L = 10^{-5}$, $r_M = 10^{-4}$, and $r_H = 5 \times 10^{-4}$. In the alternative, consider that S =1 for day 2; in this event, one new TB patient is admitted and the daily infection risks are doubled. For each susceptible cohort member at work on day 2 (which may be less than the number present on day 1 due to the chance of not being assigned to work or due to infections that occurred on day 1), a uniform random variate is generated. Given two TB patients in the facility, the comparisons for the low-, medium- and high-risk group members are, respectively, $U_L \leq 0.00002$, $U_M \leq 0.0002$, and $U_H \leq .001$, which signifies that infection occurs. As before, any worker who becomes infected is removed from the remaining susceptibles in the group. The simulation then proceeds to day 3, and so forth, for a total of 1825 days (5 years). At least 500 simulations were performed for each scenario.

Added complexity involved accounting for the development of TB disease by infected workers. Morbidity can occur if a worker's *M. tb* infection is not detected and treated, perhaps because the hospital has a poor employee infection screening program, because the infection occurs in the interval between scheduled screening tests, because the infected employee is anergic, or because the infection is detected but the worker does not undergo prophylactic antibiotic therapy. For simplicity, the incidence of TB disease and its consequences was initially modeled with the assumption that no employee infection screening program was in place such that all infections went undetected and untreated.

If a worker becomes infected, for the first 365 days thereafter the individual is assigned a daily risk of 1.4×0^{-4} of developing TB, and then is assigned a daily risk of 3.02×0^{-6} for the remainder of the simulation. These risks correspond to a probability of .05 of developing TB by one year after infection, and a probability of 0.10 of developing TB by fifty years after infection. Fifty years was assumed to be the subsequent lifetime of an otherwise healthy adult infected with *M. tb*. If a worker becomes infected, a uniform random variate U_{TB} is generated for the worker for each remaining day of the simulation. In the first year following infection, if $U_{TB} \leq .00014$ the worker develops TB on that day, whereas if $U_{TB} > .00014$ the worker remains free of disease. After the first year of infection, $U_{TB} \leq 3.02 \times 0^{-6}$ signifies that disease develops, and $U_{TB} > 3.02 \times 0^{-6}$ signifies that it does not.

If an infected individual develops TB, the individual continues to work for a three-week calendar period before the disease is diagnosed and the individual leaves on medical disability. A HCW with undiagnosed TB is a secondary source of infection for coworkers as well as for patients. Two approaches were used to model this secondary source of infection among HCW's. First, the diseased worker is simply treated as an additional TB patient who is present in the hospital for 13 workdays (i.e., 21 calendar days x 220/365) and who imparts the usual daily risks of infection to all susceptible cohort members. In the second approach, each diseased worker has 25 "close contacts" among the susceptible employees, and each close contact has probability of 0.22 of being infected given that the diseased coworker is present in the hospital for 13 workdays (i.e., 21 calendar days x 220/365). For the remaining susceptible HCW's, the diseased worker acts like another TB patient in the facility, except that the diseased worker is present for 13 days rather than 10 days.

HCW Infection with Subsequent Disease: Curve A, Figure 1, depicts the five-year time course of the mean number of infections, plus or minus one standard deviation (± SD), given X = 600, Y = 300 and Z = 100, and given T = 50 TB patients admitted annually on average and no disease development among infected HCW's. At five years, the mean ± SD was 104 ± 9.9. For comparison, Curve B depicts the time course for the same conditions except that T = 5 TB patients admitted annually on average. At five years, the mean ± SD was 13 ± 4.3. As expected, admitting fewer TB patients leads to a lower incidence of occupational infection.

For the T = 50 scenario, the five-year cumulative risks in the low-, medium- and high-risk groups are, respectively, .015, 0.14 and 0.53. The expected number of infections in each group is the product of the cumulative risk and the group size, which yields 9, 42 and 53 infections in the low-, medium- and high-risk groups, or 104 infections in total. For the T = 5 scenario, the five-year cumulative risks in the low-, medium- and high-risk groups are, respectively, .0015, .015, and .073, which correspond to 1, 5 and 7 infections for a total of 13 infections.

For the analogous scenarios with X = 850, Y = 100 and Z = 50, the five-year mean number of infections ± one SD was 6.3 ± 2.7 for the T = 5 scenario, and 53 ± 6.7 for the T = 50 scenario. As expected, having relatively fewer HCW's in the medium- and high-risk groups

resulted in fewer infections in the cohort. The five-year simulation results for the four scenarios just described are summarized in Table 1.

HCW Infection with Subsequent TB Disease and No Close Contacts: Given X = 600, Y = 300, Z = 100, and T = 50 versus T = 5 TB patients admitted annually on average, the five-year time course of the mean total number of infections was close to that shown by, respectively, Curve A and Curve B, Figure 1. At five years, the mean ± SD was 106 ± 9.9 for T = 50, and 13 ± 4.6 for T = 5. In the T = 50 scenario, the development of TB disease among cohort members resulted in approximately three "secondary" infections at five years (i.e., infections due to diseased coworkers). Moreover, at five years the mean number of disease cases ± SD was 5.1 ± 2.3; approximately one disease case developed during each year of the simulation. For this same scenario, the expected total number of infections at five years was approximately 109 (compare to the observed mean of 106), and the expected number of primary disease cases due to infection by a TB patient was approximately 4.9 (compare to the observed mean of 5.1). Note that the latter difference of 0.2 disease cases represents "secondary" disease incidence (i.e., disease cases caused by diseased coworkers).

Table 2 summarizes the five-year simulation results for the above scenarios, and for the analogous scenarios in which X = 850, Y = 100, Z = 50, and T = 5 vs. 50 TB patients admitted annually on average. Fewer TB patients admitted and/or fewer number of workers in the medium- and high-risk groups resulted in fewer disease cases and secondary infections.

Worker Infection with Subsequent TB Disease and Close Contacts: Given X = 600, Y = 300, Z = 100, and T = 50 vs. T = 5 TB patients admitted annually on average, the five-year time course of the mean total number of infections is shown by Curves C and D, respectively, in Figure 1. At five years, the mean ± SD was 140 ± 24 for T = 50, and 17 ± 8.5 for T = 5. In the T = 50 scenario, the five-year mean number of disease cases ± SD was 6.5 ± 3.5, and the five-year mean number of secondary infections ± SD was 39 ± 22.

As compared to the T = 50 scenario which accounted for disease development but not for close contacts, the presence of close contacts increased the five-year mean number of secondary infections from 3 to 39, and increased the five-year mean number of disease cases from 5.1 to 6.5. Among the former 5.1 disease cases, 4.9 were primary cases and 0.2 were secondary cases, which is a primary to secondary disease ratio of approximately 25:1. Among the 6.5 disease cases in the close-contacts scenario, 4.8 were primary cases and 1.7 were secondary cases, which is a primary to secondary disease ratio of approximately 6:2.

The light bars in Figure 2 represent a histogram of five-year infection incidence outcomes in the scenario involving X = 600, Y = 300, Z = 100, and T = 50 TB patients admitted annually on average, and accounting for subsequent TB disease and substantial infection risk among close contacts. The mean is 140, but the range is 82 to 245. For comparison, the dark bars in Figure 2 show a histogram of five-year infection outcomes for the analogous scenario that did not permit TB disease among infected workers; the mean is 104 infections and the range is 77 to 138. Figure 3 shows a histogram of five-year disease incidence outcomes in the scenario involving X = 600, Y = 300, Z = 100, and T = 50 TB patients admitted annually on

average, and accounting for subsequent TB disease and substantial infection risk among close contacts. The mean is 6.5, but the range is 0 to 26. Overall, the increase in occupational infection and disease incidence corresponds to the absence of an employee *M. tb* infection screening program with followup prophylactic antibiotic therapy.

Table 3 summarizes the 5-year simulation results for the above scenarios, and for the scenarios in which X = 850, Y = 100, Z = 50, and T = 5 vs. 50 TB patients admitted annually on average. Again, the fewer TB patients admitted and/or the fewer number of workers in the medium- and high-risk groups, the lower the number of secondary infections and disease cases.

The Effect of An Employee Infection Surveillance Program: The results described above apply to the circumstance in which an employee PPD-skin testing program is not in place, such that new *M. tb* infections among HCW's are not detected and antibiotic prophylaxis is not administered. The expected impact of an employee infection surveillance program would be to reduce the number of primary TB disease cases among infected HCW's and thereby reduce the number of secondary infections and secondary disease cases. On the other hand, a surveillance program would not impact the number of primary infections due to TB patients, as depicted in Figure 1.

Consider the close-contacts scenario described above with the change that 90% of the HCW cohort successfully participates in an infection surveillance program. This circumstance signifies that 90% of HCW's comply with skin testing, are not subject to testing error, and undergo successful antibiotic prophylaxis if infected. The Table 4 columns subheaded "12 months", "6 months" and "3 months" show the five-year values for the previous three outcomes (total number of infections, number of secondary infections, total number of disease cases) given successful periodic testing of susceptible employees at, respectively, 12-month, 6-month and 3-month intervals. For T = 50 TB patients admitted annually on average, the mean total number of infections ± SD for these three intervals are, respectively, 118 ± 15, 112 ± 14 and 109 ± 12. The reduction in the mean number of total infections from 140 without screening results from decreasing the mean total number of disease cases ± SD from 6.5 ± 3.5 without screening to 3.2 ± 2, 1.7 ± 1.6 and 1.2 ± 1.2 for the three respective intervals. In turn, the mean number of secondary infections ± SD is reduced from 39 ± 2 in the absence of screening to 18 ± 12, 10 ± 10 and 6.3 ± 7.2 for the three respective intervals.

For T = 5 TB patients admitted annually on average, the five-year mean total number of infections ± SD is reduced from 17 ± 8.5 without screening to 15 ± 6.2, 14 ± 5.9 and 13 ± 5.5 for the respective 12-month, 6-month and 3-month screening intervals. The mean total number of disease cases ± SD is reduced from 0.7 ± 1.1 without screening to 0.4 ± 0.7, 0.2 ± 0.5 and 0.2 ± 0.6 for the three respective intervals. In turn, the mean number of secondary infections ± SD is reduced from 4.2 ± 6.7 in the absence of screening to 2.4 ± 4.4, 1.2 ± 3.5 and 1 ± 3.5 for the three respective intervals. Overall, the screening results are intuitively reasonable. A shorter screening interval reduces the amount of time newly infected workers are subject to developing TB disease, and thereby reduces the number of TB disease cases and the number of secondary infections.

II. The Effect of Variable Patient Infectivity

To examine the impact of variability in patient infectivity, three scenarios were considered: (*i*) a constant infectivity parameter such that every TB patient posed the same infection risk; (*ii*) a uniformly distributed infectivity parameter over a 100-fold range, but with the same mean value as in scenario (*i*); and (*iii*) a binary infectivity parameter over a 100-fold range, but with the same mean value as in scenario (*i*). To illustrate, consider the high-risk HCW group. In scenario (*i*), the daily infection risk imparted by each patient is $r_H = 5 \times 10^{-4}$. In scenario (*ii*), the daily infection risk value for each patient is randomly selected from a uniform distribution over the interval 9.9×10^{-6} to 9.9×10^{-4}, which yields a mean r_H value of 5×10^{-4}. Therefore, patient #1 might impart a daily infection risk of 1.0×10^{-5} to all high-risk group members, patient #2 might impart a daily infection risk of 1.0×10^{-4}, and so forth. In scenario (*iii*), the daily infection risk value for each patient is randomly selected from a binary distribution such that $r_{H,HIGH} = 1.678 \times 10^{-2}$ for 2% of patients, and $r_{H,LOW} = 1.678 \times 10^{-4}$ for 98% of patients, which again yields a mean r_H value of 5×10^{-4}. Therefore, patient #1 might impart a daily infection risk of 1.678×10^{-4} to all high-risk group members, patient #2 might impart a daily infection risk of 1.678×10^{-2}, and so forth.

A given simulation again involved tracking the stochastic events of TB patient admissions, occupational *M. tb* infections, and subsequent TB disease incidence among the 1000 cohort members over a five-year period (1825 days). At least 500 simulation runs were performed for each scenario investigated.

Consider scenarios involving T = 50 versus 5 TB patients admitted annually on average, and with 90% of the HCW cohort successfully participating in an infection surveillance program with a 6-month testing interval. Table 5 shows the five-year values of the mean ± SD for the total number of infections, number of secondary infections and total number of disease cases given patient infectivity values that are constant, uniform or binary. For each average annual number of patient admissions, the respective mean values are essentially the same across the three distributions of patient infectivity (constant, uniform, binary) but the standard deviation of the total number of infections is substantially larger for the binary distribution of patient infectivity. For T = 50 TB patients admitted annually on average, the %CV of the total number of infections is 13% (14/112 x 100%) given constant patient infectivity, and 27% (30/111 x 100%) given binary patient infectivity. For T = 5 TB patients admitted annually on average, the %CV of the total number of infections is 42% (5.9/14 x 100%) given constant patient infectivity, and is 93% (13/14 x 100%) given binary patient infectivity. Figure 4 presents histograms of the five-year total number of infections for the scenario involving T = 5 TB patients admitted annually on average and a 6-month screening interval with 90% successful participation. Therefore, for any posited distribution of patient infectivity, implementing an infection screening program decreases the expected number of infections compared to no screening, but substantial variability in infection incidence remains.

III. The Impact of Immunocompromised Health Care Workers

To examine the cohort-level impact of infection among immunocompromised (IC) HCW's, one to five IC workers were seeded into the high-risk group in the scenario involving the cohort composed of X = 600, Y = 300, and Z = 100. For example, given five IC cohort members, the high-risk group has 95 healthy susceptible HCW's and 5 IC susceptible HCW's. For simplicity, an IC worker is not permitted to be a close contact for a non-IC diseased coworker. If the IC worker becomes infected, the individual is assigned a daily risk of 2.28×0^{-4} of developing TB disease for the remainder of the simulation. This daily risk corresponds to an annual probability of .08 of developing TB, which is a value consistent with published data.[1,11] To assess the worst-case outcome, it is assumed that *M. tb* infection in an IC worker would not be detected due to anergy, in which case the worker would not undergo antibiotic prophylaxis. If the infected IC worker develops disease, it is again assumed that the worker has 25 close contacts among susceptible employees, and that each close contact has probability 0.22 of being infected given that the diseased IC worker remains for three calendar weeks. For other susceptible cohort members, the diseased IC worker imparts the same daily infection risks as does a TB patient.

Immunocompromised Workers with No Infection Surveillance Program: To provide a baseline for comparison, first assume that a PPD-skin testing program is not in place. Table 6 shows the five-year values of the mean ± SD for the total number of infections, the number of secondary infections, and the total number of disease cases. Given the presence of 0, 1, 3 or 5 IC workers, the mean total number of infections ± SD was, respectively, 140 ± 24, 141 ± 25, 142 ± 25 and 144 ± 24. These slight increases from 140 total infections with no IC workers present were due to corresponding increases in the mean number of secondary infections. The latter outcome was 39 ± 22 with no IC workers present, and 40 ± 22, 42 ± 23, and 43 ± 22 with, respectively, 1, 3 or 5 IC workers present. In turn, these small increases in secondary infections contributed to small increases in the total number of disease cases. The mean number of disease cases ± SD was 6.5 ± 3.5 with no IC workers present, and 6.8 ± 3.6, 7.0 ± 3.6 and 7.3 ± 3.6 with, respectively, 1, 3 or 5 IC workers present. In summary, in the absence of an employee infection surveillance program, adding IC workers to the high-risk employee group caused an approximate 2% increase per IC worker in the number of secondary infections and number of disease cases at the cohort level.

Immunocompromised Workers with an Infection Surveillance Program: Consider that 5 IC HCW's are present in the high-risk group, and that 90% of the cohort successfully participates in a PPD skin-testing program. Table 7 lists the five-year values of the mean ± SD for the three cohort outcomes previously discussed, given the presence of 0 versus 5 IC HCW's, and given alternative screening intervals of 12 months, 6 months and 3 months. As before, the presence of IC workers slightly increased the number of total infections, secondary infections and total disesase cases in the cohort, and the use of shorter testing intervals decreased the values of these same outcomes whether or not IC HCW's were present. Table 7 also indicates that the relative cohort-level impact of *M. tb* infection among IC HCW's is greatest when overall cohort infection and disease incidence is minimized by using a 3-month screening interval. For example, consider the mean total number of disease cases. Adding IC workers to the high-risk employee group caused an approximate 3% increase per

IC worker given 12-month screenings, an 8% increase per IC worker given 6-month screenings, and a 9% increase per IC worker given 3-month screenings; in the absence of screening, the increase was 2% per IC worker. However, the absolute increment in the number of disease cases per IC worker was approximately 0.1 for all three screening intervals.

IV. Component Reliability Analysis of a Hospital TB Control Program

Occupational TB control programs in most hospital settings have the following four components: (*i*) rapid detection of TB disease in presenting patients; (*ii*) use of environmental controls including respiratory isolation of known/suspect TB cases and personal respiratory protection by HCW's when attending infectious patients; (*iii*) periodic PPD skin testing of HCW's for new infections; (*iv*) administration of prophylactic antibiotic therapy to newly infected HCW's. These components are interventions in a potential time series of events whereby HCW's can be infected by TB patients and subsequently develop disease. Given limited resources, a risk manager should know which intervention or set of interventions is most important in reducing the risk of TB disease among HCW's. A component reliability analysis was performed to quantify the relative impact of the different intervention measures

In the absence of any infection control program, the average risk of TB disease among HCW's is equal to $\lambda_I \cdot \lambda_D$, where λ_I is the average infection risk posed by TB patients who are all unrecognized, and λ_D is the subsequent risk of developing TB disease if the infection is not detected and prophylactically treated. Given that an infection control program is in place, however, Figure 5 depicts six series of events that can result in TB disease among HCW's.

An infectious TB patient who presents may or may not be identified as having the disease. Let p_1 denote the probability that TB disease is rapidly detected, so $1 - p_1$ is the probability that disease is not rapidly detected. Because λ_I is the infection risk posed by unrecognized TB patients, let $\alpha \cdot \lambda_I$ (where $0 \le \alpha \le 1$) denote the infection risk posed by recognized TB patients. In general, α is less than one because patients with recognized TB receive antibiotic therapy which decreases the *M. tb* concentration in respiratory aerosols and decreases cough frequency; in turn, both these outcomes decrease infectivity. The left-hand side of Figure 5 depicts three alternative series of events that may occur when disease is detected in TB patients, while the right-hand side depicts three alternative series when TB disease goes unrecognized.

First consider the three left-hand side event series (labeled I, II and III). Because disease is recognized, environmental controls are implemented. The usual controls are placing the patient in a negative-pressure isolation room (for protection of staff outside the room) and use of disposable particulate filter respirators while directly attending the patient. Let p_2 denote the overall efficiency of the combination of control measures in reducing exposure intensity; in the alternative, p_2 may be defined as the probability that the control measures eliminate exposure and risk. Therefore, $1 - p_2$ is the probability that infection risk is not reduced.

Although an infection surveillance program is assumed to be present, the program will be imperfect in that not all employees scheduled for testing actually undergo testing, and some newly infected employees who undergo testing have false negative test results. Therefore, let p_3 denote the probability that newly infected employees successfully undergo skin testing

such that their infections are identified, in which case $1 - p_3$ is the probability that newly infected employees are not identified. Note that the left-hand series in Figure 1 bifurcates at the screening step in a corresponding manner.

Next, consider those new infections that are identified. Let p_4 denote the probability that infected employees undergo and complete antibiotic prophylaxis; $1 - p_4$ is the probability that they do not. In correspondence, the series involving successful screening branches at the prophylaxis step. Let p_5 denote the probability that completing prophylaxis eliminates disease risk, in which case $1 - p_5$ is the probability that completing prophylaxis does not eliminate disease risk. For the event series involving successful skin testing followed by prophylaxis (Series III, Figure 5), TB disease risk equals: $\alpha \cdot \lambda_1 \cdot p_1(1 - p_2)p_3 \cdot p_4(1 - p_5)\lambda_D$. For the event series involving successful skin testing not followed by prophylaxis (Series II, Figure 5), TB disease risk equals: $\alpha \cdot \lambda_1 \cdot p_1(1 - p_2)p_3(1 - p_4)\lambda_D$. For the event series not involving successful skin testing or prophylaxis (Series I, Figure 5), TB disease risk equals: $\alpha \cdot \lambda_1 \cdot p_1(1 - p_2)(1 - p_3)\lambda_D$.

The three right-hand side event series (IV, V, and VI) in Figure 5 are the same as the respective series I, II and III, with the exceptions that the environmental controls step is absent because the TB cases are not detected, and that the infection risk posed by untreated TB patients is λ_1. For event series IV, V and VI, the TB disease risks are, respectively: $\lambda_1 \cdot (1 - p_1)(1 - p_3)\lambda_D$; $\lambda_1 \cdot (1 - p_1)p_3(1 - p_4)\lambda_D$; and $\lambda_1 \cdot (1 - p_1)p_3 \cdot p_4(1 - p_5)\lambda_D$.

The total risk of TB disease, denoted R_D, is the sum of the disease risks for the six event series in Figure 5:

$$(1) \quad R_D = \lambda_1 \cdot \lambda_D(1 - p_1)(1 - p_3 \cdot p_4 \cdot p_5) + \alpha \cdot \lambda_1 \cdot \lambda_D \cdot p_1(1 - p_2)(1 - p_3 \cdot p_4 \cdot p_5)$$

The exact value of R_D depends on knowing the values of all the input parameters which may be difficult to specify. At the same time, Equation (1) is useful in assessing the relative importance of the different intervention parameters over a range of parameter values.

Assessing Relative Impact: A simple way to assess relative impact is to pose sets of values for the intervention parameters and graph the reduction in R_D while increasing the value of each parameter one at a time. Consider the following hypothetical scenario which might be considered a "typical" scenario: $p_1 = 0.95$, $p_2 = 0.8$, $p_3 = 0.7$, $p_4 = 0.8$, $p_5 = 0.93$, and $\alpha = 0.1$. The value of p_5 is based on the observed five-year reduction in TB disease incidence among individuals completing 52 weeks of treatment with isoniazid (INH).[12] The value of α is based on the efficacy of antibiotic therapy in rapidly reducing the sputum *M. tb* concentration and reducing cough frequency[13], and the assumption that 5% of cases are difficult to treat such that a rapid decrease in *M. tb* emissions is not achieved.

The initial value of R_D is $.032\ \lambda_I \cdot \lambda_D$. Figure 6 shows the decrease in R_D with increases in p_1 through p_4 made one at a time. Decreasing p_1 affords the greatest rate of decrease in R_D, yet the final values of R_D differ by less than a factor of 2.5, as indicated at $p_i = 1$. The overall meaning of Figure 6 is the following. In a "typical" scenario, the greatest reduction in disease risk will be achieved by increasing the probability of rapid detection of TB disease, but improving the reliability of other interventions may achieve a comparable decrease.

In Figure 6, the values of p_1 through p_4 were allowed to increase to one. However, there are likely upper limits less than one for these parameters. In the absence of relevant, published survey data from a large sample of hospitals, the following values are offered as upper bounds: $p_1 \approx 0.99$, $p_2 \approx 0.99$, $p_3 \approx 0.9$, and $p_4 \approx 0.8$. The p_1 value recognizes that some TB patients will present with symptoms that are not consistent with pulmonary TB, in which case the necessary diagnostic tests will not be quickly ordered. The p_2 value assumes simultaneous use of two or more high-level controls such as a large amount of dilution ventilation (e.g., 12 air changes per hour) and high efficiency respiratory protection. The p_3 value accounts for the lack of compliance on the part of some staff in undergoing testing, and for the false negative error inherent in tuberculin skin testing. The p_4 value recognizes that some individuals will decline undergoing antiobiotic prophylaxis, and that other individuals will initiate prophylaxis but discontinue it due to adverse side effects such as hepatitis.

A Conditional Scenario for Identified TB Disease: To this point, the relative impact of different interventions has been considered across all the steps shown in Figure 5. Because the probability of rapid detection of TB disease is already high in many hospitals, HCW's most frequently encounter the scenario in which TB disease has already been identified. Given that $p_1 = 1.0$, the conditional risk of disease, denoted $R_{D|P_1=1}$, is obtained by simplifying Equation (1) to yield:

$$R_{D|P_1=1} = \alpha \cdot \lambda_I \cdot \lambda_D (1 - p_2)(1 - p_3 \cdot p_4 \cdot p_5) \quad (2)$$

Now consider a "worst-case" scenario for which: $p_2 = 0.5$, $p_3 = 0.2$, $p_4 = 0.2$, $p_5 = 0.93$, and $\alpha = 0.1$. The values of p_5 and α are the same as in the "typical" scenario because they are cinically demonstrated outocmes and/or independent of the TB control program. The initial value of $R_{D|P_1=1}$ in this scenario is $.048\ \lambda_I \cdot \lambda_D$. Figure 7 shows the decrease in R_D with increases in p_2, p_3 and p_4 made one at a time. Increasing p_2 affords the greatest rate of decrease in $R_{D|P_1=1}$, and in theory decreases $R_{D|P_1=1}$ to zero if $p_2 = 1$. Increasing either p_3 or p_4 decreases $R_{D|P_1=1}$ at a much less rapid rate, and increasing either p_3 or p_4 to one can decrease $R_{D|P_1=1}$ to only $.041\ \lambda_I \cdot \lambda_D$. The overall meaning of Figure 7 is the following. Once TB disease has been identified, the greatest reduction in disease risk will be achieved by increasing the the reliability (efficiency) of environmental controls.

V. An Analytical Risk Model for Determing the Cost Efficacy of Alternative Screening Intervals

As previously described in Section 6. IV., the stochastic simulation model can be used to examine the efficacy of alternative PPD skin testing intervals in reducing TB disease among HCW's. In the period that the simulation model was developed (1996 and 1997), the computing time necessary to run 500 simulations of just one scenario was over 20 hours. To facilitate the cost efficacy analysis of alternative screening intervals, an analytical risk model was developed that used constant rates of *M. tb* infection and TB disease development as inputs, and yielded expected disease incidence outcomes. Once the equations were developed, obtaining the results for a given scenario required less than 10 seconds of computing time. Further, the analytical equations could more readily be used by risk managers, because the equations were not specific to a programming langage or software package. All the simulation model routines were written in MATLAB® code.

The analytical risk model involves the following assumptions: (*i*) in a given interval between screenings, the time to infection is an exponential variable with rate constant λ_1 per month; (*ii*) in the absence of antibiotic prophylaxis, for the first year following infection the time to develop disease is an exponential variable with rate constant $\lambda_2 = 4.274 \times 10^{-3}$ per month, which produces a .05 risk of developing disease in the first year of infection; (*iii*) in the absence of antibiotic prophylaxis, for all years subsequent to the first year of infection the time to develop disease is an exponential variable with rate constant $\lambda_3 = 9.195 \times 10^{-5}$ per month, which produces a .05236 risk of developing disease in the 49-year period subsequent to the first year. The rate constants λ_2 and λ_3 are paired such that in the first 50 years subsequent to infection there is a 0.10 risk of developing disease given that no antibiotic prophylactic therapy is received.

Let n denote the PPD skin testing interval in months. Let $D(n)$ denote the risk of both infection *and* disease occurring in the n-month interval between screenings. If $n \leq 12$ months, $D(n)$ is given by the following integral:

$$D(n) = \int_0^n \frac{\lambda_1 \cdot \lambda_2}{\lambda_1 - \lambda_2} \left[\exp(-\lambda_2 \cdot t) - \exp(-\lambda_1 \cdot t)\right] \cdot dt \qquad (3)$$

where λ_1 and λ_2 are the same parameters previously defined. The integrand in Equation (3) is the expression for the sum of two independent exponential increments of time, in this case the time to infection and the subsequent time to disease. For example, if there is a 10% annual risk of infection such that $\lambda_1 = .00878$/month, the probability that disease occurs by the end of one year is .00256 in the absence of screening. If $n > 12$ months, a stepwise computation procedure is required, because the rate constant for disease development decreases from λ_2 to λ_3 following the first year of infection.

Let m denote the total number of exposure months being considered. The term D(m) denotes the cumulative risk of disease over m months for initially susceptible individuals given that no infection screening program is in place, in which case new infections go undetected and untreated. Let $n < m$, such that the quotient m/n is an integer. Let p denote the proportion of all susceptible employees who comply with skin testing, whose skin tests would not be subject to false negative error, and who would undergo successful antibiotic prophylaxis if infected. The fraction q equals $1 - p$. The expected cumulative risk of TB disease over m months, denoted β^*, is given by the following equation:

$$\beta^* = p \cdot D(n) \cdot \left[\sum_{i=0}^{m/n - 1} \exp(-\lambda_1 \cdot n \cdot i) \right] + q \cdot D(m) \tag{4}$$

The index i on the bracketed sum tracks the number of screenings that occur up to m months. For this analysis, m was set equal to 144 months (12 years) so that the n-month screening intervals considered (3, 6, 9, 12, 24,36 months) would cause m/n to be an integer value.

The total cost of a screening program involves the cost of placing, reading, and recording the PPD skin tests, and the cost of the "residual" TB disease cases that may arise in between the screenings. Let x (dollars) denote the average cost of a PPD skin test. Let y (dollars) denote the average cost of a TB disease case in an HCW. Let N denote the initial number of susceptible employees. Let q_1 denote the fraction of employees whose skin tests would always be false negative if infected. Let q_2 denote the fraction of employees who are always noncompliant. Let q_3 denote the fraction of employees who would not undergo successful prophylaxis if infected. Let q denote the fraction of employees who belong to either of fractions q_1, q_2 or q_3, in which case: $q = q_1 + q_2 + q_3 - q_1 \cdot q_2 - q_1 \cdot q_3 - q_2 \cdot q_3 + q_1 \cdot q_2 \cdot q_3$, where $p = 1 - q$. The expression for q assumes that memberships in the respective fractions q_1, q_2 and q_3 are mutually independent events.

The expected total cost of screening and residual disease at $m = 144$ months given an n-month screening interval is:

$$\text{Total Cost} = \left[1 - q_1(1 - q_2) - q_2\right] \cdot N \cdot x \cdot \left[\sum_{i=0}^{144/n - 1} \exp(-\lambda_1 \cdot n \cdot i) \right] + q_1(1 - q_2) \cdot N \cdot x \cdot \left(\frac{144}{n}\right) + N \cdot y \cdot \beta^* \tag{5}$$

where β^* is the cumulative disease risk defined by Equation (4) which explicitly incorporates the fraction q. The first term on the right-hand side of the equation should properly include those individuals in fraction q who undergo testing but produce false negative results; it assumed for simplicity that these individuals constitute a fraction that is minor compared to p. Also note that the cost of false positive errors in skin testing is not included, because nearly all false positives would occur in the initial baseline testing which is not considered part of the ongoing screening program.

To compute the cost of preventing a disease case over 144 months, the total cost (screening plus residual disease) is divided by the expected number of disease cases prevented. The latter number is the expected number of disease cases in the absence of screening *minus* the expected number of residual disease cases with a screening program in place. Therefore:

$$(6)\quad \text{Cost per Disease Case Prevented} = \frac{\text{Total Cost}}{\#\text{Cases}|\text{No Screening} - \#\text{Cases}|\text{Screening}}$$

The cost per disease case prevented measures the cost efficiency of the screening program. If cost efficiency were the only consideration, one would choose the screening interval that minimizes the cost per disease case prevented. In practice, the risk manager must also consider the residual risk (i.e., the expected number of residual disease cases per 1000 workers) and the target (benchmark) risk level, where the latter quantity is the *de facto* acceptable cumulative disease risk. Therefore, if a 12-month screening interval is the most cost efficient in a given scenario, a shorter interval might still be chosen if the residual disease risk is greater than the target risk level, and if the total cost of using a shorter interval is not too high. For the purpose of this analysis (performed in 1997), the acceptable 12-year cumulative disease risk (the *target risk level*) is taken as 1 per 1000, which corresponds to the general U.S. population value for 1996. In 1996, the reported TB disease rate was 8.7 per 10^5. If this rate is interpreted as an annual disease risk, the 12-year cumulative disease risk is: $1-(1-.000087)^{12} = .001$.

Results for a Perfect Screening Program: For $p = 1$, Table 8 lists the total cost (TC) and the cost per disease case prevented (C/DCP) at 12 years for alternative screening intervals of 3, 6, 9, 12, 18, 24, and 36 months, and for λ_1 values corresponding to an annual rate of infction (*ari*) of, respectively, 0.2%, 0.5%, 1.0% and 5.0%. It is assumed that x = \$10 per PPD test, that y = \$10,000 per disease case and that N = 1000 initially susceptible workers. Cost estimates for x and y were provided by R.J. Harrison, MD, MPH, California Department of Health Services, but will likely vary across facilities. For comparison, the bottom row of Table 8 labeled 144 months shows the total cost without screening, which is entirely due to disease cases. No entry is shown for the cost per disease case prevented because no cases are prevented absent screening.

Table 8 shows that over the *ari* range of 0.2% to 5.0%, the total cost tends to increase as the screening interval decreases from 36 months to 3 months, but that the cost per disease case prevented has a minimum value at a screening interval of 12 months or less. Figure 8 presents the same data for the 0.5% *ari* scenario. Curve #1 shows the total cost and curve #2 shows the cost per disease case prevented at the different screening intervals. In addition, curve #3 shows the expected number of residual disease cases per 1000 workers which for this scenario ranges from 0.37 for the 3-month screening interval to 2.48 for the 36-month interval. Although the 12-month screening interval is the most cost efficient, it permits 1.5 disease cases per 1000 at 12 years, which exceeds the target risk level of 1 per 1000. To meet the latter value, a screening interval less than 9 months would be required. It happens that an 8-month interval yields 0.99 disease cases per 1000 at 12 years.

Results for an Imperfect Screening Program: Due to the slight false negative error of the PPD skin test[14] and the incomplete efficacy of antibiotic prophylaxis, a real-world screening program will not be perfect. The maximum value of p might be 0.88 given 100% compliance with testing. Table 9 shows the total cost and the cost per disease case prevented over 12 years for the same set of parameters used in Table 8, with the change that $p = 0.88$ and $q = 0.12$ (based on $q_1 = .05$, $q_2 = 0$, $q_3 = .07$). Figure 9 presents the Table 9 data for the 0.5% *ari* scenario where curve #1 shows the total cost, curve #2 shows the cost per disease case prevented, and curve #3 shows the expected number of residual disease cases per 1000 workers at the different screening intervals. As seen by comparing Table 8 vs. Table 9, and Figure 8 vs. Figure 9, a small degree of false negative error and failure of prophylaxis does not greatly alter the costs and disease risks associated with a perfect screening program. In this case, a 6-month screening interval (for which there are 1.0 disease cases per 1000 at 12 years) rather than an 8-month screening interval would be required to achieve the target risk level.

VI. A Source-Receptor-Pathway Framework to Evaluate the Efficacy of Alternative Control Measures for Airborne Infection

A source-pathway-receptor construct was applied to airborne infection by *M. tb* particles. This framework integrates the important mechanistic factors that determine the degree of infection risk, and thereby permits comparisons of the cost-efficacy of alternative control strategies. The traditional Wells-Riley model for *M. tb* infection risk in indoor environments incorporates a steady-state *M. tb* aerosol concentration equal to the quotient of the total *M. tb* emission rate (# per hr) and the room dilution supply rate Q_V (m^3/hr). In turn, the total emission rate is the product of the number of infectors I, and the average emission rate per infector E (# infectious particles per hr). The inhaled concentration C_{INH} (# infectious particles per m^3) for a susceptible HCW in this environment equals $I \cdot E / Q_V$. For relatively low values of C_{INH} and for limited exposure duration t (hr), an individual HCW's infection risk is approximately equal to the expected dose μ_D (# infectious particles) defined as follows:

$$\mu_D = C_{INH} \cdot b \cdot t \cdot f$$

where *b* is the HCW's breathing rate (m^3/hr), and *f* is the probability of inhaled particle deposition in the alveolar region, the target site of infection.

Controls that act at the source (the TB patient) and at the receptor (the HCW) have the algebraic effect of fractionally reducing C_{INH}, while controls that act on the pathway by removing *M. tb* from air effectively add to the value of Q_V. The primary source control is having the TB patient wear a surgical mask. Let η_E denote a surgical mask's efficiency (0 – 1) in removing expelled infectious particles. Pathway controls include dilution ventilation, in-room air filtration, and upper room air ultraviolet germicidal irradiation (UVGI). Let Q_R denote the airflow rate through a recirculating in-room filter (m^3/hr), and let η_R denote the filter's efficiency (0 – 1) in removing infectious particles. Let λ_{UVGI} denote the first-order *M. tb* inactivation rate constant due to UV irradiation (hr^{-1}), and let V denote the room volume (m^3). The primary receptor control is the use of respiratory protection. Let η_S denote a respirator's efficiency (0 – 1) in removing infectious particles from inhaled air. For simplicity, consider that I = 1 for a given room air space, which is the usual circumstance in hospitals. For initial simplicity, consider that room air is well mixed. If C_{INH} is the outcome variable of interest, the source-pathway-receptor framework becomes:

$$C_{INH} = \left(\frac{E \cdot (1 - \eta_E)}{Q_V + Q_R \cdot \eta_R + \lambda_{UVGI} \cdot V} \right) \cdot (1 - \eta_S) \quad (7)$$

The first parenthetical term is the *M. tb* concentration in room air, and the second term is the overall fractional penetration through the HCW's respirator. As will be discussed subsequently in Section 6. VII – IX, room air is usually not well-mixed, in which case exposure intensity near an emission source is greater than at a distance from the source. A modified version of Equation (7) that accounts for a near-field effect is as follows:

$$(8) \qquad C_{INH,NF} = \left(\frac{E \cdot (1 - \eta_E)}{Q_V + Q_R \cdot \eta_R + \lambda_{UVGI} \cdot V} + \frac{E \cdot (1 - \eta_E)}{\beta} \right) \cdot (1 - \eta_S)$$

where β is the air flow rate (m^3/hr) between the near-field zone and the remainder of the room. In a strict sense, Equation (8) somewhat overstates the efficacy of upper-room air UVGI, because it does not restrict the germicidal effect of UV irradiation to only the upper portion of the room. Details of a more appropriate three-zone model for upper-room air UVGI are provided in Section 6.VII.

A different sort of two-zone model was applied to the circumstance in which a TB patient is placed in a respiratory isolaton room that experiences leakage of air into the adjoining hospital ward. A small degree of outward air leakage is expected just from opening the isolation room door to enter and exit the room. Let L denote the fraction (0 – 1) of the patient room ventilation rate that leaks outward into the adjoining ward. In this construct, the patient room and the adjoining ward both have defined volumes and mechanical ventilation rates, and both spaces might be equipped with upper-room air UVGI and recirculating air filters. In the two-zone model equation below, the subscript "P" denotes measures applied to the patient room, and the subscript "W" denotes measures applied to the general ward environment. Although it is unlikely that susceptible HCW's in the general ward environ-ment would wear respirators, or that the isolated TB patient would wear a surgical mask, these latter measures terms are included for the sake of completeness. For simplicity, it is assumed that the ward houses only one TB patient, although multiple TB patients on a ward can be accommodated with this approach. The inhalation concentration in the general ward environment, $C_{INH,W}$, is given by:

$$(9) \quad C_{INH,W} =$$

$$\left(Q_{V,P} \cdot L \cdot \frac{E \cdot (1 - \eta_E)}{Q_{V,P} + Q_{R,P} \cdot \eta_{R,P} + \lambda_{UVGI,P} \cdot V_P} \right) \cdot \left(\frac{1}{Q_{V,W} + Q_{R,W} \cdot \eta_{R,W} + \lambda_{UVGI,W} \cdot V_W} \right) \cdot (1 - \eta_S)$$

The first parenthetical term is the number of viable *M. tb* particles per hour that escape from the TB patient room into the general ward environment. The denominator in the second parenthetical term is the effective ventilation rate (m^3/hr) in the general ward environment. The product of these two terms is the *M. tb* concentration in the general ward environment. room air, and the second term is the overall fractional penetration through the HCW's respirator. The third term is the overall fractional penetration through the HCW's respirator.

Equation (9) was used to assess the importance of rapid identification and isolation of TB patients by applying it to three scenarios. In the base case, the infectious TB patient is undiagnosed and is admitted to the general ward. The *M. tb* particle emission rate is $E = 0.25\ hr^{-1}$. No recirculating air filters or UVGI are present ($Q_{R,W} = 0$, $\lambda_{UVGI,W} = 0$). The ward volume is 250 m^3, and $Q_{R,W} = 470\ m^3$/hr such that there are 1.9 ACH. The patient

does not wear a surgical mask and HCW's do not wear respirators ($\eta_E = 0$, $\eta_S = 0$). For this base case, remove the first parenthetical term from Equation (9), but insert $E \cdot (1 - \eta_E)$ in the denominator of the second parenthetical term. In Figure 10, the curve labeled "base case (undiagnosed)" shows a cohort cumulative infection risk parameter D as a function of the length of patient stay, where D is a function of $C_{INH,W}$. For the Figure 10 scenario:

$$D = 10 \cdot C_{INH,W} \cdot t$$

where it is assumed that ten (10) HCW's are exposed, that each breathes at rate 1 m^3/hr, and that all inhaled *M. tb* particles deposit in the pulmonary region.

In the second case, the TB patient remains undaignosed but enhanced mechanical ventilation, in-room air filtration, or upper-room air UVGI increase the effective ventilationrate from 470 m^3/hr to 1500 m^3/hr, or 6 ACH. In Figure 10, the curve labeled "enhanced removal (undiagnosed)" shows the cohort cumulative infection risk parameter D as a function of the length of patient stay. The value of D is is reduced to approximately 30% of the base case value.

In the third case, the patient is unisolated for 2 hours and is then placed in respiratory isolation and begins chemotherapy. It is assumed that E linearly decreases to zero over a 48-hr period, that L = .05 (5% leakage), that $Q_{V,P} = 300$ m^3, and that $Q_{R,P}$ and $\lambda_{UVGI,P}$ are zero. In Figure 10, the curve labeled "chemotherapy + isolation" shows the cohort cumulative infection risk parameter D as a function of the length of patient stay. The value of D is reduced to approximately 2% of the base case value. More than half the risk accumulates during the first two hours in the hospital, which again indicates the importance of rapid isolation.

Equation (7) was used to assess the efficacy of different types of respirators versus increasing the effective air cleaning rate for a bronchoscopy scenario described by Catanzaro in which the estimated *M. tb* particle emission rate was E = 249 hr^{-1}.[15] The different respirator devices considered were: (1) a surgical mask (which is not properly a respirator); (2) a disposable dust/mist respirator (akin to the current filtering facepiece Type N95 respirator); (3) an elastomeric halfmask respirator with high efficiency filters (akin to the Type N100 filter); and (4) a powered air-purifying respirator with high efficiency filters. Based on published data, estimated efficiency (η_S) values for these four devices were, respectively, 0.58, 0.94, 0.98 and 0.996.[16] Figure 11 shows the reduction in the cohort infection risk parameter D given a 2.5-hr exposure period in the bronchoscopy suite over a range of air cleaning rates (effective ventilation rates) in ACH. For the Figure 11 scenario:

$$D = 13 \cdot C_{INH} \cdot 2.5$$

where it is assumed that 13 HCW's are exposed, that each breathes at rate 1 m^3/hr, and that all inhaled *M. tb* particles deposit in the pulmonary region. Wearing personal respiratory protection during this high-risk procedure is predicted to be far more effective than increasing the effective ventilation rate.

VII. A Multi-Zone Model Evaluation of the Efficacy of Upper-Room Air Ultraviolet Germicidal Irradiation

For existing TB patient isolation rooms, the 1994 CDC guidelines recommended a ventilation rate of at least six air changes per hour (ACH). For newly constructed isolation rooms, at least 12 ACH were recommended. Many isolation rooms currently receive less than 6 ACH,[17] and renovating facilities to achieve rates of 6 – 12 ACH can be expensive. The cost issue leads to an interest in means other than mecanical ventilation to remove viable *M. tb* from room air. One method is the use of upper-room air ultraviolet germicidal irradiation (UVGI).

For upper-room air irradiation, UV lamps are suspended from the ceiling or attached to the walls; the bottom of the lamp is usually shielded to direct radiation in the horizontal and upward directions. The objective of this configuration is to inactivate *M. tb* in the upper part of the room while minimizing radiation exposure to persons in the lower part of the room. If the room is relatively well-mixed, inactivation of *M. tb* in the upper zone effectively reduces the viable *M. tb* concentration in the lower zone.

Probably the best study of upper-room air UVGI was conducted in 1971 by Richard Riley and colleagues.[18] Viable *M. bovis* BCG aerosol was released in a test room, and a presumably uniform room concentration was attained by using a mixing fan. Once aerosol release ceased, the concentration decay of viable *M. bovis* was measured, with and without upper-room air UVGI, at a sampling point 0.8 m off the floor near the center of the room. As described, the total room volume was 64 m^3, with floor dimensions of 18.4 m^2 and a ceiling height of 3.5 m. On the first test day, one 17-watt (W) lamp was operated with the UV tubes facing the ceiling and baffled to prevent radiation below the edges of the lamp fixture. In this configuration, the irradiated upper room zone nominally extended down 0.61 m from the ceiling, so the theoretical upper zone volume V_U was 11.2 m^3. On the second and third test days, a 29-W lamp was operated in addition to the 17-W lamp. This 29-W lamp was operated with the UV tubes facing the floor and baffled to control the downward inclination of radiation. For the second and third test days, the irradiated upper zone nominally extended down approximately 1.65 m (5 ft 5 in) from the ceiling; the theoretical upper zone volume V_U was 30.4 m^3. No mechanical ventilation was operating in the room during the experiments, and the door to the room was sealed. However, air infiltration and exfiltration was possible through one (or more) windows which were presumably located in the room's lower zone. A room diagram was not provided, and measurements of air flows, air speeds, air temperature, humidity, and UV radiation intensity were not made.

Table 10 summarizes the data reported for the three test days. The slopes of the observed semi-log concentration decay curves were given in terms of equivalent room air changes per hour (Eq ACH). Consider the first test day. The reported slopes were 2 Eq ACH with UV lights off, and 12 Eq ACH with one 17-W UV light on. Based on this difference, Riley et al. inferred that UVGI with one 17-W fixture added 10 Eq ACH. Given a perfectly mixed room volume of 64 m^3, 12 Eq ACH represents an effective ventilation rate Q_E = 12.8 m^3/min.

Given that bacilli are emitted from a source at constant rate G, the steady-state concentration at all points in a well-mixed room, $C_{WM,SS}$, would equal G/12.8.

Interpreting the slope of a semi-logarithmic concentration decay curve in terms of Eq ACH implicitly assumes that the spatial profile of the contaminant concentration across the room adheres to a well-mixed room construct. However, previous work has shown that different positions in a room can receive different effective ventilation rates leading to substantial differences in contaminant concentrations, yet the slopes of the semi-logarithmic concentration decay curves at these positions can be similar.[19] Therefore, a three-zone model was formulated to describe air movement in the test room, and reasonable model parameters were found that reproduced the reported decay slopes in Table 10. Based on the three-zone model parameters, the predicted steady-state concentrations near the emission source were found to be 2.4- to 5.8-fold higher than those predicted using the Eq ACH reported by Riley and colleagues. Near-field exposure intensity is especially relevant because HCW's are usually in close proximity to the TB patients they attend. Therefore, the published *M. bovis* decay data could easily have been misinterpreted to overestimate UVGI efficacy.

The Three Zone Model: Consider a hemispherical near-field zone 1 m in radius around the *M. bovis* aerosol generator; the latter was likely placed on a table or the room floor (Figure 12). The hemisphere geometry also represents the potential near-field zone around a TB patient lying on a bed, and 1 m approximates the distance between a HCW and the patient. The near-field zone volume V_{NF} is 2.1 m^3 (i.e, $\frac{2}{3}\pi r^3$), in which case the remaining lower zone volume V_L is 50.7 m^3 for the first test day, and 31.5 m^3 for the second and third test days.

To assign interzonal air exchange values, assume that the average random air speed in the test room was 3 m/min, which represents relatively still air. In a multi-zone model, it is assumed that air moves into a given zone through half the inter-zonal surface area, and moves out of the zone through the other half. Therefore: β_1 = 9.2 m^2 x 3 m/min = 28 m^3/min, and β_2 = 3.1 m^2 x 3 m/min = 9.6 m^3 /min (340 cfm). In the β_2 calculation, it is assumed that the base of the hemisphere lies on a physical surface (a table, floor or bed), in which case its surface area is not available for air flow. Therefore, β_2 is the product of the average air speed and half the surface area of a hemisphere (πr^2). For the assumed upper and near-field zone volumes, the magnitudes of β_1 and β_2 are substantial with respect to the number of air exchanges per unit time. That is, β_1 / V_U ranges from 0.94 min^{-1} (second and third test days) to 2.5 min^{-1} (first test day), and β_2 / V_{NF} is 4.6 min^{-1}.

The three-zone model is based on a material balance applied to the number of viable *M. bovis* in each zone of the room. The following set of differential equations describes the rate of change of the viable *M. bovis* concentration with time in the respective upper, lower, and near-field zones, with ongoing emission at constant rate G into the near-field zone:

$$(10) \qquad \frac{dC_U}{dt} = \frac{\beta_1}{V_U} \cdot C_L(t) - \frac{\left[(k_1 + k_2) \cdot V_U + \beta_1\right]}{V_U} \cdot C_U(t)$$

$$(11) \qquad \frac{dC_L}{dt} = \frac{\beta_2}{V_L} \cdot C_{NF}(t) + \frac{\beta_1}{V_L} \cdot C_U(t) - \frac{(k_1 \cdot V_L + \beta_1 + \beta_2 + Q)}{V_L} \cdot C_L(t)$$

$$(12) \qquad \frac{dC_{NF}}{dt} = \frac{G}{V_{NF}} + \frac{\beta_2}{V_{NF}} \cdot C_L(t) - \frac{(k_1 \cdot V_{NF} + \beta_2)}{V_{NF}} C_{NF}(t)$$

In these equations, k_1 is the rate constant for the natural die-off of *M. bovis* in air and k_2 is the rate constant for the UV-induced inactivation of *M. bovis*. Based on data for *M. tb* summarized by Hopewell,[13] it is estimated that $k_1 = .00235\ min^{-1}$. The analytical solutions to these equations are given in the publication describing this analysis,[20] which is also appended to this report.

Based on the three-zone model with the previously posited parameter values for the first test day ($V_U = 11.2\ m^3$, $V_L = 50.7\ m^3$, $V_{NF} = 2.1\ m^3$, $\beta_1 = 28\ m^3$ /min, $\beta_2 = 9.6\ m^3$ /min, $k_1 = .00235\ min^{-1}$), and with $Q = 2\ m^3$/min (which produces an observed slope of 2 Eq ACH with UV lights off), an observed slope of 12 Eq ACH with UV lights on requires that $k_2 = 1.28\ min^{-1}$. Table 1 lists the k_2 values for the three test days required to reproduce the reported Eq ACH values with UV lights on. The value of k_2 was computed using an iterative procedure.

For the posited room conditions pertaining on the first test day with $k_2 = 1.28\ min^{-1}$ (which produces the observed slope of 12 Eq ACH), the three-zone model predicts the near-field steady-state concentration to be G/5.3, which is 2.4-fold greater than the estimate $C_{WM,SS}$ = G/12.8 for the same test day based on the well-mixed room assump-tion. That is, if a room is not well mixed, $C_{WM,SS}$ underestimates the steady-state bacilli concentration near the source. For the three test days under analysis, the ratio $C_{NF,SS}/C_{WM,SS}$ ranges from 2.4–5.8. Again, the three-zone model predicts higher concentrations near the source than would be predicted using the Riley et al. decay curve slopes and the well-mixed room assumption. Limited air flow between zones also signifies that the steady-state bacilli concentrations will differ by room location. For example, again consider the first test day. Given the previously posited parameter values with UV lights on, the three-zone model predicts that: $C_{NF,SS}$ = G/5.3, $C_{L,SS}$ = G/11.6, and $C_{U,SS}$ = G/17.6. This 3.3-fold range in concentrations reflects a room that is, of course, not well-mixed.

The following question arises: Shouldn't the lower effective ventilation rate in the near-field zone be reflected in the slope of the semi-log decay curve at this same position? For exam-

ple, on the first test day, shouldn't the observed slope in the near-field zone be considerably less than 12 Eq ACH? The answer is, not necessarily.

Consider the set of three-zone model decay equations corresponding to the first test day with UV lights on, but starting from an initial uniform room concentration of 100 per m^3 (this concentration is a convenient value that does not correspond to the actual *M. bovis* concentrations). For the parameter values discussed above, Figure 13 shows the predicted semi-log decay curves in the three zones. Although the initial portions of these curves are nonlinear, they are transient and easy to miss. After a short time, all three curves appear as straight lines with the same slope. The value of this slope corresponds to the least negative of the three eigenvalues (λ_1, λ_2, λ_3) for the system of decay equations for the three-zone model. If by convention, $|\lambda_1| < |\lambda_2| < |\lambda_3|$, then for the three zone-model parameter values posited for test day one, $\lambda_1 = -0.20\ \text{min}^{-1}$, $\lambda_2 = -4.06\ \text{min}^{-1}$, and $\lambda_3 = -4.87\ \text{min}^{-1}$. The actual decay equations are as follows:

$$C_U(t) = 72.5 \cdot e^{-0.20 \cdot t} + 24.9 \cdot e^{-4.06 \cdot t} + 2.6 \cdot e^{-4.87 \cdot t}$$

$$C_L(t) = 103.9 \cdot e^{-0.20 \cdot t} - 2.8 \cdot e^{-4.06 \cdot t} - 1.1 \cdot e^{-4.87 \cdot t}$$

$$C_{NF}(t) = 108.6 \cdot e^{-0.20 \cdot t} - 25.2 \cdot e^{-4.06 \cdot t} + 16.6 \cdot e^{-4.87 \cdot t}$$

In the above equations, the exponential terms involving λ_2 and λ_3 effectively disappear after two minutes, in which case all three trajectories appear as simple exponential decays governed by the dominant rate constant, $\lambda_1 = -0.20\ \text{min}^{-1}$ (= 12 Eq ACH).

VIII. A Two-Zone Markov Model of a TB Patient Isolation Room

Deterministic equations such as formulated for the three-zone model in Section 6.VII. are useful in describing expected concentrations for specified parameter values. However, where small numbers of airborne particles are present, as is usually the case for *M. tb* aerosols, deterministic equations are unrealistic for two reasons – they assume a continuity in the concentration value which in reality can fluctuate abruptly, and they do not describe the substantial variability in concentration that may pertain. Therefore, an explicitly probabilistic three-state Markov model was developed to describe *M. tb* particle concentrations in a TB patient isolation room. The three states were the near-field zone surrounding a TB patient (state 2), the remainder of the room (state 1), and being exhausted from the room such that the particle could not return (state 0).

Figure 14 depicts a hypothetical room. A near-field zone with volume V_N contains the emission source, and the remainder of the room constitutes a far-field zone with volume V_F. Supply air enters, and exhaust air exits, the far-field zone at rate Q (m^3/sec). Air is exchanged between the near- and far-field zones at rate β (m^3/sec), which is the product of the room random air speed and the free surface area of the near- and far-field interface, divided by two. Contaminant particles are emitted directly into the near-field zone. An upper room zone is not included to keep the model simple; further, upper-room air UVGI is not commonly used in TB patient isolation rooms.

The transition probability matrix **P** for this system is:

$$\mathbf{P} = \begin{array}{c} \\ 0 \\ 1 \\ 2 \end{array} \begin{array}{c} \begin{array}{ccc} 0 & 1 & 2 \end{array} \\ \begin{bmatrix} 1 & 0 & 0 \\ \left(1-e^{-((Q+\beta)/V_F)}\right)\dfrac{Q}{Q+\beta} & e^{-((Q+\beta)/V_F)} & \left(1-e^{-((Q+\beta)/V_F)}\right)\dfrac{\beta}{Q+\beta} \\ 0 & 1-e^{-(\beta/V_N)} & e^{-(\beta/V_N)} \end{bmatrix} \end{array} \tag{13}$$

State 0 (exhausted from the room) is an absorbing state such that $P_{00} = 1$. A particle in state 1 (the far-field zone) can move to state 0 with exponential rate parameter Q/V_F, or to state 2 (the near-field zone) with exponential rate parameter β/V_F. Therefore, a particle leaves state 1 with an overall exponential rate parameter $(Q+\beta)/V_F$. The probability that it remains in state 1 over one time step is $P_{11} = e^{-(Q+\beta)/V_F}$. The probability that it leaves state 1 is the complement $1-e^{-(Q+\beta)/V_F}$. Given that the particle leaves state 1, the probability that it moves to state 0 is $Q/(Q+\beta)$, and the probability that it moves to state 2 is $\beta/(Q+\beta)$. Therefore, $P_{10} = \left(1-e^{-(Q+\beta)/V_F}\right)\left[Q/\left(Q+\beta\right)\right]$, and $P_{12} = \left(1-e^{-(Q+\beta)/V_F}\right)\left[\beta/\left(Q+\beta\right)\right]$.

With regard to a particle in state 2, it cannot enter state 0 in one time step (because it must first move through state 1), so $P_{20} = 0$. However, the particle can enter state 1 with exponential rate parameter β / V_N. Therefore, the probability that it remains in state 2 over one time step is $P_{22} = e^{-\beta / V_N}$, and the probability that it enters state 1 is $P_{21} = 1 - e^{-\beta / V_N}$.

Given that N_0 particles are in the near-field zone and none are in the far-field zone at time zero, and given that no additional particles are released, the expected value and variance of the far-field and near-field particle concentrations at time t are given by the following equations, where j = 1 for the far-field zone and j = 2 for the near-field zone:

(14) $$E\left[C_j(t)\right] = \frac{N_0 \times P_{2j}^t}{V_j}$$

(15) $$Var\left[C_j(t)\right] = \frac{N_0 \times P_{2j}^t \times \left(1 - P_{2j}^t\right)}{V_j^2}$$

For a scenario involving ongoing particle release starting at time zero, assume that at time q in sec (where $q = 0,1,2,\ldots,t$), G_q particles are released into the near-field zone, where the G_q values are deterministic but may vary across the time steps. The expected value and variance of the far-field and near-field particle concentrations at time t are given by the following equations, where j = 1 for the far-field zone and j = 2 for the near-field zone:

(16) $$E\left[C_j(t)\right] = \frac{\sum_{q=0}^{t} G_q \times P_{2j}^{t-q}}{V_j}$$

(17) $$Var\left[C_j(t)\right] = \frac{\sum_{q=0}^{t} G_q \times P_{2j}^{t-q} \times \left(1 - P_{2j}^{t-q}\right)}{V_j^2}$$

To illustrate the model, let the near-field zone be a 1-m radius hemisphere centered on a patient lying on a bed, in which case $V_N = 2.1\ m^3$. Let $V_F = 47.9\ m^3$, such that the total room volume ($V_N + V_F$) is 50 m^3; the latter is a reasonable value for a patient isolation room. Let $Q = .0833\ m^3/sec$, which corresponds to six nominal room air changes per hour and adheres to the 1994 CDC guidelines for existing TB patient isolation rooms. Let $\beta = 0.32\ m^3/sec$, which corresponds to an air speed of 0.1 m/sec; the latter represents relatively still air and corresponds to the median air speed measured in a survey of indoor work-places.[21] Specifying V_N, V_F, Q and β also specifies the P_{ij} values in the Equation (13) matrix P.

Assume that no *M. tb* particles are initially present, but that at time zero, $N_0 = 10$ *M. tb* particles are released by a cough into the near-field zone, with no subsequent release; for simplicity, assume that no particle carries more than one bacillus. Therefore, the near-field *M. tb* particle concentration is 4.8 per m^3 at time zero (N_0/V_N). The solid lines labeled $E[C_2(t)]$ and $E[C_1(t)]$ in Figure 15 depict the expected values of the near-field and far-field *M. tb* concentrations, respectively, over the first 60 secs following the pulse release. There is a rapid decrease in $E[C_2(t)]$ from 4.8 per m^3 to 0.21 per m^3 by t = 40 sec, at which time it is close to $E[C_1(t)] = 0.19$ per m^3. The subsequent decrease in both expected concentrations is relatively gradual. The dotted line immediately above each solid line is the approximate 95th percentile value for the corresponding particle concentration. For example, at t = 25 sec, $E[C_2(t)] = 0.29$ per m^3, and the probability is 98% that $C_2(t) \leq 0.95$ per m^3. The approximate 95th percentile values for $C_2(t)$ and $C_1(t)$ were found by computing the binomial probabilities for the possible particle numbers in each zone based on the values of P_{22}^t and P_{21}^t, respectively, and then finding that particle number in each zone for which the cumulative probability was closest to 95%. For example, at t = 25 sec, $\Pr[N_2(25) \leq 1] = 0.88$, and $\Pr[N_2(25) \leq 2] = 0.98$. The event $N_2(25) \leq 2$ corresponds to $C_2(25) \leq 0.95$ per m^3, in which case 0.95 per m^3 was plotted as the approximate 95th percentile value for the near-field *M. tb* concentration.

The health significance of variability in the near-field concentration is that it increases the variability in the risk of infection, which in turn increases uncertainty in selecting appropriate control measures. To explain this idea, assume that a susceptible HCW is in a TB patient's near-field zone over a T-sec interval. The worker's infection risk is a function of the expected number of *M. tb* particles that are inhaled and deposited in the pulmonary region during this interval, denoted D(T). In turn, D(T) is the product of the average *M. tb* particle concentration over the interval, the air volume inhaled by the worker over the interval, b (m^3), and the inhaled particle deposition fraction in the alveolar region, f_D (0 to 1), which is the target site for infection:

$$D(T) = \frac{b \times f_D}{T} \sum_{t=0}^{T-1} C_2(t)$$

where $C_2(t)$ denotes the near-field *M. tb* particle concentration at time t. The summed concentrations run from t = 0 to t = T – 1, and not to t = T, because the concentration value $C_2(T)$ pertains only after the Tth time step. Dividing the summed concentrations by T yields the average concentration over the interval.

Because it is thought that the infectious dose is one *M. tb* bacillus, infection risk R is modeled by the one-hit expression: $R = 1 - e^{-D(T)}$.[22,23] However, if D(T) is a small number, say, $\leq .05$, then a good approximation is: $R \cong D(T)$. Because D(T) is a function of the

random variable $C_2(t)$, D(T) and R are also random variables. The expected infection risk, E[R], and the variance of the infection risk, Var[R], are approximately equal to E[D(T)] and Var[D(t)], respectively. The latter quantities are defined by:

$$E[D(T)] = \frac{b \times f_D}{T} \sum_{t=0}^{T-1} E\left[C_2(t)\right]$$

$$Var[D(T)] = \left(\frac{b \times f_D}{T}\right)^2 \left[\sum_{t=0}^{T-1} Var\left[C_2(t)\right] + 2 \sum_{t=0}^{T-2} \sum_{s>t}^{T-1} Cov\left[C_2(t), C_2(s)\right]\right]$$

The $E\left[C_2(t)\right]$ and $Var\left[C_2(t)\right]$ terms correspond to previous Equations (11) and (12), respectively, but a concise analytical expression is not available for $Cov\left[C_2(t), C_2(s)\right]$. Instead, the value of Var[D(T)] can be approximated by Monte Carlo simulation as follows.

In a given simulation run, each particle is followed for T – 1 one-sec time steps. For each particle at each time step, a uniform random variate U between 0 and 1 is generated. If the particle is in state 2, at the next time step the particle moves to state 1 if $U \le P_{21}$, or remains in state 2 if $P_{21} < U \le 1$. If the particle is in state 1, at the next time step the particle moves to state 0 if $U \le P_{10}$, remains in state 1 if $P_{10} < U \le \left(P_{10} + P_{11}\right)$, or moves to state 2 if $\left(P_{10} + P_{11}\right) < U \le 1$. If the particle is in state 0, the particle remains in state 0. The number of particles in state 2 at time step t is divided by the near-field volume to obtain $C_2(t)$. To compute the expected pulmonary dose, the T successive C_2 values are summed and divided by T to yield the TWA value for C_2, which is multiplied by the factor $\left(b \times f_D\right)$ to give D(T) for the simulation run. For this analysis, 10^5 simulation runs were performed, and the variance of the 10^5 values for D(T) was computed.

Returning to the scenario depicted in Figure 15, assume that the HCW's exposure starts at time zero when $N_0 = 10$ *M. tb* particles are released into the near-field zone (with no subsequent release), and lasts for T = 300 sec. Further assume that the HCW inhales b = .083 m^3 in 300 sec, which corresponds to inhaling one m^3/hr. Because the aerodynamic diameter of an *M. tb* particle is approximately 3 μm, let $f_D = 0.3$.[24] Based on the Monte Carlo simulation, E[D(T)] = .0069, in which case E[R] ≅ .0069. Further, Var[D(T)] ≅ 2.8×10^{-6} (the %CV of the estimate is < 2%), in which case the standard deviation SD[R] ≅ .0017, and the associated %CV[R] ≅ 25%. These values signify that while the expected infection risk is .0069 for the exposure period, there is a reasonable chance that it can be as high as .0097 (the approximate 95th percentile value: E[R] + 1.645 SD[R]). Figure 16 is a histogram of 10^5 simulation outcomes of the approximate R value for this scenario; the outcomes reasonably conform to a normal distribution. The mean is .0069, the standard deviation is .0017, and 5.9% of the values exceed .0097. Note that while an infection risk on the order of .01 (1%) may seem small, experiencing just ten similar exposures produces a cumulative infection risk of 9.6%, or: $1-(1-.01)^{10} = .096$.

IX. A Multi-State Markov Model Describing Contaminant Dispersion in Indoor Air

One drawback of the two-zone Markov model described in Section 6. VIII. is that it can yields an unrealistic spatial discontinuity in concentration. For example, if the predicted near field concentration is, say, 1000 particles per m^3, then one cm away across the zonal boundary the predicted far field concentration might be 1 particle per m^3. Finer detail in terms of describing a continuous concentration gradient with distance from the source is provided by a turbulent eddy diffusion model. For an emission point source in space, the simplest construct is spherical diffusion due to turbulent air motion (zero velocity on average) with no reflecting boundaries. For a pulse release of M particles, the spherical diffusion model predicts the concentration ($\#/m^3$) at time t (sec) and radial distance *r* (m) from the source to be:

$$C(r,t) = \frac{M}{(4 \cdot \pi \cdot D \cdot t)^{1.5}} e^{-\frac{1}{2}\left(\frac{r^2}{2 \cdot t \cdot D}\right)} \tag{18}$$

where D (m^2/sec) is the turbulent eddy diffusion coefficient, which is assumed to be constant over time and space. D is distinct from, and far greater in magnitude than, molecular diffusivity. Molecular diffusion coefficients in air are on the order of 10^{-5} m^2/sec, whereas reported D values for turbulent diffusion in indoor industrial environments range from .0014 to 0.19 m^2/sec.[25]

The above equation can be modified to account for advection along a room axis, to account for wall reflection and to partially account for removal by exhaust air. A turbulent diffusion model developed by Drivas and colleagues is as follows:[26]

$$C(x,y,z,t) = \frac{M_{x_0,y_0,z_0}}{(4 \cdot \pi \cdot D \cdot t)^{1.5}} \cdot R_x \cdot R_y \cdot R_z \cdot e^{-\left(\frac{Q}{V}t\right)} \tag{19}$$

where M_{x_0,y_0,z_0} is the number of particles released at room position (x_0, y_0, z_0); Q is the room exhaust air rate (m^3/sec); V is the room volume (m^3); and R_x, R_y and R_z are wall reflection terms along the *x*-, *y*- and *z*-axis, respectively, and represent infinite but convergent sums of exponential terms.

A problem with Equation (19), hereafter termed the Drivas model, is that at a given instance in time removal by exhaust air applies to particles at all room positions, whereas only those particles near an exhaust outlet would be subject to removal. This is problem is shared by the near-field/far-field model. Further, the Drivas model cannot account for in-room barriers and reflective surfaces, which may be important to consider in some circumstances. A Markov chain approach was used to formulate two models describing the dispersion of particles in room air. Markov model I is mathematically equivalent to the Drivas model and is computationally simple. Markov model II accounts for the positions of air inlets and outlets, for reflection by walls and other in-room surfaces, and for advective flow as well as diffusion.

Model II is much more complex than model I, but is still tractable. Both models yield concentration values with an explicit probabilistic interpretation.

The basic idea is that particle diffusion in room air can be treated as a simultaneous random walk along three orthogonal room axes (x,y,z), and that a continuous-time diffusion process can be discretized as movment over a suitably small time step. Consider a diffusion process without drift operating along the *x*-axis, where X(t) denotes the position of a diffusing particle at time t (sec). For simplicity, let X(0) = 0, the origin. In one time step of duration Δt (sec), the particle can move length Δx (m) to the right with probability *p*, or Δx to the left with probability *p*, such that there is no drift. Let *h* denote the probability that the particle holds its position (does not move), where 2p + h = 1. After $n = t/\Delta t$ time steps, the expected particle position is E[X(t)] = 0, and the variance is:

Eq. (20)
$$\mathrm{Var}[X(t)] = 2 \cdot p \cdot \frac{(\Delta x)^2}{\Delta t} \cdot t$$

The quantity $p \cdot (\Delta x)^2 / \Delta t$ corresponds to the diffusion coefficient D (m^2 /sec):

Eq. (21)
$$D = p \cdot \frac{(\Delta x)^2}{\Delta t}$$

The probability law of the random walk particle position X(t) is related to the binomial distribution, but with parameters $\mu = 0$ and $\sigma^2 = 2 \cdot p \cdot \left[(\Delta x)^2 / \Delta t\right] \cdot t$. However, for a large number of time steps *n*, which may constitute a short time duration t, the probability distribution tends toward the same normal distribution used to describe a continuous-time diffusion process. Next, assume the particle can simultaneously diffuse along the *y*-axis and *z*-axis in an independent and identically distributed manner, such that E[Y(t)] = E[Z(t)] = 0, and Var[Y(t)] = Var[Z(t)] = Var[X(t)]. Given that the particle position is (0,0,0) at time zero, the probability that the particle position is (x,y,z) at time t is well approximated by the same joint distribution implicit in Equation (18), where $r = \sqrt{x^2 + y^2 + z^2}$.

The Random Walk and Markov Model I: The random walk of a particle in one or more dimensions is a Markov process, because the particle's next move depends only on its current position (state). The probability of the particle's position along each axis is described by an independent Markov chain. To explain, let **PX** denote the single-step transition probability matrix for the *x*-axis position. If one uses a 0.1-m length increment, a length of 10 m, say, along the room's *x*-axis corresponds to a 100 x 100 matrix **PX**, where each state represents a room cell of length 0.1 m.

The matrix **PX** is defined in Figure 17. The numbers outside the matrix index the state numbers. States 1 and 100 border the room walls, and states 2-99 are interior room positions. For the moment, it is assumed that the particle never leaves room air. For a particle in an interior state, in the next time step it can hold with probability *h*, or move to the adjacent higher or lower state with probability *p*. For a particle in a wall border state, in the next time

step it can hold with probability $h + p$, or move to the adjacent state with probability p. This set of transition probabilities yields a uniform probability distribution at equilibrium, that is, a particle has the same chance of being in any given state. The value of p that corresponds to a particular value of D is determined by Equation (21) after specifying Δt (as well as Δx). In turn, $h = 1 - 2p$. Given that a particle is currently in state i, the probability that the particle is in state j after $n = t/\Delta t$ time steps is denoted $PX_{i,j}^{t/\Delta t}$, which corresponds to the i^{th} row and j^{th} column entry in the matrix $\mathbf{PX}^{(n)}$, or $\mathbf{PX}$ multiplied by itself n times. $\mathbf{PX}^{(n)}$ specifies the probability distribution of the particle's position along the room's x-axis after n time steps.

Similarly, let $\mathbf{PY}$ and $\mathbf{PZ}$ denote the transition probability matrices for the particle's y-axis and z-axis positions, respectively. The number of states in $\mathbf{PY}$ and $\mathbf{PZ}$ correspond to the respective room width and height divided by the 0.1-m length increment. Given that a particle starts in room position (x_0, y_0, z_0), where the three values denote the initial state number in the matrices $\mathbf{PX}$, $\mathbf{PY}$ and $\mathbf{PZ}$, respectively, the probability that the particle is at room position (x,y,z) at time t is the product of the three independent probabilities: $\left(PX_{x_0,x}^{t/\Delta t}\right)\left(PY_{y_0,y}^{t/\Delta t}\right)\left(PZ_{z_0,z}^{t/\Delta t}\right)$.

Next, let $V_{(x,y,z)}$ denote a volume element (m^3) at room position (x,y,z); for the 0.1-m length increment, $V_{(x,y,z)} = .001\ m^3$. Again, let M_{x_0,y_0,z_0} denote the number of particles released as a pulse at room position (x_0, y_0, z_0). Given that no particles leave room air, the expected particle concentration at room position (x,y,z) at time t after the release is given by:

$$E[C(x,y,z,t)] = \frac{M_{(x_0,y_0,z_0)}}{V_{(x,y,z)}} \cdot PX_{x_0,x}^{t/\Delta t} \cdot PY_{y_0,y}^{t/\Delta t} \cdot PZ_{z_0,z}^{t/\Delta t}$$

The above expression is equivalent to the Drivas model except for the dilution ventilation factor $e^{-(Q/V)\cdot t}$. By multiplying the right-hand side of the expression by $e^{-(Q/V)\cdot t}$, Markov model I is obtained:

Eq. (22)
$$E[C(x,y,z,t)] = \frac{M_{(x_0,y_0,z_0)}}{V_{(x,y,z)}} \cdot PX_{x_0,x}^{t/\Delta t} \cdot PY_{y_0,y}^{t/\Delta t} \cdot PZ_{z_0,z}^{t/\Delta t} \cdot e^{-\left(\frac{Q}{V}t\right)}$$

Note that the published form of the Drivas model also incorporates a pollutant surface deposition factor, $e^{-(w_d \cdot A/V)\cdot t}$, where w_d is the deposition rate on surfaces (m/sec), and A is the surface area (m^2) available for deposition. Markov model I can be made equivalent by multiplying the the right-hand side of Equation (22) by $e^{-(w_d \cdot A/V)\cdot t}$.

The Random Walk and Markov Model II: The room is divided into cubic cells with length aspect Δx, and the positions of air inlets and outlets are specified. Given m cells in the room, there is a corresponding transition probability matrix **P** with dimensions $(m + 1)$ x $(m + 1)$. **P** has has one state for each cell in the room plus an additional absorbing state that represents particle removal from room air. For simplicity, it is assumed that the only particle loss mechanism is removal by exhaust air, and that once exhausted from the room, a particle cannot reenter. However, other particle loss mechanisms can be accommodated, as well as absorbing states corresponding to these removal pathways.

In one time step, a particle in a given room cell can hold its position or move to a physically contiguous "nearest neighbor" cell. An interior room cell has six nearest neighbors. A cell that borders one wall (or surface) has five nearest neighbors. A cell that borders two walls (or surfaces) has four nearest neighbors, and a room corner cell has three nearest neighbors. A cell bordering the exhaust air outlet can be considered to have six nearest neighbors if one counts the absorbing state as a neighbor, although a particle that enters the absorbing state can never leave that state.

The complete set of equations specifying the single-step transition probabilities is presented in Appendix 1, but the underlying concepts are described here for a particle in an interior room cell (state). First, assume that turbulent diffusion is the only mechanism of particle movement. In Markov model I, the probability that a particle in a given chain holds its position is: $h = 1 - 2p$, in which case the probability that the particle simultaneously holds its position in the three independent chains is: $h^3 = (1-2p)^3$. It follows that in Markov model II, the probability that an interior cell particle holds its position, denoted $h_{I,D}$ (where the subscript D signifies that only diffusive flow is considered), is given by:

Eq. (23) $$h_{I,D} = (1-2p)^3$$

where p is defined by Equation (21). In turn, if the particle leaves the cell, it can move with equal likelihood to one of six nearest neighbors. Therefore, the probability that the interior cell particle moves to a given neighboring cell, denoted $p_{I,D}$ is:

Eq. (24) $$p_{I,D} = \frac{1}{6}\cdot(1-h_{I,D})$$

Next, assume that a particle in an interior cell is can move by advection as well as diffusion. Let s_A denote the advective air speed (m/sec). For simplicity, consider that advective flow is perpendicular to only one cell face, in which case a cell with face area $(\Delta x)^2$ receives an advective air supply in m^3/sec equal to $s_A \cdot (\Delta x)^2$. Because a cell has volume $(\Delta x)^3$, this advective air supply divided by the cell volume corresponds to $s_A / \Delta x$ air changes per sec. If air in a cell is assumed well-mixed, the advective air supply can be treated as a "dilution" air supply. The probability that a particle is not removed due to advection in time step Δt is

denoted $h_{I,A}$ (where the subscript A signifies that only advective flow is considered), and is specified by:

Eq. (25) $$h_{I,A} = e^{-\left(\frac{s_A}{\Delta x}\right)\Delta t}$$

If particle removal from the cell by diffusive flow and by advective flow are treated as independent mechanisms, the probability that the particle holds its position is the product $(h_{I,D})(h_{I,A})$. To recapitulate, where an interior cell particle can move only by diffusion, the probability that it holds its position is $h_{I,D}$, but where the particle can move by advection or diffusion, the probability that it holds its position is the product of $h_{I,D}$ and $h_{I,A}$.

If only diffusive flow applies, the probability that a particle moves to a given neighboring cell is specified by $p_{I,D}$ in Equation (24). However, where both diffusive and advective flows apply, the probabilities that a particle moves to the "downstream" neighboring cell (in the direction of advective flow), denoted $p_{I,down}$, or to one of the five other neighboring cells, denoted $p_{I,other}$, are respectively given by:

Eq. (26) $$p_{I,down} = \frac{(1/6)\cdot\alpha + (s_A/\Delta x)\cdot\Delta t}{\alpha + (s_A/\Delta x)\cdot\Delta t}\cdot(1 - h_{I,D}\cdot h_{I,A})$$

Eq. (27) $$p_{I,other} = \frac{(1/6)\cdot\alpha}{\alpha + (s_A/\Delta x)\cdot\Delta t}\cdot(1 - h_{I,D}\cdot h_{I,A})$$

where $\alpha = -\ln(h_{I,D})$. The derivation of Equations (26) and (27) is provided in Appendix 1. For a particle in a cell bordering the exhaust air outlet, $p_{I,down}$ is also the probability that the particle is exhausted from the room, that is, enters the absorbing state. Note that this general construct represents a three-dimensional random walk with drift along the room axis in the direction of the advective flow.

Given a specified matrix **P**, and given the release of M particles at time zero in state *i* corresponding to room position (x_0, y_0, z_0), the expected concentration in state *j* corresponding to room position (x,y,z) after $t/\Delta t$ time steps is:

Eq. (28) $$E[C(x,y,z,t)] = \frac{M_{(x_0,y_0,z_0)}}{(\Delta x)^3}\cdot P_{i,j}^{t/\Delta t}$$

An Illustrative Scenario: Consider a hypothetical room, 3 m x 3 m x 3 m. The room is isothermal and receives six nominal air changes per hour. Based on $\Delta x = 0.2$ m, the room is divided into 3375 cubic cells, and the **P** matrix is 3376 x 3376. Air enters through a 3 m x 0.6 m register running the length of the left-hand wall at height position 1.4 m to 2 m. Air is

exhausted through a register of the same dimensions at the same height position on the right-hand wall. The supply air discharge velocity is .025 m/sec.

An algorithm presented in reference 24 predicts the turbulent diffusion coefficient for this room to be .0189 m^2/sec. For Δx = 0.2 m, Δt = 1/30 sec and D = .0189 m^2/sec, the transition probabilities for interior cell particles not subject to advective flow are $h_{I,D}$ = 0.90845 and $p_{I,D}$ = .01526. For simplicity, it is assumed that all advective flow goes uniformly from left to right in the 1.4-m to 2-m height zone, in which case s_A = .025 m/sec and $h_{I,A}$ = 0.99584. For interior cell particles in the 1.4-m to 2-m height zone, the transition probabilities are $(h_{I,D})(h_{I,A})$ = 0.90467, $p_{I,down}$ = .01919, and $p_{I,other}$ = .01523. The transition probabilities for particles in cells bordering wall surfaces can be found by the formulae in Appendix 1.

To provide a baseline for comparison, results are first described if the room were sealed with no air supply (Q = 0). Figure 18 depicts the expected particle concentrations at three room positions in the first five minutes after the release of 2700 particles at position x_0 = 1.1 m, y_0 = 1.5 m, z_0 = 1.5 m, where all axes run from 0 m to 3 m. The three locations are: (1) x = 0.1 m, y = 1.5 m, z = 1.5 m, which is 1 m upstream from the release point and next to the air supply register; (2) x = 2.1 m, y = 1.5 m, z = 1.5 m, which is 1 m downstream from the release point; and (3) x = 2.9 m, y = 1.5 m, z = 1.5 m, which is 1.8 m downstream from the release point and next to the exhaust outlet. Note that these (x,y,z) tuples are the midpoint coordinates of the 0.2-m cubic cells. The solid-line curves are the concentrations predicted by Markov model II, and the dashed-line curves are the concentrations predicted by Markov model I per Equation (22). For the latter model, the matrices **PX**, **PY** and **PZ** are each 15 x 15 in dimension, and the parameters Δx = 0.2 m, Δt = 1/30 sec and D = .0189 m^2/sec correspond to h = 0.9685 and p = .01575.

As seen in Figure 18, the concentration curves predicted by the two models are essentially coincident. Moreover, a particle concentration of 100 per m^3 eventually develops at all room positions, which is the value expected by uniformly distributing 2700 particles in a 27 m^3 volume.

Figures 19-21 depict the expected concentrations at the same respective room positions given Q = .045 m^3/sec, which corresponds to six nominal air changes per hour. Again, the solid-line and dashed-line curves are the concentrations predicted by, respectively, models II and I. Figure 19 shows the concentrations at location (1), which is 1 m upstream from the release point and next to the air inlet. Model II describes a lower concentration than does model I; for example, the peak level in the former model (200 per m^3) is 33% lower than the peak value in the latter (300 per m^3). This result is intuitively reasonable. There is less tendency for particles to diffuse against the advective flow towards the air inlet, and the discharge of clean air at the inlet exerts a greater local dilution effect than if clean air were somehow uniformly discharged at all room positions, as assumed in model I.

Figure 20 shows the expected concentrations at location (2), which is 1 m downstream from the release point. Model II describes a higher concentration than does model I in the first 1¼ minutes, and a lower concentration thereafter; for example, the peak level in the former model (330 per m^3) is 70% higher than the peak value in the latter (195 per m^3). This result is also intuitively reasonable, because there is a greater initial tendency for particles to migrate towards location (2) due to the advective flow. The impact of advection is also seen by comparing $p_{I,down} = .01919$ (the transition probability to the right-hand neighboring cell due to both advection and diffusion) and $p_{I,D} = .01526$ (the transition probability to the right-hand neighboring cell due to diffusion alone). Note that advection has a substantial effect even though the advective air speed is only .025 m/sec.

Figure 21 shows the expected concentrations at location (3), which is 1.8 m downstream from the release point and next to the exhaust outlet. After the first ½ minute, model II describes a lower concentration than does model I. This result is somewhat counterintuitive. Given that all particles are eventually exhausted at the outlet, it might be expected that the particle concentration would be higher near the outlet than if particles were somehow uniformly exhausted from all room positions, as assumed in model I. However, the room had a relatively large 1.8 m^2 exhaust outlet area, which decreases the exiting particle concentration in cells adjacent to the outlet. A smaller exhaust area would funnel a greater number of particles through a smaller volume adjacent to the outlet and increase the local particle concentration.

The Effect of An In-Room Barrier: Consider a pulse release of particles immediately in front of an individual. If the person's back faces the advective flow stream, the particle concentration in the breathing zone will likely be higher than if the individual's body somehow presented no barrier to the advective flow. One reason is that the body decreases or eliminates advective flow immediately in front of the person (on the downstream side). A second reason is that the body reflects particles diffusing in the upstream direction. The net effect is that particles tend to remain relatively longer in front of the person before migrating away.

To approximate this scenario, model II for the 3-m cubic room was modified as follows. A barrier representing a person was placed along the *x*-axis at 0.8 m to 1 m from the left-hand wall, midway along the *y*-axis from 1.2 m to 1.8 m, and along the *z*-axis at 0 m to 1.8 m from the floor. Therefore, the barrier's depth, width and height were, respectively, 0.2 m, 0.6 m, and 1.8 m. That portion of the advective air flow hitting the left-hand face of the barrier (at height 1.4 m to 1.8 m) was evenly split around the ends of the barrier in the same height zone, but made to return to a uniform flow pattern 0.4 downstream from the right-hand face of the barrier at $x = 1.4$ m. In effect, a wake zone free of advective flow was created in front of the barrier on the downstream side (on the *x*-axis from 1 m to 1.4 m, on the *y*-axis from 1.2 m to 1.8 m, and on the *z*-axis from 1.4 m to 1.8 m). For simplicity, the turbulent diffusion coefficient was kept the same in the wake zone as elsewhere in the room. As before, assume that 2700 particles are released at room position $x_0 = 1.1$ m, $y_0 = 1.5$ m, $z_0 = 1.5$ m, which is intended to represent a person's breathing zone position.

Figure 22 shows the particle concentration (on a logarithmic scale) at the release position over the first minute. The solid line curve is the concentration profile with the barrier present, and the dashed-line curve is the concentration without the barrier. The particle concentration at the time of release is the same in both scenarios (3.38×10^5 per m^3), but the concentration initially decreases less rapidly with the barrier present. The 5-min TWA values with and without the barrier are 800 per m^3 versus 630 per m^3, respectively. Therefore, the barrier increased the 5-min TWA value by 27%.

Section 7 – Discussion and Conclusions

The Stochastic Simulation Model: It is not argued that the modeling results represent the typical experience in a hospital with 1000 staff members. Rather, hypothetical scenarios were posed to illustrate the approach and demonstrate how a variety of factors could be investigated. At the same time, the parameter values posited were reasonable. These parameters included the daily infection risks (r_L, r_M and r_H), the relative number of workers in the three risk groups, the number of workdays per year, the annual number of TB patient admissions, the length of TB patient infectiousness, the probability of developing TB once infected, the duration of continuing work while diseased, a diseased worker's number of close contacts, and the probability of a diseased worker infecting a close contact. In general, published information on these parameters is sparse, but some relevant data are now discussed.

Based on a mail questionnaire survey of hospital epidemiologists, employee infection rates in 1992 as reported for 109 hospitals had a median value of 0.5% and a range of 0% to 7.7%; median infection rates for the previous three years were reported to be, respectively, 0.26%, 0.35% and 0.42%.[5] Based on 1992 data reported for 210 hospitals, the mean infection rate among "higher-risk" employees (bronchoscopists and respiratory therapists) was 1.9% in hospitals that treated ≥ 6 TB patients annually, and 0.2% in hospitals that treated < 6 TB patients annually.[27] For the same hospitals for the period 1989-1992, the median annual number of TB cases admitted was 5.6 and the range was 0 to 492.[26]

Several aspects of the simulation scenarios are consistent with these data. First, the annual numbers of TB patients admitted (5 vs. 50) fall within the reported range of 0 to 492. Second, the year one infection rates in all the scenarios summarized in Tables 1- 3 fall within the 0 - 7.7% range of annual infection rates reported for hospitals in 1992. For example, in the scenario involving X = 600, Y = 300, Z = 100, T = 50 TB patients admitted annually on average, and accounting for disease development and close contacts (see Figure 1, Curve C), the year one infection rate was 2.9% (29 infections among 1000 cohort members). Third, both the simulated and reported infection rates increased with more TB patient admissions.

Note that the values of r_L, r_M and r_H posited for the simulation model could not be extrapolated from these data or from other reports because sufficient detail was not provided. That is, for a defined time period no study has ever provided complete information including the number of TB patients admitted, their lengths of admission; the number of susceptible employees in different occupational groups who did or did not attend TB patients, the number of days each of these employees worked, and the infection rates experienced in different occupational groups. However, the posited daily infection risks led to annual infection rates within the range of values reported not only for all hospital staff, but for groups of high-risk employees as well.[7,27]

Modeling primary and secondary TB disease incidence involved the following subset of assumptions: (*i*) an otherwise healthy individual has a 5% chance of developing disease in the first year following infection; (*ii*) a diseased worker remains on the job for three calendar weeks while infectious; (*iii*) a diseased worker has 25 close contacts; and (*iv*) close contacts

have a 22% chance of being infected. Assumption (*i*) was based on values reported in the literature.[4] With regard to assumption (*ii*), among eight workers in an Atlanta hospital who developed occupational TB, on average the employees spent 21 days on the job while potentially infectious.[7] For assumption (*iii*), no data were located concerning the number of close contacts on the job; instead, it was speculated that 25 was a reasonable number given that close contacts include employees who work in physical proximity or with whom the individual socializes. Assumption (*iv*) was based on data reported for TB case contact investigations in two Canadian provinces for the period 1966-1971. Among Caucasians of age ≥ 20 yr who were described as casual contacts ("close friends, office associates"), the *M. tb* infection risk was approximately 0.22.[28]

As previously mentioned, in the scenario involving X = 600, Y = 300, Z = 100, T = 50 TB patients admitted annually on average, and accounting for disease development and close contacts, the primary to secondary TB disease ratio was approximately 6:2 ratio. This ratio is similar to that reported in two investigations. Among emergency department staff at a Dallas hospital who were infected by a TB patient, five workers developed TB while a sixth worker developed TB after infection by a diseased "close associate" (primary to secondary disease ratio, 5:1).[29] At the Atlanta hospital where eight workers developed TB, it was determined that at least one and possibly two of the cases involved worker-to-worker transmission (primary to secondary disease ratio, 7:1 or 6:2).[7]

The simulation model was used to investigate the impact of alternative screening intervals for *M. tb* infection, the impact of variability in patient infectivity, and the impact of *M. tb* infection among immunocompromisd HCW's. As previously described, infection screening with followup antibiotic prophylaxis reduces the incidence of TB disease among HCW's with primary infections (due to patient-to-worker transmission), and thereby reduces the incidence of secondary infections and TB disease among HCW's (due to worker-to-worker transmission). Because shorter screening intervals permits less time for HCW's with an unidentified new infections to develop TB disease, the shorter the screening interval, the greater the reduction in incidence. With regard to variability in patient infectivity, the model showed that a binary type of infectivity generates substantial variability in infection incidence among HCW's. The model also provided the following interesting result. When comparing a uniform distribution of infectivity over a 100-fold range, versus a binary distribution of infectivity over a 100-fold range and with the same mean infectivity value as for the uniform distribution, the uniform distribution did not increase the variability in infection incidence among HCW's, but the binary distribution greatly increased infection incidence variability.

The Cohort-Level Impact of Infection among Immunocompromised Health Care Workers: According to the simulation model, the presence of a small number of immunocompromised (IC) individuals in a large HCW cohort is predicted to have little effect on *M. tb* infection and TB disease incidence at the cohort level. In fact, the results of the simulation modeling might be considered worst-case outcomes for two reasons: (*i*) IC workers were always seeded into the high-risk group which was subject to a high annual infection rate; and (*ii*) infections among IC workers were not detected by PPD skin testing. In the high-risk group, the annual infection risk due to TB patients was 0.14, which corresponded to a five-year cumulative infection risk of 0.53; the latter value was 4-fold to 35-fold greater than in the low- and

medium-risk groups, respectively. To explain the computation, given an annual average of 50 TB patient admissions and a 10-day stay per patient, there were on average 500 patient days per year. For a high-risk group member, the daily infection risk was: (500/365) x $\left(5 \times 10^{-4}\right) = 6.8 \times 10^{-4}$. Given 220 days worked in one year, the annual infection risk was: $1-(1-.00068)^{220} = 0.14$. Given 1100 days worked in five years, the cumulative infection risk was: $1-(1-.00068)^{1100} = 0.53$. In contrast, the cumulative risks were .015 and 0.14 for low- and medium-risk group members, respectively, where the latter probabilities were computed in a similar manner.

Second, it was assumed that *M. tb* infections among IC workers would not be detected due to anergy, in which case infected IC workers were permitted the maximum time within the simulation period to develop disease subsequent to infection. For example, consider the scenario where an annual PPD skin testing program was in place. If an IC worker became infected on day one, the individual had a full five years to develop disease, which resulted in probability 0.34 of developing TB by the end of the simulation, or $1-(1-.000228)^{1824} = 0.34$. In contrast, if a non-IC worker became infected on day one, and if the worker's infection was detected by PPD skin testing 12 months later, the non-IC worker had only a one-year period in which to develop disease; this circumstance led to a seven-fold lower disease probability of .05, or $1-(1-.00014)^{364} = .05$.

Given the seven-fold difference in TB disease risk in the latter example, it is initially surprising that the presence of IC workers did not exert a greater effect at the cohort level. The explanation involves two considerations: (*i*) the unconditional probability of disease; and (*ii*) the expected increment in secondary infections and disease cases per IC worker. First, the previous disease probabilities of 0.34 and .05 for IC and non-IC workers, respectively, are conditioned on infection occurring on day one. However, an individual has equal likelihood of being infected at any point in the five-year simulation period, and infections occurring later in the simulation period lead to smaller differences between IC and non-IC workers. For example, if infection occurred at day 1460 (year 4) and no screening occurred thereafter, the conditional disease probabilities for the IC and non-IC workers would be .08 and .05, respectively, which represents only a 1.6-fold difference.

To simultaneously account for the time of infection and the subsequent risk of disease, the unconditional probability of TB disease is computed by the following expression:

$$\Pr[\text{Disease}] = \sum_{i=1}^{N} \Pr\left[\text{Disease} \mid \text{Infection on the } i^{\text{th}} \text{day}\right] \text{x} \Pr\left[\text{Infection on the } i^{\text{th}} \text{day}\right]$$

where *i* indexes the number of days over which the infection/disease process pertains. For a non-IC worker, the computation is difficult because the risk rate for developing TB disease subsequent to infection is not constant, and the time available for developing disease may be decreased by treating the infection prophylactically subsequent to identification by PPD skin testing. Details of the computation method have been published elsewhere,[30] but some pertinent results are presented for high-risk group members.

Given no screening program in place, the five-year unconditional cumulative probability of developing TB disease due to infection by a TB patient is .026 for a non-IC worker and 0.11 for an IC worker, which is a four-fold rather than a seven-fold difference in disease risk. However, the relative difference does increase if the non-IC worker is part of a screening program, because the non-IC worker's risk of developing TB disease is decreased. For example, if the non-IC worker is skin tested annually, the five-year unconditional cumulative probability of developing TB disease due to infection by a TB patient is reduced from .026 to .015; in this case, there is again a seven-fold difference in disease probabilities between IC and non-IC workers.

Next, consider the expected increment in the number of secondary infections and disease cases per IC worker. An individual's expected contribution to the cohort's total number of disease cases is equal to the individual's risk of developing disease. If no screening program is in place, and if one IC worker replaces one non-IC worker in the high-risk group, the expected increment in primary disease cases is: 0.11 - .026 = .084. Given that a diseased worker infects 5.5 close contacts on average [i.e., (25 close contacts)(0.22)], the expected increment in secondary infections among close contacts is: (5.5)(0.11 - .026) = 0.46. In turn, some fraction of this increment will become secondary TB disease cases. If for simplicity it is assumed that no screening program is in place, this fraction is approximately .05, and the expected total increment in secondary disease cases is: (.05)(0.46) = .023. Therefore, the expected increment in the cohort total number of disease cases due to one IC worker is: .084 + .023 = 0.11. These expected increments are slight underestimates because a diseased IC worker acts like an additional TB patient among those susceptible employees outside the group of close contacts.

In summary, the presence of IC individuals in a HCW cohort subject to *M. tb* infection is expected to only slightly increase the incidence of secondary infection and TB disease at the cohort level. Other than considerations of personal health consequences for the IC worker, there is no compelling reason to keep IC individuals from performing tasks that potentially subject them to *M. tb* aerosol exposure. At the same time, it is advisable to offer more frequent screening examinations of such IC workers, and thereby increase the chance of early detection of new *M. tb* infection and/or TB disease.

***Cost Effectiveness*:** Cataloguing of current dollar costs for different control measures, and comparisons of specific controls (e.g., in-room air filter #7 versus Type N95 respirator #20), were not pursued in this project. The reason is that costs continually change as new technology is developed and market demand fluctuates, and a final cost analysis depends not only on the current dollar costs of implementing different measures, but on the degree of risk currently experienced by a facility. In this context, it is the ability to estimate reductions in infection and disease risk afforded by different measures that is important to develop. Therefore, analytical engineering and component reliability frameworks were constructed to inform cost-efficacy analyses and decision-making in general.

The component reliability analysis showed that if a facility has a poor record in identifying TB disease in presenting patients, expenditures to increase the general level of suspicion and efficiency of identifying and isolating TB patients will be most cost-effective. The source-

pathway-receptor construct led to a similar conclusion for HCW's who do not attend TB patients. That is, engineering efforts to increase the rate of *M. tb* particle removal from the general hospital air and from isolation room air, are far less effective than rapidly identifying and isolating suspect TB patients. This idea is consistent with a common belief among infection control practitioners that rapid identification and isolation of TB patients is the most important component of a TB control program. On the other hand, the component reliability analysis showed that if the facility is already highly efficient in identifying and isolating TB patients, expenditures to increase the efficiency of environmental controls will be the most cost-effective control measure, particularly among HCW's who attend TB patients. In a similar vein, the source-pathway-receptor construct showed that for HCW's who enter TB patient isolation rooms, personal respiratory protection is substantially more effective than increasing the *M. tb* removal rate from isolation room air via increasing effective room ventilation. These latter findings do not appear to correspond to beliefs commonly held by infection control practitioners.

The three-zone model of a TB patient isolation room with upper-room air UVGI, and the two-zone Markov model of an isolation room without UVGI, also showed the limited efficacy of increasing the removal/inactivation rate of *M. tb* particles from the general room air. The reason is that an attending HCW is usually in close proximity to the TB patient, the source of the *M. tb* particles, such that the HCW is exposed to a near-field *M. tb* particle concentration. However, controls such as mechanical dilution ventilation, in-room air filtration, and upper-room air UVGI act on *M. tb* particles in the far field, and cannot remove/inactivate M. tb particles directly emitted into the HCW's breathing zone in the near field. The results presented for the three-zone model also have a broader application. That is, determinations of an enginering control's efficacy in reducing the steady-state or long-term average airborne contaminant concentration should not be based on analyzing slopes of concentration decay curves, but on steady-state measurements, because decay slope values can be misleading. The effective contaminant removal rate at different room positions may differ markedly (leading to different average contaminant levels at these room positions), yet the slopes of concentration decay curves at these same room positions can be similar in value.

As noted previously, the analytical risk model for the effect of an *M. tb* infection screening program in reducing nosocomial TB disease among HCW's is apparently the first effort at quantifying the cost-efficacy of alternative screening intervals. The analytical formulae permit risk managers to design a screening program based on the estimated annual rate of infection in a facility and a defined target risk of disease (suggested to be 1 per 1000 in a 12-year interval). An important finding visually shown in Figure 9 is that for HCW's subject to a relatively "low" annual infection risk of 0.5%, an infection screening interval of 6 months rather than 12 months is necessary to meet the target risk level, yet this interval is only slightly less cost effective than using the 12-month interval recommended by the 1994 CDC guidelines.

The Markov Models: Probabilistic models based on Markov chain techniques were developed to describe particle dispersion in, and removal from, room air. Markov models are complementary to other techniques for indoor air modeling such as simple turbulent diffusion models and computational fluid dynamics (CFD) models. The latter are increasingly being applied to indoor air quality studies and specifically to workplace settings. The main advantages of the Markov modeling approach may be its relative simplicity and explicit probabilistic treatment of contaminant dispersion and removal processes.

For preventing occupational *M. tb* infection, an important implication of the Markov models is the following. Because relatively small numbers of *M. tb* particles are usually present, the failure to account for the probabilistic nature of particle dispersion and fate may lead to formulating an exposure control strategy that is inconsistent with the intended goal. For example, the tuberculosis standard proposed by the Occupational Safety and Health Administration (OSHA) requires that when a room or area is vacated by a TB patient, the room must be ventilated to achieve a 99.9% "removal efficiency" before employees may enter without respiratory protection.[10] Therefore, if a room receives six nominal air changes per hour, the ventilation system must be run for 69 mins, at which time the *M. tb* particle concentration is expected to be 0.1% of the initial concentration. Because OSHA did not propose an acceptable concentration of *M. tb* in air, OSHA may have intended that 99.9% "removal efficiency" also signify a 99.9% probability that no *M. tb* particles are present in room air upon entry. However, requiring 99.9% "removal efficiency" fails to provide 99.9% probability that no *M. tb* particles are present.

To illustrate, consider a room having V = 50 m^3 and Q = 300 m^3/hr, but let $N_0 = 40$ *M. tb* particles. Such a scenario might involve a bronchoscopy on a pulmonary TB patient who emits 250 *M. tb* particles per hour over the course of a 1.5 hr procedure, as reported in a case study.[15] It can be shown that the number of *M. tb* particles in room air would be approximately 40 by the end of the bronchoscopy in the room just specified. For simplicity, if the room is assumed to be well-mixed, and if the dilution ventilation system operates for 69 mins after the procedure, the probability that any given particle remains is .001. The binomial probability that none of the 40 *M. tb* particles remain is 0.961, or only 96.1%.

Beyond their application to *M. tb* and other infectious aerosols, a useful property of the Markov models is the ability to account for multiple in-room sources of contaminant. For example, in Markov model II, by specifying the cell location of each source and the number of particles released at time zero, the particle concentration at a given receptor cell at time t due to all sources is easily computed from the matrix $P^{(t/\Delta t)}$ as follows:

Eq. (29)
$$E[C(x,y,z,t)] = \frac{1}{(\Delta x)^3}\sum_{i=1}^{k} M_i \cdot P_{i,j}^{t/\Delta t}$$

where i indexes the source cell, $i = 1,2,\ldots, k$; M_i is the number of particles released in the i^{th} source cell; and j indexes the receptor cell (x,y,z).

Moreover, one can account for ongoing contaminant emission by multiple in-room sources, where the emission rate (# particles per sec) at a given source need not be constant. For example, one might model the emission rate at one source as exponentially decreasing, the rate at a second source as sinusoidal, and the rate at a third source as constant. The particle concentration at a given receptor cell $j = (x,y,z)$ at time t is:

Eq. (30)

$$E[C(x,y,z,t)] = \frac{1}{(\Delta x)^3} \sum_{i=1}^{k} \left[\sum_{q=0}^{t/\Delta t} (M_i)_q \cdot P_{i,j}^{t/\Delta t - q} \right]$$

where i again indexes the source cell; $(M_i)_q$ is the number of particles released in the i^{th} source cell at time q; and $P_{i,j}^0 = 0$ and $P_{i,i}^0 = 1$. If desired, the times of emission events and the number of particles emitted per event can also be modeled as probabilistic entities.[31]

A current limitation is that the Markov models do not independently predict the the room air flow patterns and the turbulent diffusion coefficient, and are conceptual rather than physics-based constructs. It is anticipated that these Markov models can eventually be combined with deterministic physics-based approaches to more realistically predict contaminant concentrations at room locations of interest.

REFERENCES

1. Bloom, B.R. and C.J.L. Murray: Tuberculosis: Commentary on a Reemergent Killer. *Science 257*:1055-1064, 1992.

2. Menzies, D., A. Fanning, L. Yuan, and M. Fitzgerald: Tuberculosis among Health Care Workers. *New Engl. J. Med. 332*:92-98, 1995.

3. Sepkowitz, K.A.: Tuberculosis and the Health Care Worker: A Historical Perspective. *Ann. Int. Med. 120*:71-79, 1994.

4. American Thoracic Society/Centers for Disease Control: Diagnostic Standards and Classification of Tuberculosis. *Am. Rev. Respir. Dis. 142*:725-735, 1990.

5. Fridkin, S.K., L. Manangan, E. Bolyard, and W.R. Jarvis: SHEA-CDC TB Survey, Part I: Status of TB Infection Control Programs at Member Hospitals, 1989-1992. *Infect. Control Hosp. Epidemiol. 16*:129-134, 1995.

6. Nardell, E.: Editorial: Is a tuberculosis exposure a tuberculosis exposure if no one is infected? *Infect. Control Hosp. Epidemiol. 19*:484-486, 1998.

7. Zaza, S., H.M. Blumberg, C. Beck-Sague, W.H. Haas, et al.: Nosocomial Transmission of *Mycobacterium tuberculosis*: Role of Health Care Workers in Outbreak Propagation. *J. Infect. Dis. 172*:1542-1549, 1995.

8. National Institute for Occupational Safety and Health: NIOSH Recommended Guidelines for Personal Respiratory Protection of Workers in Health-Care Facilities Potentially Exposed to Tuberculosis. U.S. Department of Health and Social Services, CDCP, NIOSH, Atlanta, GA, September 1992.

9. Centers for Disease Control and Prevention: Guidelines for Preventing the Transmission of *Mycobacterium tuberculosis* in Health-Care Facilities, 1994. *Morb. Mort. Wkly. Rep. 43(RR-13)*:1-132, 1994.

10. Occupational Safety and Health Administration: "Occupational Exposure to Tuberculosis; Proposed Rule." Federal Register 62:54159-54308 (17 October 1997).

11. Moreno, S., J. Baraia-Etxaburu, E. Bouza, F. Parras, M. Perez-Tascon, P. Miralles, T. Vicente, J.C. Alberdi, J. Cosin, and D. Lopez-Gay: Risk for Developing Tuberculosis among Anergic Patients with HIV. *Ann. Intern. Med. 119*:194-198, 1993.

12. International Union Against Tuberculosis Committee on Prophylaxis: Efficacy of Various Durations of Isoniazid Preventive Therapy for Tuberculosis: five years of follow-up in the IUAT trial. *Bull. WHO 60*:555-564, 1982.

13. Hopewell, P.C.: "Factors Influencing the Transmission and Infectivity of *Mycobacterium tuberculosis*: Implications for Clinical and Public Health Management." In: Sande M.A., Hudson L.D., Root R.K., eds. *Respiratory Infections*. New York, NY: Churchill Livingstone, 1986. pp. 191-216.

14. Huebner R.E, M.F. Schein, J.B. Bass Jr. Tuberculosis Commentary: The Tuberculin Skin Test. C*lin Infect Dis. 17*:968-975, 1993.

15. Catanzaro, A.: Nosocomial Tuberculosis. *Am Rev Resp Dis. 125*:559-562, 1982.

16. Nicas, M.: Respiratory Protection and the Risk of *Mycobacterium tuberculosis* Infection. *Am. J. Ind. Med. 27*:317-333, 1995.

17. Nagin, D., N. Pavelchak, M. London, R.P. DePersis and J. Melius: "Control of Tuberculosis in the Workplace." In: *Occupational Medicine State of the Art Reviews, Volume 9*, 1994. Pp. 609-630.

18. Riley, R.L., M. Knight, and G. Middlebrook: Ultraviolet Susceptibility of BCG and Virulent Tubercle Bacilli. *Am. Rev. Resp. Dis. 113*:413-418, 1976.

19. Nicas, M.: Estimating Exposure Intensity in An Imperfectly Mixed Room. *Am. Ind. Hyg. Assoc. J. 57*:542-550, 1996.

20. Nicas, M. and S.L. Miller: A Multi-Zone Model Evaluation of the Efficacy of Upper-Room Air Ultraviolet Germicidal Irradiation, *Appl. Occup. Environ. Hyg. 14*:317-328, 1999

21. Baldwin, P.E.J., and A.D. Maynard: A Survey of Wind Speeds in Indoor Workplaces. *Ann. Occup. Hyg. 42*:303-313, 1998.

22. Wells, W.F.: *Airborne Contagion and Air Hygiene.* Cambridge, MA: Harvard University Press, 1955. pp. 105-141.

23. Riley, R.L. and E.A. Nardell: Clearing the Air: The Theory and Application of Ultraviolet Air Disinfection. *Am. Rev. Resp. Dis. 139*:1286-1294, 1989.

24. Hinds, W.C.: *Aerosol Technology.* New York: John Wiley & Sons, page 220.

25. Keil, C.B. and D.R. Krupinski: Eddy Diffusivity Measurements for Exposure Modeling. Abstract #182. American Industrial Hygiene Conference and Exposition, Dallas, TX, May 1997.

26. Drivas, P.J., P.A. Valberg, B.L. Murphy and R. Wilson: Modeling Indoor Air Exposure from Short-Term Point Source Releases. *Indoor Air 6*:271-277, 1996.

27. Fridkin, S.K., L. Manangan, E. Bolyard, and W.R. Jarvis: SHEA-CDC TB Survey, Part II: Efficacy of TB Infection Control Programs at Member Hospitals, 1989-1992. *Infect. Control Hosp. Epidemiol. 16*:135-140, 1995.

28. Grzybowski, S., G.D. Barnett and K. Styblo: Contacts of Cases of Active Pulmonary Tuberculosis. *Bull. Internat. Union Tuberculosis 50*:90-106, 1975.

29. Haley, C.E., R.C. McDonald, L. Rossi, W.D. Jones, R.W. Haley, and J.P. Luby: Tuberculosis Epidemic among Hospital Personnel. *Infection Control and Hosp. Epidemiol. 10*:204-210, 1989.

30. Nicas, M.: A Risk/Cost Analysis of Alternative Screening Intervals for Occupational Tuberculosis Infection. *Am. Ind. Hyg. Assoc. J. 59*:104-112, 1998

31. Nicas, M.: Markov Modeling of Contaminant Concentrations in Indoor Air, *Am. Ind. Hyg. Assoc. J.*, in press.

Grant-Related Publications:

1. **Nicas, M.** and E. Seto: A Simulation Model for Occupational Tuberculosis Transmission, *Risk Anal. 17*:606-616, 1997

2. **Nicas, M.** A Risk/Cost Analysis of Alternative Screening Intervals for Occupational Tuberculosis Infection, *Am. Ind. Hyg. Assoc. J. 59*:104-112, 1998

3. **Nicas, M.**: Assessing the Relative Importance of the Components of an Occupational Tuberculosis Control Program, *J. Occup. Environ. Med. 40*:648-654, 1998

4. Nazaroff, W., **M. Nicas** and S. Miller: Framework for Evaluating Measures to Control Nosocomial Tuberculosis Transmission, *Indoor Air 8*:205-218, 1998

5. **Nicas, M.** and S. Miller: A Multi-Zone Model Evaluation of the Efficacy of Upper-Room Air Ultraviolet Germicidal Irradiation, *Appl. Occup. Environ. Hyg. 14*:317-328, 1999

6. **Nicas, M.**: Markov Modeling of Contaminant Concentrations in Indoor Air, *Am. Ind. Hyg. Assoc. J.*, in press

7. **Nicas, M.**: Regulating the Risk of Tuberculosis Transmission among Health Care Workers, *Am. Ind. Hyg. Assoc. J.*, in press

8. **Nicas, M.**: Modeling Turbulent Diffusion and Advection of Indoor Air Contaminants by Markov Chains, submitted to *Ann. Occup. Hyg.*

Intended Future Grant-Related Publications:

Nicas, M. and E. Seto: Variability in Tuberculosis Infection and Disease Incidence as Assessed by a Simulation Model, manuscript in preparation

Fischer, S.L., S. Miller and **M. Nicas**: Time Series Analysis of Carbon Monoxide Levels Measured in the Near-Field and Far-Field of An In-Room Source, manuscript in preparation

Appendix 1
Single-State Transition Probabilities for Markov Model II

The probabilities are derived with reference to those in Markov model I. For convenience, the formulae for p (the jump probability to one of the adjacent states) and h (the hold probability) for an interior state particle in a given Markov chain in model I are reproduced below:

Eq. (A1) $$p = \frac{D \cdot \Delta t}{(\Delta x)^2}$$

Eq. (A2) $$h = 1 - 2 \cdot p$$

For a particle in a wall border state (at the ends of the Markov chain), the respective hold and jump probabilities are:

Eq. (A3) $$\text{Hold Probability} = h + p = 1 - p$$

Eq. (A4) $$\text{Jump Probability} = p$$

The wall border probabilities are specified to create a uniform probability distribution at equilibrium. More formally, if there are m states in the chain, and if π_i denotes the probability that a particle is in the i^{th} state after a large number of transitions (where $\sum_{i=1}^{m} \pi_i = 1$), then Equations A1 – A4 lead to: $\pi_i = 1/m$, for $i = 1,2,\ldots, m$.

Given that a particle cannot leave the room, the particle position described by model II has a corresponding position in each of the three independent chains in model I. For the moment, assume that a particle can move only by diffusion. The probability that a model II interior cell particle holds its position is the product of the independent probabilities that it holds its position in each of the three model I chains:

Eq. (A5) $$h_{I,D} = h^3$$

The corresponding probability that the model II interior cell particle moves to a given nearest neighbor (of which there are six) is 1/6 times $1 - h_{I,D}$, or:

Eq. (A6) $$p_{I,D} = \frac{1}{6} \cdot \left(1 - h^3\right)$$

Similarly, a model II particle that borders one specific wall surface has a wall border position in one model I chain, and interior cell positions in the other two model I chains. The probability that it holds its position is the product of the probabilities that it holds its wall-border position in the first chain and holds its interior cell positions in the other two chains, or:

Eq. (A7) $$h_{\text{one-wall,D}} = (h+p)\cdot h^2$$

The corresponding probability that a model II particle bordering one wall surface moves to a given nearest neighbor (of which there are five) is 1/5 times $1 - h_{\text{one-wall,D}}$, or:

Eq. (A8) $$p_{\text{one-wall,D}} = \frac{1}{5}\cdot\left(1 - (h+p)\cdot h^2\right)$$

By similar arguments, the respective hold and jump probabilities for a model II particle that borders two wall surfaces or three wall surfaces can be derived:

Eq. (A9) $$h_{\text{two-walls,D}} = (h+p)^2\cdot h$$

Eq. (A10) $$p_{\text{two-walls,D}} = \frac{1}{4}\cdot\left(1 - (h+p)^2\cdot h\right)$$

Eq. (A11) $$h_{\text{three-walls,D}} = (h+p)^3$$

Eq. (A12) $$p_{\text{three-walls,D}} = \frac{1}{3}\cdot\left(1 - (h+p)^3\right)$$

Next, assume that a particle can move by advective flow as well as diffusion, where s_A is the advective air speed. For simplicity, assume that advective flow is perpendicular to only one cell face with area $(\Delta x)^2$. The advective air supply, $s_A\cdot(\Delta x)^2$, divided by the cell volume, $(\Delta x)^3$, corresponds to $s_A/\Delta x$ air changes per sec and is treated as dilution air. Now, consider any cell subject to advective flow in Markov model II. The probability that a particle in the cell is not removed by advection in interval Δt is denoted $h_{\cdot,A}$ (where the dot subscript signifies that the cell's position need not be specified), and is given by:

Eq. (A13) $$h_{\cdot,A} = e^{-\left(\frac{s_A}{\Delta x}\right)\Delta t}$$

If particle removal from the cell by diffusive flow and by advective flow are treated as independent mechanisms, the probability that the particle holds its position is the product of the hold probability based on diffusion alone and the hold probability based on advection alone. Therefore:

Eq. (A14) Hold Probability for an Interior Cell Particle $= h_{I,D} \cdot h_{\cdot,A}$

Eq. (A15) Hold Probability for a One-Wall Border Particle $= h_{\text{one-wall},D} \cdot h_{\cdot,A}$

Eq. (A16) Hold Probability for a Two-Wall Border Particle $= h_{\text{two-wall},D} \cdot h_{\cdot,A}$

Eq. (A17) Hold Probability for a Three-Wall Border Particle $= h_{\text{three-wall},D} \cdot h_{\cdot,A}$

If $s_A = 0$, these expressions simplify to the hold probabilities due to diffusion alone. The derivation of the jump probabilities where both diffusion and advection apply is presented for an interior cell particle. The hold probability can be written as:

$$h_{I,D} \cdot h_{\cdot,A} = e^{\ln(h_{I,D})} \cdot e^{-\left(\frac{s_A}{\Delta x}\right)\Delta t} = e^{-\left[-\ln(h_{I,D}) + \left(\frac{s_A}{\Delta x}\right)\Delta t\right]}$$

For notational simplicity, let $\alpha = -\ln(h_{I,D})$, in which case:

$$e^{-\left[-\ln(h_{I,D}) + \left(\frac{s_A}{\Delta x}\right)\Delta t\right]} = e^{-\left[\alpha + \left(\frac{s_A}{\Delta x}\right)\Delta t\right]}$$

The power term $\alpha + (s_A / \Delta x) \cdot \Delta t$ is a type of exponential rate, and can be treated as the sum of six independent rates. The quantity $(1/6) \cdot \alpha + (s_A / \Delta x) \cdot \Delta t$ is the rate at which a particle moves to the downstream neighboring cell (by diffusion or advection), where it is assumed for simplicity that advective flow from a cell is in just one direction. The quantity $(1/6) \cdot \alpha$ is the respective rate at which the particle moves to each of the other five neighboring cells (by diffusion alone). Given that the particle moves, the probability that it moves to a specific neighboring cell is the rate of movement to that cell divided by the total rate of movement. Because the probability that the particle moves is $1 - h_{I,D} \cdot h_{\cdot,A}$, it follows that:

Eq. (A18) $$p_{I,\text{down}} = \frac{(1/6) \cdot \alpha + (s_A / \Delta x) \cdot \Delta t}{\alpha + (s_A / \Delta x) \cdot \Delta t} \cdot (1 - h_{I,D} \cdot h_{I,A})$$

Eq. (A19) $$p_{I,\text{other}} = \frac{(1/6) \cdot \alpha}{\alpha + (s_A / \Delta x) \cdot \Delta t} \cdot (1 - h_{I,D} \cdot h_{I,A})$$

By similar arguments, the jump probabilities for a particle in the other cells can be derived:

Eq. (A20) $$p_{\text{one-wall,down}} = \frac{(1/5)\cdot\left[-\ln\left(h_{\text{one-wall,D}}\right)\right] + \left(s_A/\Delta x\right)\cdot\Delta t}{\left[-\ln\left(h_{\text{one-wall,D}}\right)\right] + \left(s_A/\Delta x\right)\cdot\Delta t}\cdot\left(1 - h_{\text{one-wall,D}}\cdot h_{\cdot,A}\right)$$

Eq. (A21) $$p_{\text{one-wall,other}} = \frac{(1/5)\cdot\left[-\ln\left(h_{\text{one-wall,D}}\right)\right]}{\left[-\ln\left(h_{\text{one-wall,D}}\right)\right] + \left(s_A/\Delta x\right)\cdot\Delta t}\cdot\left(1 - h_{\text{one-wall,D}}\cdot h_{\cdot,A}\right)$$

Eq. (A22) $$p_{\text{two-wall,down}} = \frac{(1/4)\cdot\left[-\ln\left(h_{\text{two-wall,D}}\right)\right] + \left(s_A/\Delta x\right)\cdot\Delta t}{\left[-\ln\left(h_{\text{two-wall,D}}\right)\right] + \left(s_A/\Delta x\right)\cdot\Delta t}\cdot\left(1 - h_{\text{two-wall,D}}\cdot h_{\cdot,A}\right)$$

Eq. (A23) $$p_{\text{two-wall,other}} = \frac{(1/4)\cdot\left[-\ln\left(h_{\text{two-wall,D}}\right)\right]}{\left[-\ln\left(h_{\text{two-wall,D}}\right)\right] + \left(s_A/\Delta x\right)\cdot\Delta t}\cdot\left(1 - h_{\text{two-wall,D}}\cdot h_{\cdot,A}\right)$$

Eq. (A24) $$p_{\text{three-wall,down}} = \frac{(1/3)\cdot\left[-\ln\left(h_{\text{three-wall,D}}\right)\right] + \left(s_A/\Delta x\right)\cdot\Delta t}{\left[-\ln\left(h_{\text{three-wall,D}}\right)\right] + \left(s_A/\Delta x\right)\cdot\Delta t}\cdot\left(1 - h_{\text{three-wall,D}}\cdot h_{\cdot,A}\right)$$

Eq. (A25) $$p_{\text{three-wall,other}} = \frac{(1/3)\cdot\left[-\ln\left(h_{\text{three-wall,D}}\right)\right]}{\left[-\ln\left(h_{\text{three-wall,D}}\right)\right] + \left(s_A/\Delta x\right)\cdot\Delta t}\cdot\left(1 - h_{\text{three-wall,D}}\cdot h_{\cdot,A}\right)$$

Table 1

The mean number of total infections plus or minus one standard deviation at five years without accounting for subsequent TB disease among health care workers.

Risk Group Sizes	Mean TB Patients/Yr	Total Infections
X = 600, Y = 300, Z = 100	5	12.5 ± 4.3
	50	103.7 ± 9.9
X = 850, Y = 100, Z = 50	5	6.3 ± 2.7
	50	53.1 ± 6.7

Table 2

The mean number of total and secondary infections plus or minus one standard deviation, and the mean number of disease cases plus or minus one standard deviation, at five years when accounting for subsequent TB disease among health care workers but no close contacts.

Risk Group Sizes	Mean TB Patients/Yr	Total Infections	Secondary Infections	Disease Cases
X = 600, Y = 300, Z = 100	5	13 ± 4.6	0.4 ± 0.8	0.6 ± 0.8
	50	106.3 ± 9.9	2.9 ± 2.1	5.1 ± 2.3
X = 850, Y = 100, Z = 50	5	6.5 ± 2.9	0.1 ± 0.3	0.3 ± 0.5
	50	53.8 ± 6.6	0.8 ± 1.1	2.7 ± 1.8

Table 3

The mean number of total and secondary infections plus or minus one standard deviation, and mean number of disease cases plus or minus one standard deviation, at five years when accounting for subsequent TB disease among health care workers plus close contacts.

Risk Group Sizes	Mean TB Patients/Yr	Total Infections $\bar{x} \pm s$	Secondary Infections $\bar{x} \pm s$	Disease Cases $\bar{x} \pm s$
X = 600, Y = 300, Z = 100	5	16.7 ± 8.5	4.2 ± 6.7	0.7 ± 1.1
	50	140.2 ± 24	38.6 ± 22	6.5 ± 3.5
X = 850, Y = 100, Z = 50	5	8.6 ± 6.3	2.4 ± 5.3	0.4 ± 0.8
	50	70.6 ± 16	19.1 ± 14	3.4 ± 2.4

Table 4

The mean plus or minus one standard deviation of the total number of infections, the number of secondary infections, and the total number of disease cases at the end of five years, given 5 vs. 50 TB patients admitted annually on average, constant patient infectivity, PPD skin testing programs of varying test frequency, and 0% vs. 90% successful participation.

Cohort Outcome	0% Screened	90% Screened at 12 months	90% Screened at 6 months	90% Screened at 3 months
	50 TB patients admitted annually on average			
Total Number of Infections	140 ± 24	118 ± 15	112 ± 14	109 ± 12
Number of Secondary Infections	39 ± 22	18 ± 12	10 ± 10	6.3 ± 7.2
Total Number of Disease Cases	6.5 ± 3.5	3.2 ± 2	1.7 ± 1.6	1.2 ± 1.2
	5 TB patients admitted annually on average			
Total Number of Infections	17 ± 8.5	15 ± 6.2	14 ± 5.9	13 ± 5.5
Number of Secondary Infections	4.2 ± 6.7	2.4 ± 4.4	1.2 ± 3.5	1.0 ± 3.5
Total Number of Disease Cases	0.7 ± 1.1	0.4 ± 0.7	0.2 ± 0.5	0.2 ± 0.6

Table 5

The mean plus or minus one standard deviation of the total number of infections, the number of secondary infections, and the total number of disease cases at the end of five years given: X = 600, Y = 300, Z = 100; T = 5 vs. 50 TB patients admitted annually on average; a PPD skin testing program with a 6-month testing frequency and 90% successful participation; and three distributions of patient infectivity values: (*i*) constant infectivity; (*ii*) uniformly distributed infectivity; and (*iii*) binary infectivity.

Cohort Outcome	Distribution of Patient Infectivity		
	Constant	Uniform	Binary
	50 TB patients admitted annually on average		
Total Number of Infections	112 ± 14	112 ± 13	111 ± 30
Number of Secondary Infections	10 ± 10	10 ± 9.0	11 ± 11
Total Number of Disease Cases	1.7 ± 1.6	1.8 ± 1.5	1.8 ± 1.7
	5 TB patients admitted annually on average		
Total Number of Infections	14 ± 5.9	14 ± 5.6	14 ± 13
Number of Secondary Infections	1.2 ± 3.5	1.3 ± 3.1	1.4 ± 4.3
Total Number of Disease Cases	0.2 ± 0.5	0.2 ± 0.5	0.2 ± 0.6

Table 6

The mean plus or minus one standard deviation of the total number of infections, the number of secondary infections, and the total number of disease cases at the end of five years, given: X = 600, Y = 300, Z = 100; no PPD skin testing program in place; and 1, 3 or 5 immmuno-compromised workers in the high-risk group.

	Cohort Outcome		
Number of Immunocompromised Workers	Total Number of Infections	Number of Secondary Infections	Total Number of Disease Cases
0	140 ± 24	39 ± 22	6.5 ± 3.5
1	141 ± 25	40 ± 22	6.8 ± 3.6
3	142 ± 25	42 ± 23	7.0 ± 3.6
5	144 ± 24	43 ± 22	7.3 ± 3.6

Table 7

The mean plus or minus one standard deviation of the total number of infections, the number of secondary infections, and the total number of disease cases at the end of five years, given: X = 600, Y = 300, Z = 100; zero (0) versus five (5) immmunocompromised workers in the high-rsik group; and PPD skin testing programs of varying test frequency

Number of Immunocompromised Workers	Cohort Outcome: Total Number of Infections	Number of Secondary Infections	Total Number of Disease Cases
	3 month screening interval		
0	109 ± 12	6.3 ± 7.2	1.2 ± 1.2
5	115 ± 13	9.5 ± 8.8	1.7 ± 1.4
	6 month screening interval		
0	112 ± 14	10 ± 10	1.7 ± 1.6
5	117 ± 14	14 ± 11	2.4 ± 1.7
	12 month screening interval		
0	118 ± 15	18 ± 12	3.2 ± 2
5	123 ± 15	21 ± 13	3.6 ± 2.1

Table 8

The total cost (TC) and the cost per disease case prevented (C/DCP) in thousands of dollars at 12 years given different annual rates of infection, alternative screening intervals, 1000 initially susceptible employees, and a perfect screening program, $p = 1.0$ (0% false negative error in skin testing, 0% noncompliance with testing, 0% failure of prophylaxis).

Screening Interval (months)	Annual Rate of Infection 0.2% TC	0.2% C/DCP	0.5% TC	0.5% C/DCP	1.0% TC	1.0% C/DCP	5.0% TC	5.0% C/DCP
3	480	431	479	175	478	89	463	21
6	242	252	246	104	252	55	286	15
9	164	202	171	85	180	46	242	15
12	126	189	134	82	148	46	234	18
18	88	190	99	87	118	53	234	25
24	69	190	82	92	103	59	235	32
36	50	197	65	103	88	72	237	45
144*	13	--	31	--	61	--	250	--

* denotes no screening

Table 9

The total cost (TC) and the cost per disease case prevented (C/DCP) in thousands of dollars at 12 years given different annual rates of infection, alternative screening intervals, 1000 initially susceptible employees, and an imperfect screening program, $p = 0.88$ (5% false negative error in skin testing, 0% noncompliance with testing, 7% failure of prophylaxis).

Screening Interval	Annual Rate of Infection							
	0.2%		0.5%		1.0%		5.0%	
(months)	TC	C/DCP	TC	C/DCP	TC	C/DCP	TC	C/DCP
3	481	490	482	199	484	103	490	25
6	244	287	249	119	257	63	309	18
9	165	230	173	98	185	54	261	18
12	127	216	136	94	152	54	249	21
18	88	215	101	99	121	61	245	29
24	69	216	83	105	105	68	243	38
36	50	224	66	118	90	83	243	53
144*	13	--	31	--	61	--	250	--

* denotes no screening

Table 10

Three-Zone Model Parameters for the *M. bovis* UVGI Room Study

	Day 1[A]	Day 2[B]	Day 3[B]
Reported Eq ACH, UV Off	2	2.5[C]	4
Reported Eq ACH, UV On	12	21	37
Required k_2 value (min^{-1})	1.28	0.80	1.95
$C_{WM,SS}$ (#/m^3) with UV On based on reported Eq ACH	G/12.8	G/22.5	G/39.5
$C_{NF,SS}$ (#/m^3) with UV On based on reported Eq ACH	G/5.3	G/6.0	G/6.8
$C_{NF,SS} / C_{WM,SS}$	2.4	3.8	5.8
$C_{L,SS}$ (#/m^3) with UV On based on reported Eq ACH	G/11.6	G/15.7	G/23.4
$C_{U,SS}$ (#/m^3) with UV On based on reported Eq ACH	G/17.6	G/29.4	G/72.9
$C_{NF,SS} / C_{U,SS}$	3.3	4.9	10.7

(A) One 17-W UV light fixture was operated on the first test day.
(B) One 17-W and one 29-W UV light fixture (supplying a total of 46 W) were operated on the second and third test days.
(C) The Eq ACH with UV lights off was reported as an estimate of 2 to 3 Eq ACH. The midpoint value of 2.5 Eq ACH was chosen for this analysis.

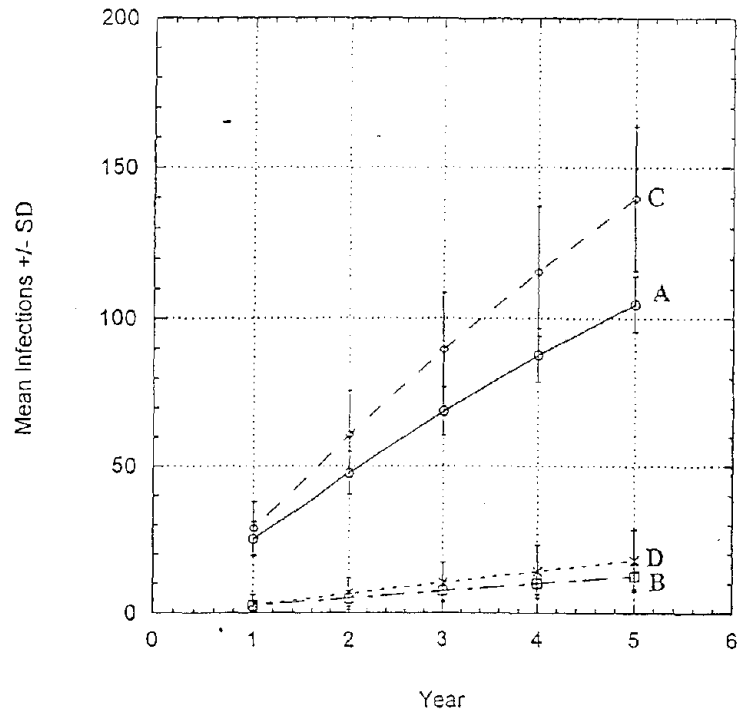

Figure 1 - The mean number of total infections plus or minus one standard deviation at at one-year intervals over the five-year simulation period for four scenarios involving X = 600, Y = 300, and Z = 100 susceptible workers. Curves A and B correspond to, respectively, T = 50 and T = 5 TB patients admitted annually on average in the scenario that does not account for subsequent TB disease among infected workers. Curves C and D correspond to, respectively, T = 50 and T = 5 TB patients admitted annually on average in the scenario that accounts for subsequent TB disease among infected workers plus 25 close contacts per diseased worker.

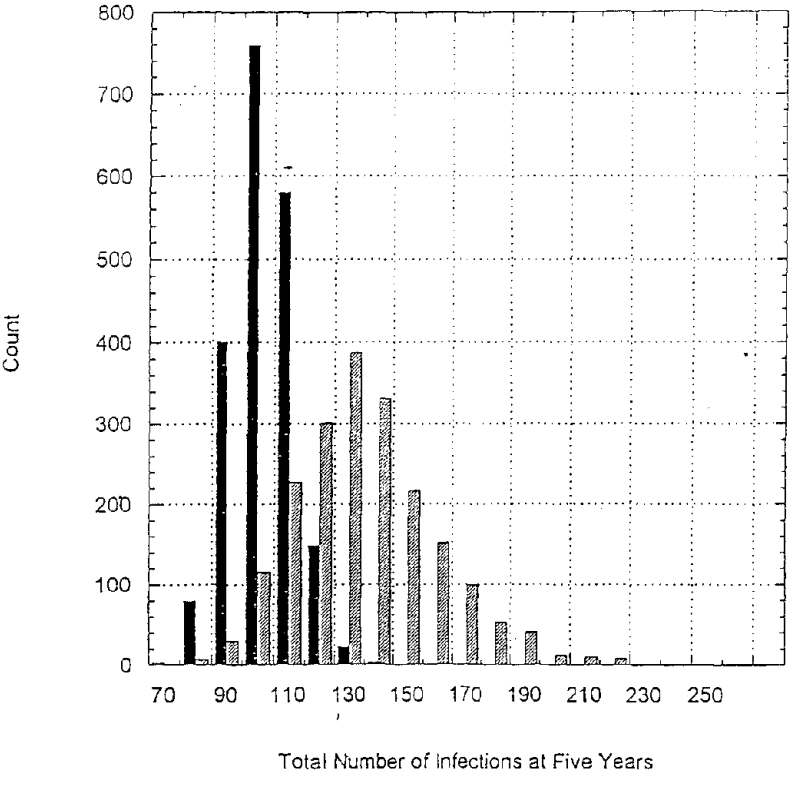

Figure 2 - The distribution of simulation outcomes of the total number of infections at five years in two scenarios involving X = 600, Y = 300, and Z = 100 susceptible workers, and T = 50 TB patients admitted annually on average. The dark bars represent the distribution in the scenario that does not account for subsequent TB disease among infected workers. The light bars represent the distribution in the scenario that accounts for subsequent TB disease among infected workers plus 25 close contacts per diseased worker.

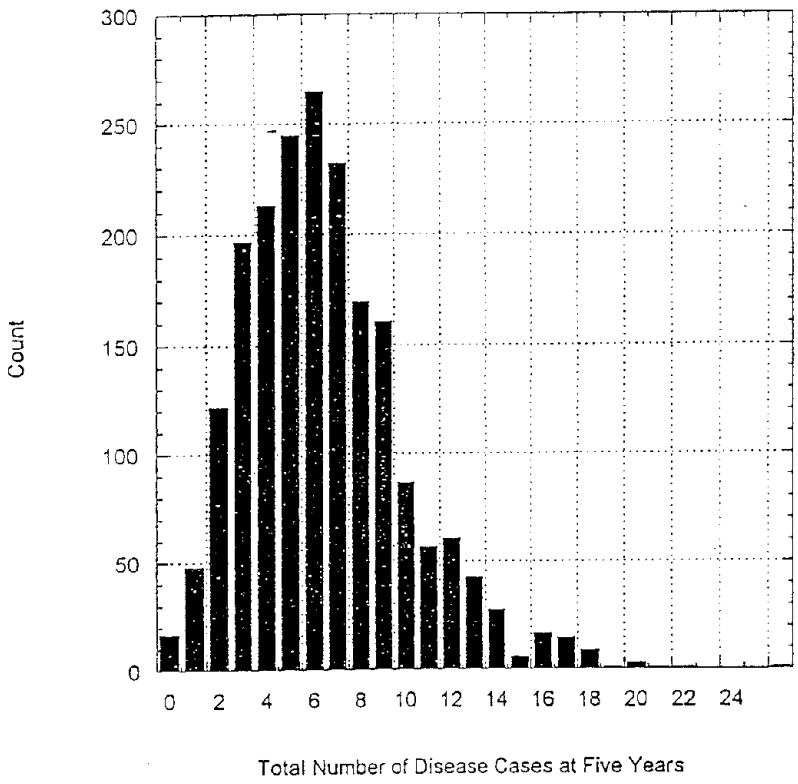

Figure 3 - The distribution of simulation outcomes of the total number of disease cases at five years in the scenario involving X = 600, Y = 300, and Z = 100 susceptible workers, T = 50 TB patients admitted annually on average, and accounting for subsequent TB disease among infected workers plus 25 close contacts per diseased worker.

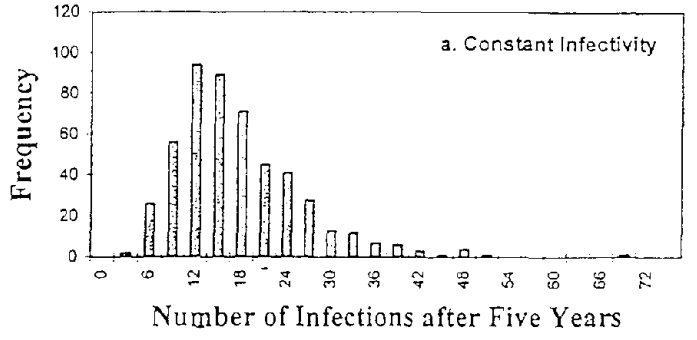

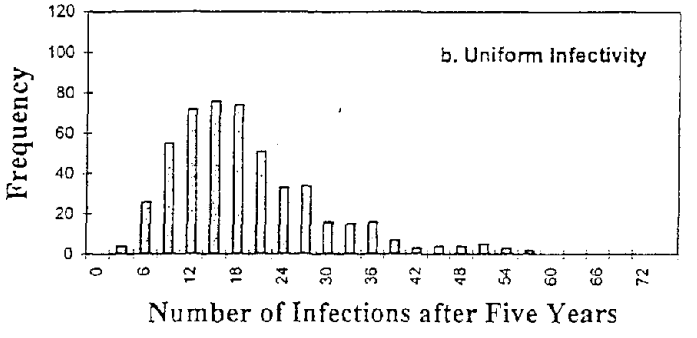

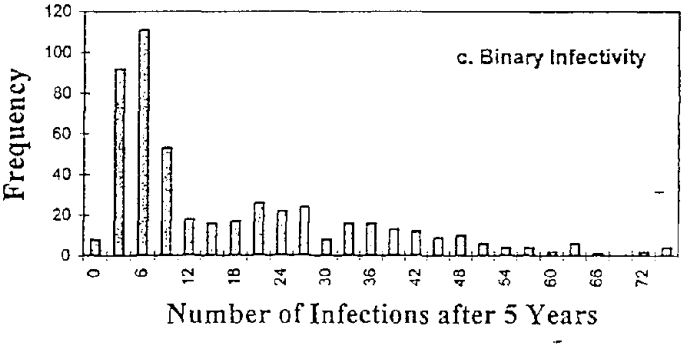

Figure 4 – The distribution of simulation outcomes of the total number of infections at five years in the scenario involving X = 600, Y = 300, and Z = 100 susceptible workers, T = 5 TB patients admitted annually on average, accounting for subsequent TB disease among infected workers (plus 25 close contacts per diseased worker), and 90% successful participation in an infection surveillance program with a 6-month PPD skin testing interval. In **panel (a)**, constant infectivity per patient was assumed. In **panel (b)**, a uniform distribution of patient infectivity was assumed. In **panel (c)**, a binary distribution of patient infectivity was assumed.

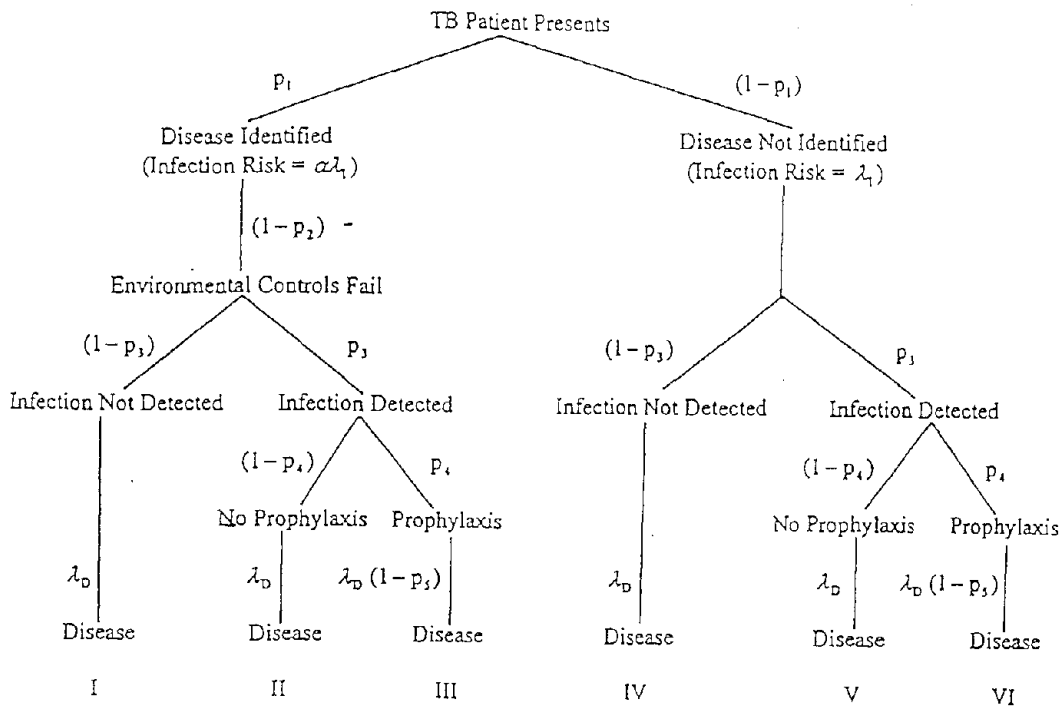

Figure 5 - Six event series that can lead to occupational tuberculosis disease among susceptible healthcare workers in the presence of an infection/disease control program. The notation is summarized below:

λ_I = average infection risk to employees due to patients with undetected TB disease

α = fraction of average infection risk to employees due to early treatment of patients with identified TB disease

λ_D = risk of developing TB disease subsequent to infection without antibiotic prophylaxis

p_1 = probability that TB disease in a presenting patient is rapidly detected

p_2 = probability that environmental controls eliminate exposure to infectious aerosol

p_3 = probability that a new infection in an employee is detected

p_4 = probability that a newly infected employee undergoes antiobiotic prophylaxis

p_5 = probability that antiobiotic prophylaxis eliminates the risk of developing TB disease

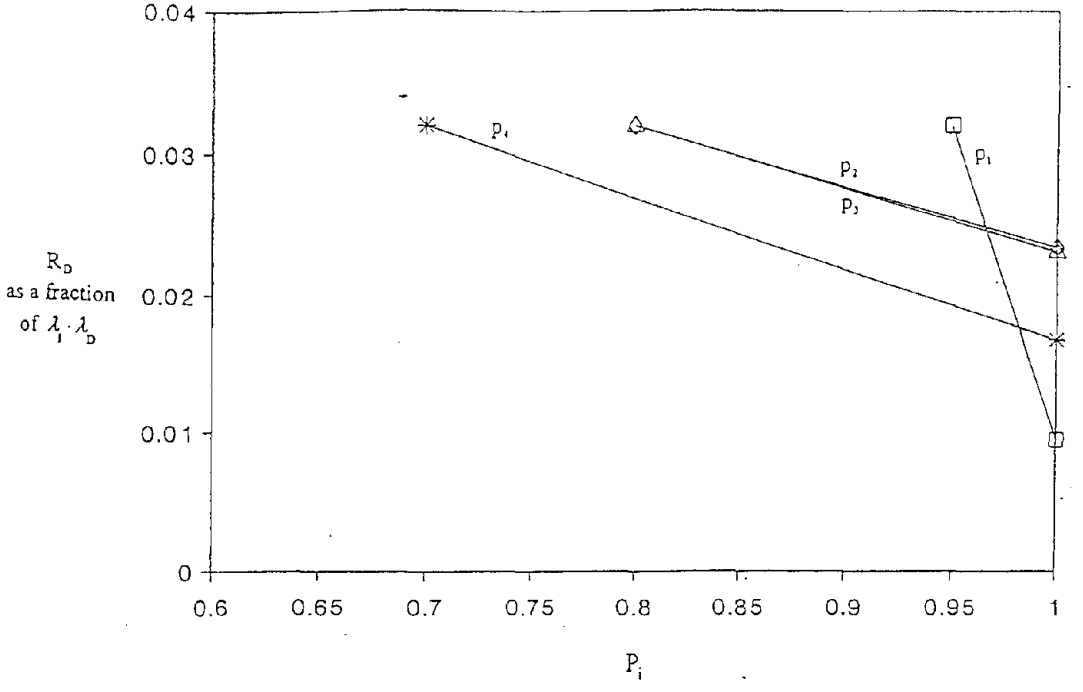

Figure 6 - The decrease in occupational tuberculosis disease risk, R_D, with one-at-a-time increases in the respective intervention parameters p_1, p_2, p_3, and p_4. The initial parameter values are $p_1 = 0.95$, $p_2 = 0.8$, $p_3 = 0.7$, $p_4 = 0.8$, $p_5 = 0.93$, and $\alpha = 0.1$. The values of p_1 through p_4 constitute a "typical" scenario. The p_1 line is indicated by the squares, the p_2 line by the diamonds, the p_3 line by the asterisks, and the p_4 line by the triangles.

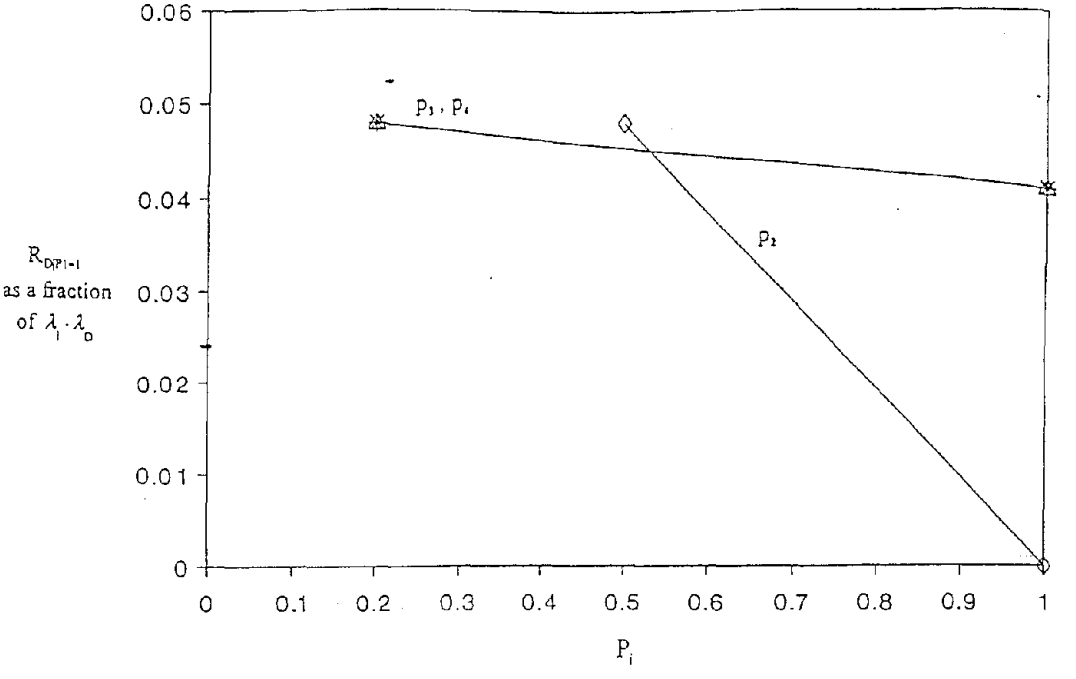

Figure 7 - The decrease in occupational tuberculosis disease risk given that patient disease has been identified, $R_{D|P_i=1}$, with one-at-a-time increases in the respective intervention parameters p_2, p_3, and p_4. The initial parameter values are $p_2 = 0.5$, $p_3 = 0.2$, $p_4 = 0.2$, $p_5 = 0.93$, and $\alpha = 0.1$. The low values of p_2 through p_4 constitute a "worst-case" scenario. The p_2 line is indicated by the diamonds, the p_3 line by the asterisks, and the p_4 line by the triangles.

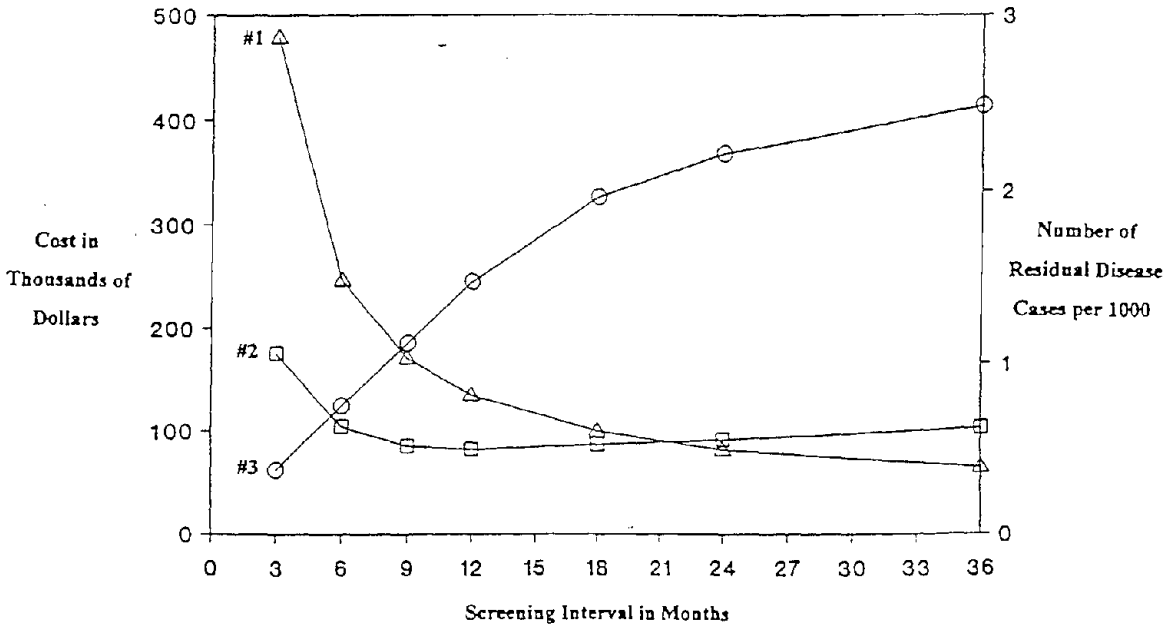

Figure 8 - Costs and residual disease risks at 12 years for alternative *M. tb* infection screening intervals given an annual rate of infection of 0.5%, costs of $10 per PPD skin test and $10,000 per TB disease case, and a perfect screening program, $p = 1.0$ (based on $q_1 = 0$, $q_2 = 0$, $q_3 = 0$). Curve #1 (triangles) shows the total cost (in thousands of dollars). Curve #2 (squares) shows the cost per disease case prevented (in thousands of dollars). Curve #3 (circles) shows the expected number of residual disease cases per 1000 initially susceptible employees.

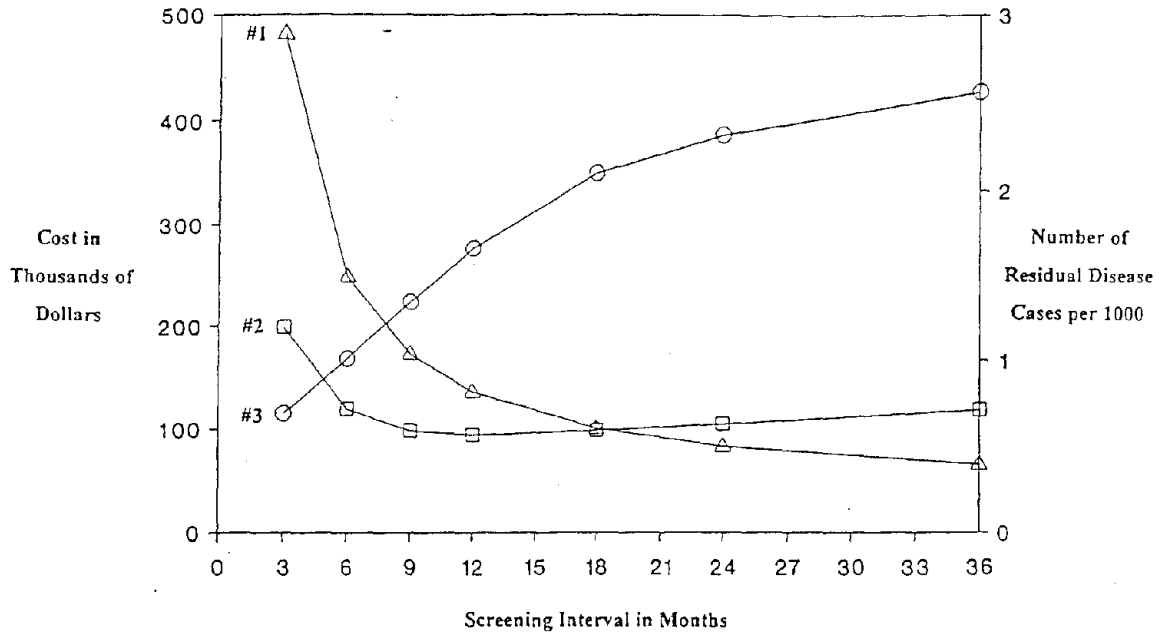

Figure 9 - Costs and residual disease risks at 12 years for alternative *M. tb* infection screening intervals given an annual rate of infection of 0.5%, costs of $10 per PPD skin test and $10,000 per TB disease case, and an imperfect screening program with $p = 0.88$ (based on $q_1 = .05$, $q_2 = 0$, $q_3 = .07$). Curve #1 (triangles) shows the total cost (in thousands of dollars). Curve #2 (squares) shows the cost per disease case prevented (in thousands of dollars). Curve #3 (circles) shows the expected number of residual disease cases per 1000 initially susceptible employees.

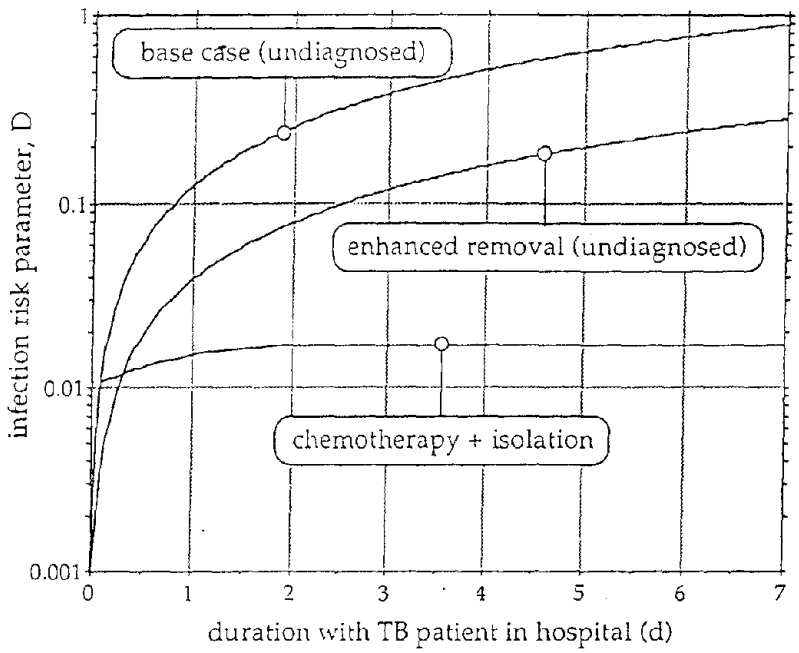

Figure 10 - Predicted cumulative infection risk parameter D since the time (days) of TB patient admission for a single infectious patient in a hospital ward.

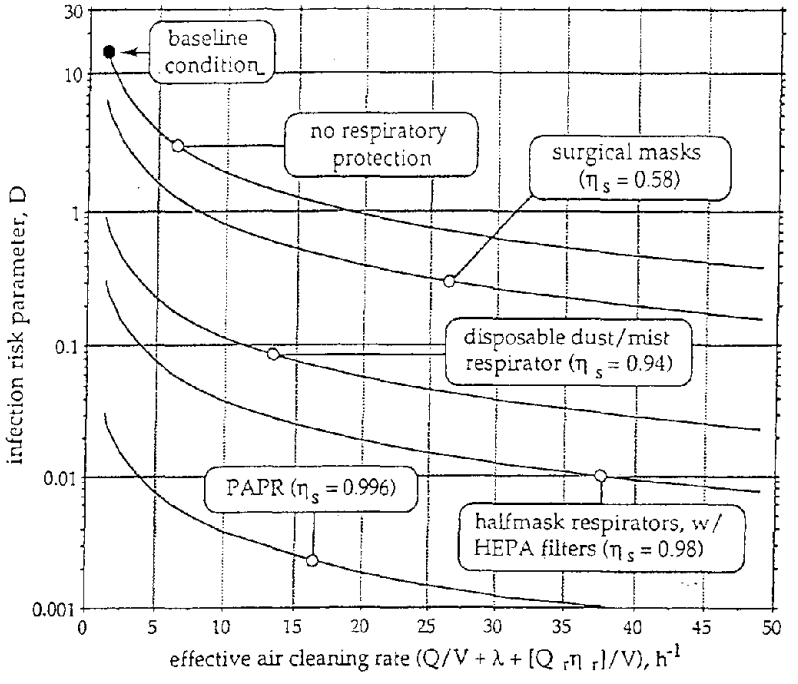

Figure 11 - Predicted infection risk parameter D for a scenario involving exposure of 13 health care workers for 150 minutes to a highly infectious TB patient during a bronchoscopy procedure, as described by Catanzaro, reference 14. The efficacy of wearing four alternative respirator devices (with respective efficiencies η_s) and of increasing the air cleaning rate (the effective ventilation rate) in ACH is shown.

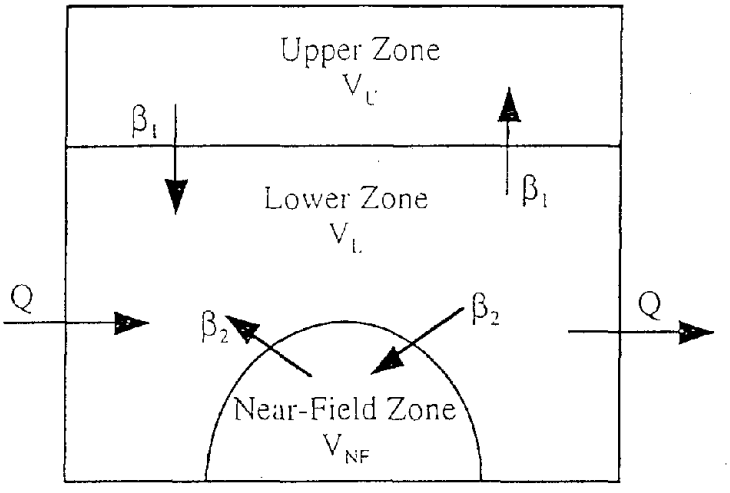

Figure 12 - A schematic representation of a three-zone room. V_U, V_L and V_{NF} are the respective upper zone, lower zone and near-field zone volumes (m^3). Q is the total room supply/exhaust air rate (m^3/min), with all air supply and exit points in the lower zone. β_1 is the air-exchange rate between the upper and lower zones (m^3/min). β_2 is the air-exchange rate between the lower and near-field zones (m^3/min).

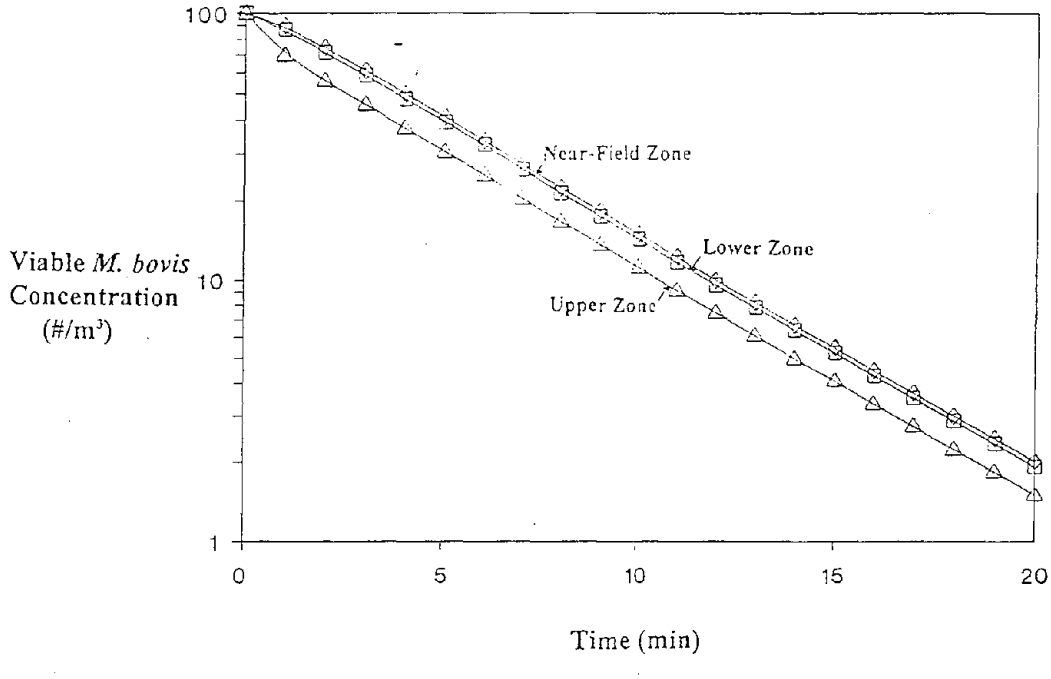

Figure 13 - The decay in the viable *M. bovis* concentration according to the three-zone model, where the initial concentration is 100 per m^3 in all three zones. Model parameter values are as follows: $V_U = 11.2\ m^3$, $V_L = 50.7\ m^3$, $V_{NF} = 2.1\ m^3$, $Q = 2\ m^3/min$, $\beta_1 = 28\ m^3/min$, $\beta_2 = 9.6\ m^3/min$, $k_1 = .00235\ min^{-1}$, $k_2 = 1.28\ min^{-1}$.

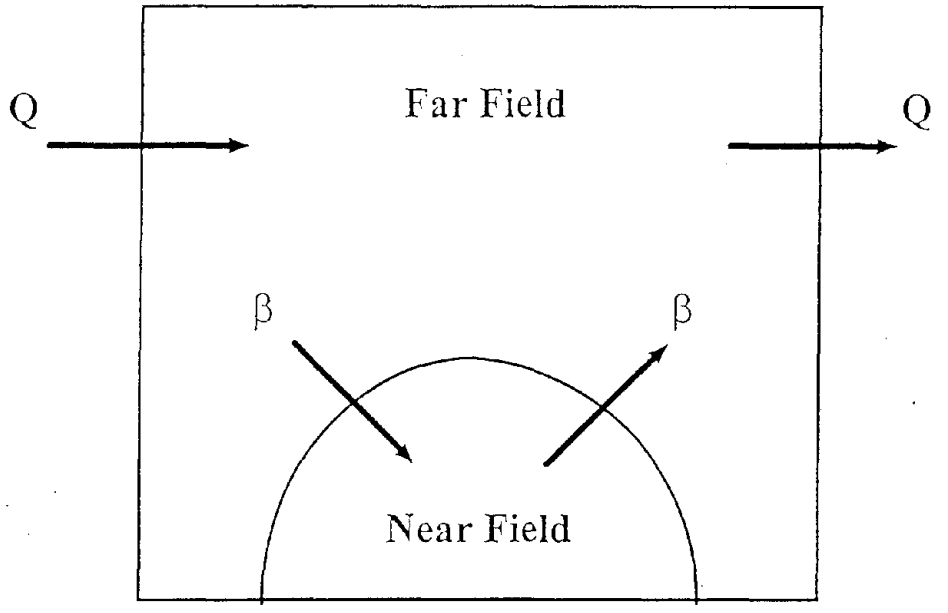

Figure 14 - A hypothetical two-zone room containing a near-field zone around a contaminant emission source; the remainder of the room constitutes the far-field zone. Supply air enters and room air exits the far field at rate Q (m^3/sec). A balanced random air flow at rate β (m^3/sec) occurs between the near-field and far-field zones.

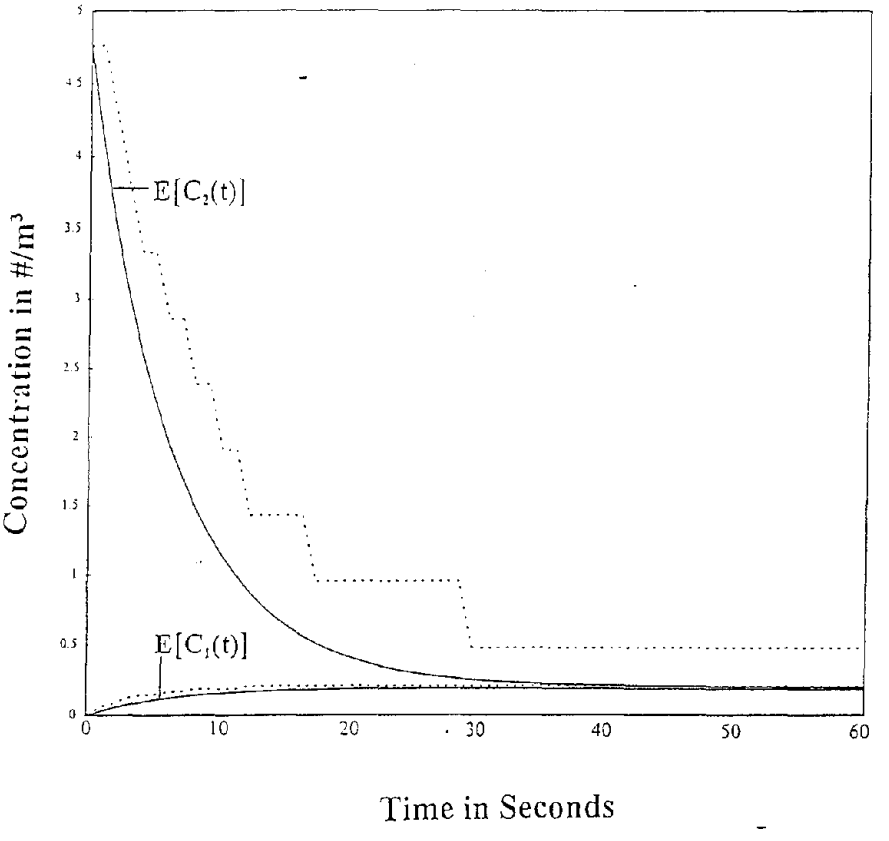

Figure 15 - The *M. tb* particle concentrations in the near-field and far-field zones in the first 60 seconds following a pulse release of 10 particles into the near field at time zero. The solid-line curve labeled $E[C_2(t)]$ is the expected near-field particle concentration, and the solid-line curve labeled $E[C_1(t)]$ is the expected far-field particle concentration. The dotted line immediately above each expected concentration curve is the approximate 95th percentile value for the corresponding particle concentration. For example, at t = 25 sec, the expected near-field particle concentration is 0.29 per m^3, and there is an approximate 95% probability that the near-field concentration is ≤ 0.95 per m^3.

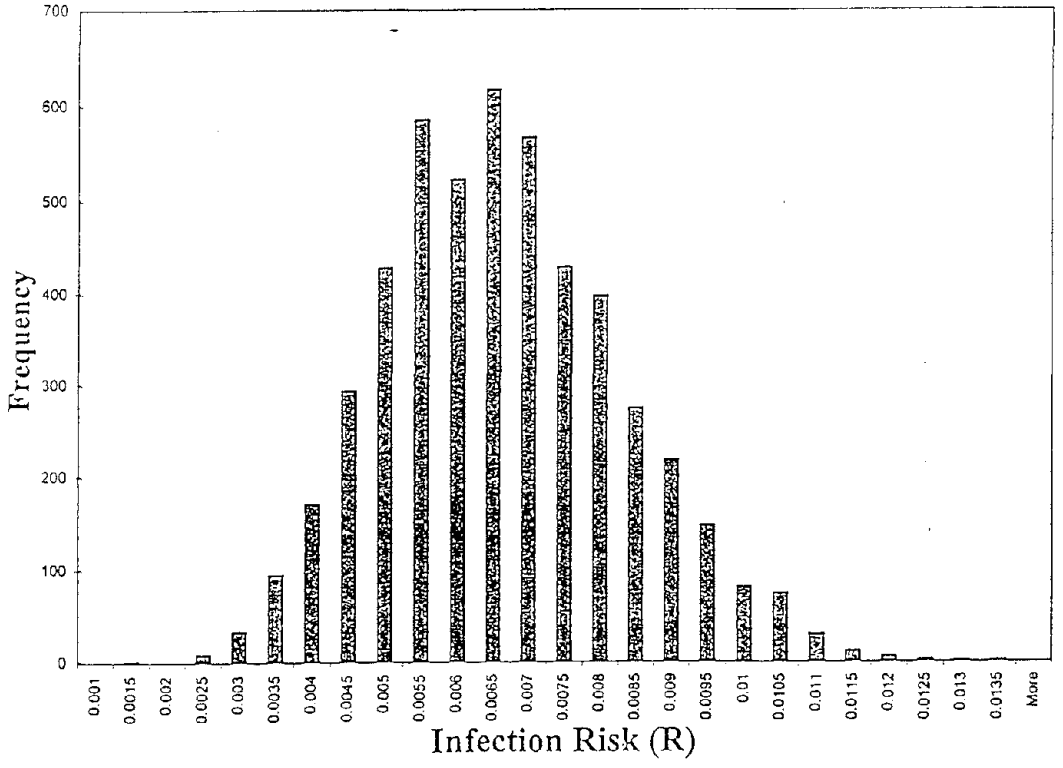

Figure 16 - The distribution of approximate *M. tb* infection risk values across 10^5 simulations of a near-field/far-field scenario in which a health care worker is in the near field of a tuberculosis patient for five minutes immediately after the patient emits 10 *M. tb* particles. For this distribution, E[R] ≅ .0069 and SD[R] ≅ .0017.

$$
PX = \begin{array}{c} \\ 1 \\ 2 \\ 3 \\ \cdot \\ \cdot \\ 98 \\ 99 \\ 100 \end{array}
\begin{array}{c}
\begin{array}{ccccccccc} 1 & 2 & 3 & & & 98 & 99 & 100 \end{array} \\
\begin{bmatrix}
h+p & p & 0 & 0 & \cdots & 0 & 0 & 0 \\
p & h & p & 0 & \cdots & 0 & 0 & 0 \\
0 & p & h & p & \cdots & 0 & 0 & 0 \\
\cdots & \cdots & \cdots & \cdots & \cdots & \cdots & \cdots & \cdots \\
\cdots & \cdots & \cdots & \cdots & \cdots & \cdots & \cdots & \cdots \\
0 & 0 & 0 & \cdots & p & h & p & 0 \\
0 & 0 & 0 & \cdots & 0 & p & h & p \\
0 & 0 & 0 & \cdots & 0 & 0 & p & h+p
\end{bmatrix}
\end{array}
$$

Figure 17– The single-step transition probability matrix **P** for the particle position along a 10-m room axis divided into one hundred 0.1-m segments.

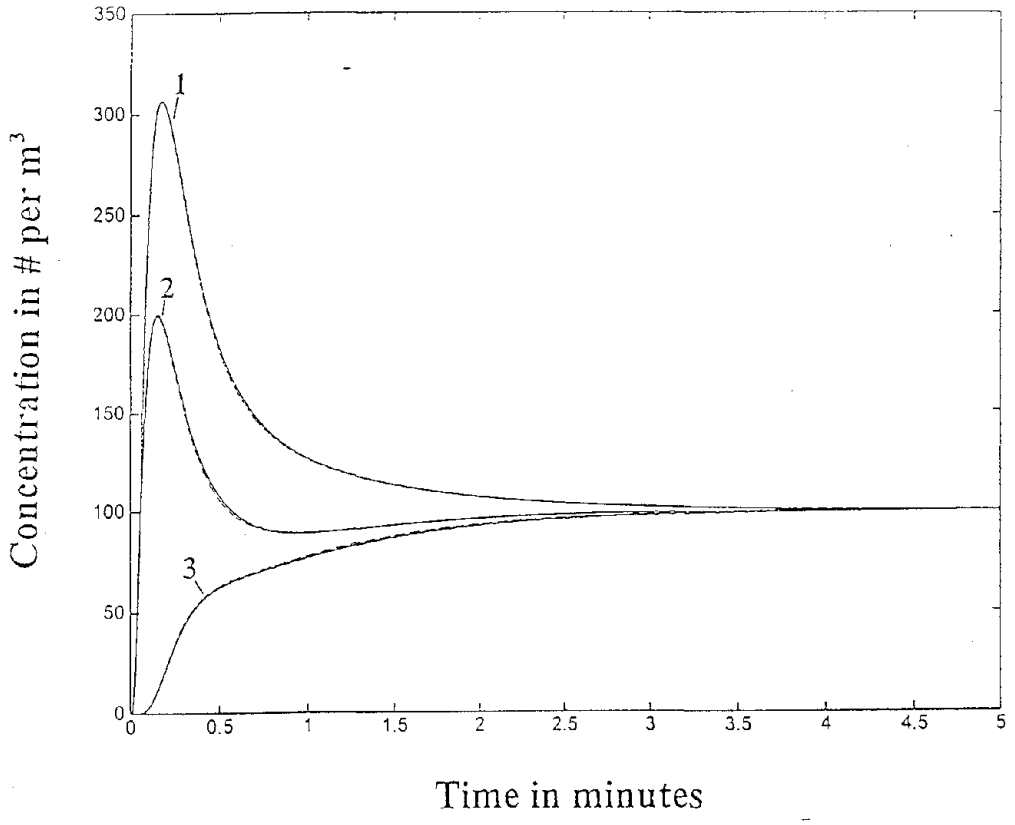

Figure 18 – The expected particle concentrations at three room positions predicted by Markov model I (dashed-line curves) and Markov model II (solid-line curves) following the pulse release of 2700 particles at source midpoint position (x = 1.1 m, y = 1.5 m, z = 1.5 m). The receptor midpoint positions are: (1) x = 0.1 m, y = 1.5 m, z = 1.5 m; (2) x = 2.1 m, y = 1.5 m, z = 1.5 m; and (3) x = 2.9 m, y = 1.5 m, z = 1.5 m. The room is 3 m x 3 m x 3 m, and receives no air supply.

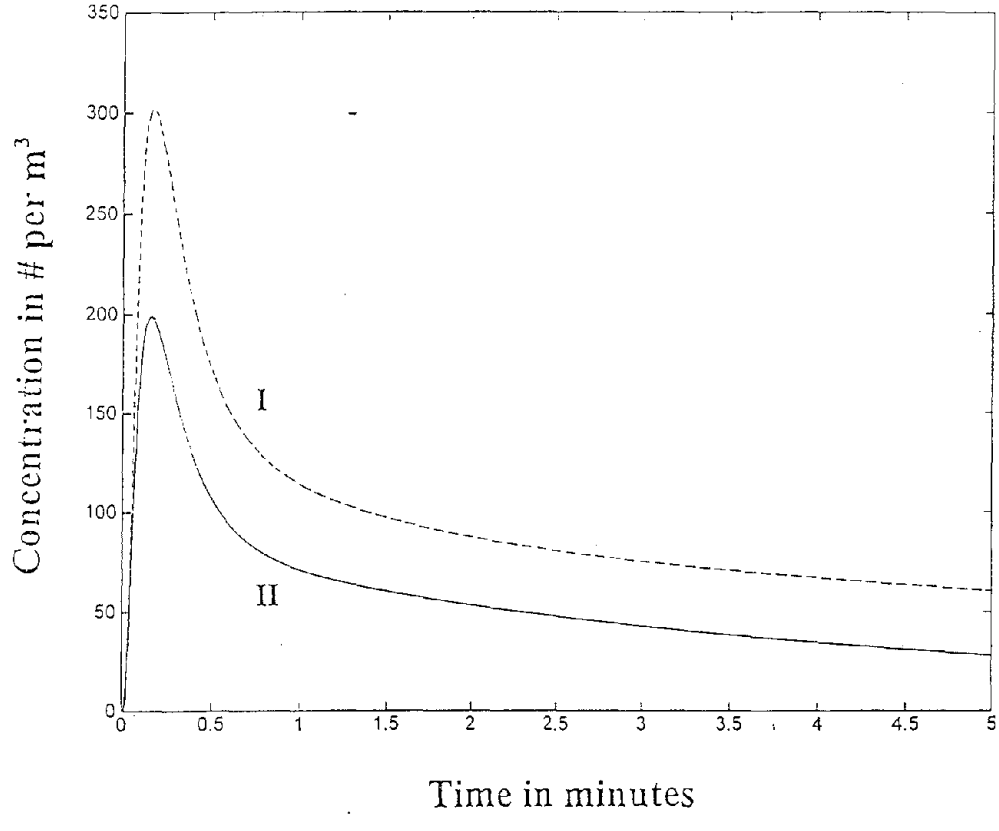

Figure 19 – The expected particle concentrations at receptor midpoint position (x = 0.1 m, y = 1.5 m, z = 1.5 m) predicted by Markov model I (the dashed-line curve labeled I) and Markov model II (the solid-line curve labeled II) following the pulse release of 2700 particles at source midpoint position (x = 1.1 m, y = 1.5 m, z = 1.5 m). The room is 3 m x 3 m x 3 m, and receives 6 nominal air changes per hour. The receptor position adjoins an air inlet and is 1 m upstream from the release position.

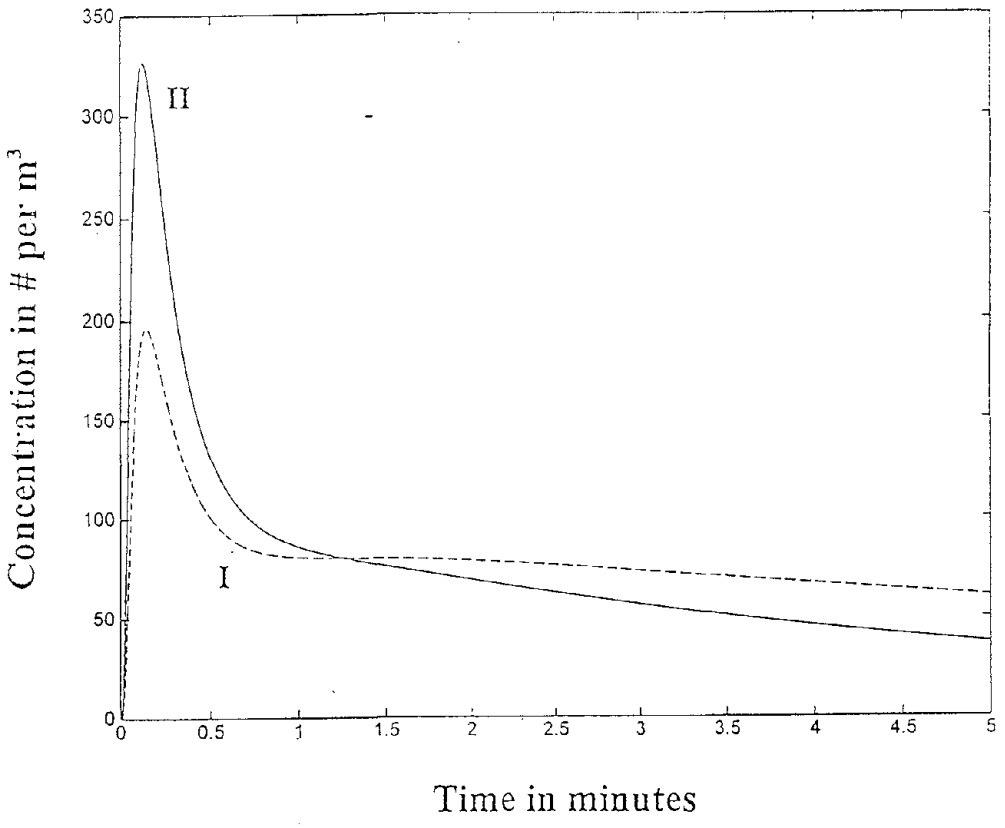

Figure 20 – The expected particle concentrations at receptor midpoint position ($x = 2.1$ m, $y = 1.5$ m, $z = 1.5$ m) predicted by Markov model I (the dashed-line curve labeled I) and Markov model II (the solid-line curve labeled II) following the pulse release of 2700 particles at source midpoint position ($x = 1.1$ m, $y = 1.5$ m, $z = 1.5$ m). The room is 3 m x 3 m x 3 m, and receives 6 nominal air changes per hour. The receptor position is in the room interior and 1 m downstream from the release position.

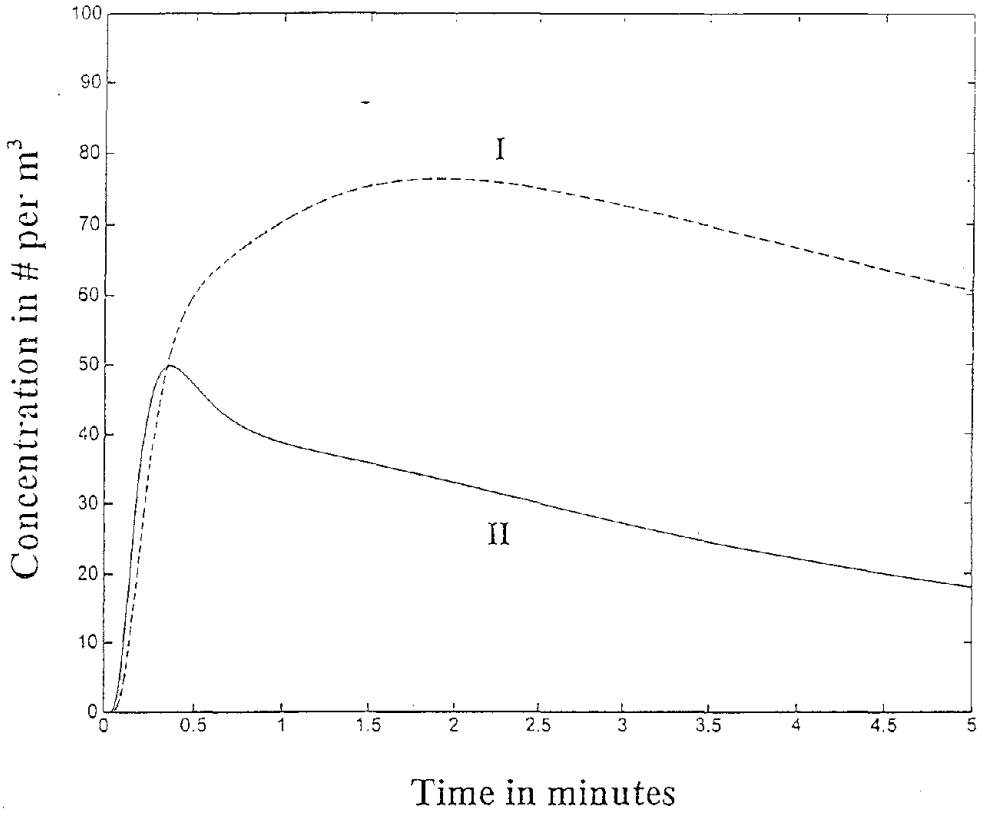

Figure 21 – The expected particle concentrations at receptor midpoint position (x = 2.9 m, y = 1.5 m, z = 1.5 m) predicted by Markov model I (the dashed-line curve labeled I) and Markov model II (the solid-line curve labeled II) following the pulse release of 2700 particles at source midpoint position (x = 1.1 m, y = 1.5 m, z = 1.5 m). The room is 3 m x 3 m x 3 m, and receives 6 nominal air changes per hour. The receptor position adjoins an air outlet and is 1.8 m downstream from the release position.

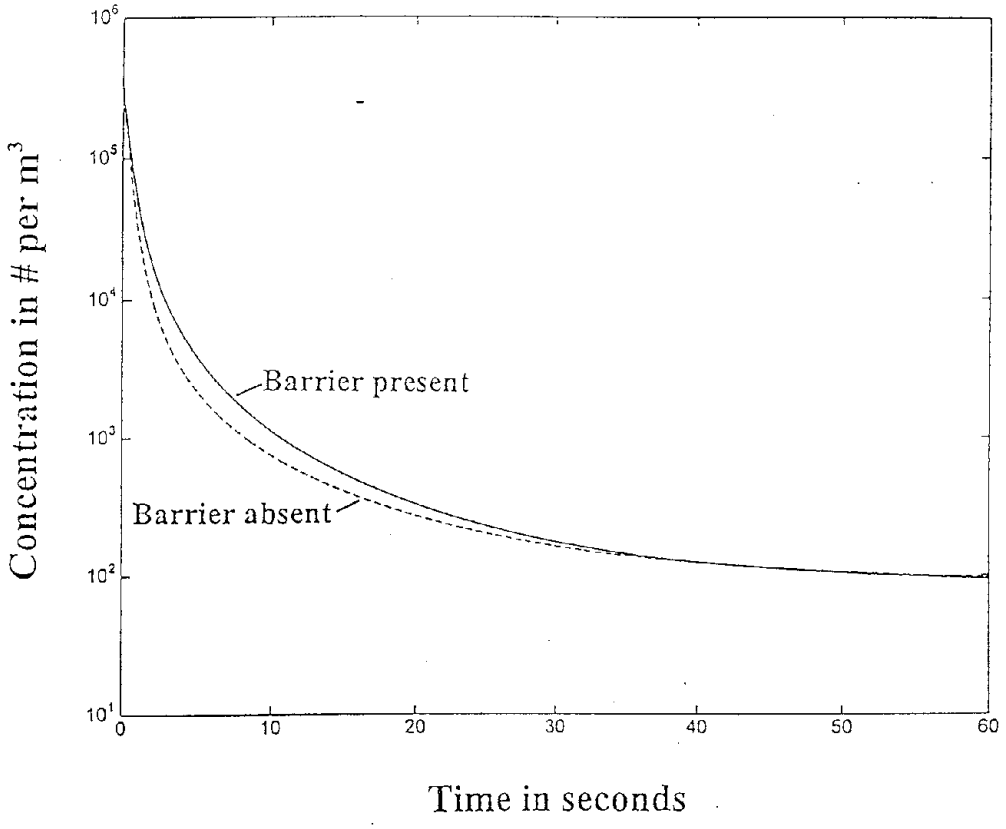

Figure 22 – The expected particle concentrations at source midpoint position (x = 1.1 m, y = 1.5 m, z = 1.5 m) following the pulse release of 2700 particles predicted by Markov model II with a barrrier immediately upstream of the source position (the solid-line curve) or with no barrier (the dashed-line curve). The room is 3 m x 3 m x 3 m, and receives 6 nominal air changes per hour.